University of New Mexico
UNM Digital Repository

Civil Engineering ETDs Engineering ETDs

Spring 4-12-2018

Assessing the power of remotely-sensed snow cover extent to improve understanding of snowpack-streamflow dynamics: an application of MODIS snow cover in Western U.S. mountain watersheds

Jennifer N. Van Osdel
Master's Student, Civil Engineering

Follow this and additional works at: https://digitalrepository.unm.edu/ce_etds

Part of the Civil and Environmental Engineering Commons

Recommended Citation

Van Osdel, Jennifer N.. "Assessing the power of remotely-sensed snow cover extent to improve understanding of snowpack-streamflow dynamics: an application of MODIS snow cover in Western U.S. mountain watersheds." (2018). https://digitalrepository.unm.edu/ce_etds/202

This Thesis is brought to you for free and open access by the Engineering ETDs at UNM Digital Repository. It has been accepted for inclusion in Civil Engineering ETDs by an authorized administrator of UNM Digital Repository. For more information, please contact disc@unm.edu.

Jennifer Nicole Van Osdel
Candidate

Civil Engineering
Department

This thesis is approved, and it is acceptable in quality and form for publication:

Approved by the Thesis Committee:

Dr. Mark Stone, Chair

Dr. Julie Coonrod

Dr. Joseph Galewsky

Assessing the power of remotely-sensed snow cover extent to improve understanding of snowpack-streamflow dynamics: an application of MODIS snow cover in Western U.S. mountain watersheds

by

Jennifer Nicole Van Osdel

B.A., Computer Science and Mathematics, Gustavus Adolphus, 2011

THESIS

Submitted in Partial Fulfillment of the
Requirements for the Degree of

Master of Science
Civil Engineering

The University of New Mexico
Albuquerque, New Mexico

May 2018

Acknowledgements

I would like to thank my advisor, Mark Stone, for guiding me through the mental and academic hurtles of graduate school and keeping me from going down the rabbit hole on more occasions than I can count. I would like to thank Julie Coonrod, who got me interested in geospatial analysis and has served as an invaluable female mentor. I would also like to thank Joe Galewsky for listening to numerous iterations of my research proposal and for sharing his climate change expertise.

A special thank you to Mark and Joe for including me on that fateful research trip to Nepal in the winter of 2014 which would become the inspiration for my research and would lead to the founding of UNM4Nepal, where I was able to immerse myself in the world of non-profit international development. And to the UNM4Nepal community and all of the people that I have met through those experiences, thank you for your hard work, dedication, and friendship.

Thank you to the National Science Foundation for believing in me and supporting my research through the NSF Graduate Research Fellowship Program.

I am forever grateful to my best friend, Katelyn Bladel, who by a twist of fate, ended up at UNM for her Master's of Fine Arts at the same time as me. Thank you for keeping me sane and full of cupcakes.

Last, but certainly not least, I would like to thank my husband, Devin Lachowsky, who has been an unending supply of support throughout this process. Thank you for your support and undying belief that I could conquer this graduate school beast. And of course, thank you for making margaritas for the nights I had to work late. I love you.

Assessing the power of remotely-sensed snow cover extent to improve understanding of snowpack-streamflow dynamics:

an application of MODIS snow cover in Western U.S. mountain watersheds

by

Jennifer Nicole Van Osdel

B.A., Computer Science and Mathematics, Gustavus Adolphus College, 2011

M.S., Civil Engineering, University of New Mexico, 2018

Abstract

Mountain snowpacks provide essential water for socio-economic systems around the world, with nearly two billion people living in snow sensitive regions. Therefore, methods for characterizing the snowpack-streamflow dynamics at the watershed level are essential for understanding how changes in temperature and precipitation due to climate change will affect the water supply in these regions. However, in-situ snowpack measurements, such as snow water equivalent (SWE), are often unavailable or insufficient due to the financial and logistical constraints of installing snowpack monitoring systems. Remotely-sensed snow cover extent (SCE), or the proportion of a watershed that is covered in snow, has been previously integrated into snowmelt models and used to assess the relationships between snowmelt and streamflow. However, no research was found that provided a comprehensive analysis of the ability of SCE to characterize snowpack-streamflow dynamics in a way that supports analysis between and within watersheds. This study develops and tests a methodology for characterizing the snowpack-streamflow dynamics of a watershed using SCE-based metrics that capture the shape and key temporal inflections in the SCE curve – start of snow season, start of snow melt, end of snow season, and average SCE. The results demonstrate that SCE and streamflow sufficiently characterize snowpack-streamflow dynamics to allow for inter-watershed comparison and intra-watershed pattern recognition. The techniques developed and tested in this study allow for the characterization of snowpack-streamflow dynamics in remote and unmonitored watersheds to support future research into how those dynamics may change under future climate change scenarios.

Contents

List of Figures viii

List of Tables xii

1. Introduction 1

2. Methodology and Data Sources 6

- 2.1 Initial watershed selection 8
- 2.2 Snow cover extent 9
- 2.3 Streamflow 11
- 2.4 Average water year 13
- 2.5 Final watershed selection 14
- 2.6 Snow season characterization 17
- 2.7 Additional Data sources 21
  - 2.7.1 Snow water equivalent 21
  - 2.7.2 Climate 23
  - 2.7.3 Elevation 24

3. Results 25

- 3.1 Inter-watershed variability 25
  - 3.1.1 Climatological variance 26
  - 3.1.2 Snow water equivalent 30
  - 3.1.3 Streamflow 35

3.2 Intra-watershed patterns 39
3.2.1 Snow water equivalent 40
3.2.2 Streamflow 48
3.3 Snowpack-streamflow dynamics in hydrologically distinct watersheds 55
3.3.1 Watershed descriptions 55
3.3.2 Initial analysis of snowpack-streamflow dynamics 60
3.3.3 Compact analysis using hysteresis loops and delta graphs 67
4. Discussion 70
4.1 SCE and inter-watershed variability 70
4.2 SCE and intra-watershed patterns 72
4.3 Snowpack-streamflow dynamics in hydrologically distinct watersheds 76
4.4 Guidelines for the use of snow cover extent 79
5. Conclusion 80
Appendices 83
Appendix A: Term definitions 83
Appendix B: SCE smoothing algorithm 83
Appendix C: Snow season characterization 90
Appendix D: Selecting metrics for analysis 116
References 128

List of Figures

Figure 1: Data processing flow diagram for main data sources.. 8

Figure 2: Logarithmic regression of drainage area with (a) peak Q and (b) peak Q normalized by drainage area. 13

Figure 3: Initial GAGESII reference watersheds in the Mountain West characterized by their status after final watershed selection. Study watersheds represent the final watershed selection for this study. 17

Figure 4: SCE distribution for all study watersheds with respect to the 8-day period in the average water year. 18

Figure 5: Characterization of the snow season using a threshold method for SCE to identify the start of the snow season, start of snow melt, and end of the snow season. ... 21

Figure 6: Map of study watersheds containing one or more SNOTEL stations. 23

Figure 7: Linear regression of (a) SOS, (b) SOMelt, (c) EOS, and (d) AvgSCE against the mean annual temperature from PRISM for all study watersheds. 28

Figure 8: Linear regression of EOS against the inverse square root of mean annual precipitation from PRISM for all study watersheds. 30

Figure 9: Linear regression of SQRT(PeakSWE) against (a) SOMelt, (b) EOS, and (c) AvgSCE for watersheds containing one or more SNOTEL stations. Metrics for watersheds with multiple stations were averaged. 32

Figure 10: Multiple linear regression of SQRT(PeakSWE) using elevation and (a) SOS, (b) SOMelt, and (c) AvgSCE for watersheds containing one or more SNOTEL stations. Overlaid measured vs. predicted SQRT(PeakSWE) against each metric are on the left.

The linear regressions of measured vs. predicted SQRT(PeakSWE) are on the right. Metrics for watersheds with multiple stations were averaged. 34

Figure 11: Linear regression of SQRT(PeakQ) against (a) SOS, (b) SOMelt, (c) EOS, and (d) AvgSCE for watersheds containing one or more SNOTEL stations. Metrics for watersheds with multiple stations were averaged. 37

Figure 12: Multiple linear regression of SQRT(PeakQ) using AvgSCE and precipitation. Overlaid measured vs. predicted SQRT(PeakQ) against AvgSCE are on the left. The linear regressions of measured vs. predicted SQRT(PeakQ) are on the right. 39

Figure 13: 8-day SCE vs SWE from the average water year for every study watershed containing one or more SNOTEL stations. Metrics for watersheds with multiple stations were averaged. 41

Figure 14: Delta graphs of 8-day SCE vs 8-day SWE from the average water year for every study watershed containing at least one SNOTEL station for the (a) accumulation season, (b) ablation season, and (c) off-season. Metrics for watersheds with multiple stations were averaged. 44

Figure 15: MODIS SCE versus SNOTEL SWE for the Yellowstone River Watershed for each 8-day period (left) and average 8-day period (right) using SNOTEL station (a) 670 and (b) 683. 47

Figure 16: Delta graphs of 8-day SCE versus 8-day SWE for all 16 water years (left) and the average water year (right) in Yellowstone River Watershed for SNOTEL stations (a) 670 and (b) 683. 48

Figure 17: SCE vs normalized streamflow for every 8-day period in the average water year for each study watershed. The snow season for each watershed was characterized to determine the timings of the accumulation, ablation, and off seasons. 50

Figure 18: Delta graphs of 8-day SCE vs 8-day streamflow from the average water year for every study watershed for the (a) accumulation season, (b) ablation season, and (c) off-season. 52

Figure 19: SCE versus streamflow for the Yellowstone River Watershed for each 8-day period (left) and average 8-day period (right)... 54

Figure 20: Delta graphs for 8-day SCE vs. 8-day streamflow for all 16 water years (left) and the average water year (right) of the Yellowstone River Watershed. 54

Figure 21: Map of the three watersheds in this case study. Yellowstone River Watershed is in the upper-right corner in northwestern Wyoming. Gila River Watershed is in the lower-right corner in southwest New Mexico. Upper Van Duzen Watershed is in the upper-left corner in northern California with a more detailed view in the inset in the lower-left corner.. 57

Figure 22: Basin delineation and elevation for the Yellowstone River Watershed (GAGESII ID 06191500). The location of the U.S.G.S. streamgage is indicated by with a star. 58

Figure 23: Basin delineation and elevation for the Gila River Watershed (GAGESII ID 09430500). The location of the U.S.G.S. streamgage is indicated by a star..................... 58

Figure 24: Basin delineation and elevation for the Upper Van Duzen River Watershed (GAGESII ID 11478500). The location of the U.S.G.S. streamgage is indicated by a star. 59

Figure 25: Monthly (a) mean annual temperature (°C) and (b) proportion of total annual precipitation for the average water year for the Yellowstone River, Gila River, and Upper Van Duzen River Watersheds. The total annual precipitations for the average water year for Yellowstone, Gila, and Upper Van Duzen are 747 mm, 458 mm, and 1705 mm, respectively. 62

Figure 26: Distribution of SCE for the 8-day periods of all 16 water years divided by season along with the SCE and streamflow for the average water year for (a) Yellowstone River Watershed, (b) Gila River Watershed, and (c) Upper Van Duzen Watershed........ 65

Figure 27: Streamflow for every 8-day period from 2000 to 2016 mapped against the period of the water year for the (a) Yellowstone River Watershed, (b) Gila River Watershed, and (c) Upper Van Duzen Watershed. 66

Figure 28: Hysteresis loops (left) and delta graphs (right) for (a) Yellowstone River Watershed, (b) Gila River Watershed, and (c) Upper Van Duzen Watershed. 69

Figure 29: Snow cover extent (SCE) before and after smoothing along with the cloud cover extent (CCE) for watershed 06191500 in the Upper Rockies. The cloud ratio is 0.1842.. 85

Figure 30: Snow cover extent (SCE) before and after smoothing along with the cloud cover extent (CCE) for watershed 12035000 in the Pacific Northwest. The cloud ratio is 1.193.. 85

List of Tables

Table 1: R^2, R, and p values for the correlational analysis between AvgAnnualTMean and each of SOS, EOS, SOMelt, and AvgSCE. 27

Table 2: R^2, R, and p values for the correlational analysis between INVSQRT(AvgAnnualPPT) and each of SOS, EOS, SOMelt, and AvgSCE. 29

Table 3: R^2, R, and p values for the correlational analysis between each of the SCE metrics – SOS, EOS, SOMelt, and AvgSCE – and SQRT(PeakSWE). 31

Table 4: R^2, R, and p values for the correlational analysis between each of the SCE metrics – SOS, EOS, SOMelt, and AvgSCE – and SQRT(PeakQ). 36

1. Introduction

Mountain snowpacks provide essential water for socio-economic systems in the Western United States and around the world. Nearly two billion people live in snow sensitive regions, meaning that their water supply depends on snowmelt and that those supplies face significant pressures due to climate change (Mankin et al, 2015). Yet in-situ knowledge of snowpack dynamics is limited by the financial and logistical constraints of snowpack monitoring systems like the Natural Resources Conservation Service's Snow Telemetry (SNOTEL) program. The prevalence of snowpack measurements in other countries is often worse and does not necessarily match the importance and fragility of their winter snowpacks.

Understanding the snowpack-streamflow dynamics of mountain watersheds is crucial to understanding how water gets to our fields, cities, and industries as well as how those dynamics may change under rising temperatures. In an idealized snow-dependent watershed, solid precipitation during the winter months accumulates in the basin with very little melt until temperatures rise sufficiently in the spring to trigger the snowmelt, or ablation, season. During this time, snow depletes quickly and makes its way as runoff to the river where it creates a spike in streamflow known as a spring pulse. This pulse generally consists of a quick increase to a peak streamflow before a longer attenuation period as the rate and volume of snowmelt runoff slows.

Long-term changes in temperature and precipitation due to climate change have and will affect snowpack, streamflow, and many aspects of the dynamics between the two. Alterations in the snowpack-streamflow dynamics of mountain watersheds, such as an earlier spring streamflow pulse, affect water supply from both surface (Hidalgo et al, 2009) and groundwater (Eckhardt and Ulbrich, 2003) sources; hydropower production (Eckhardt and Ulbrich, 2003; Vicuna et al, 2008); agricultural water demand (Hay et al, 2010); stream ecology (Rahel and Olden, 2008); water quality (Whitehead et al, 2009); and wildfire frequency and severity (Westerling et al, 2006), among numerous other critical natural and human systems.

Climate change affects snowpack and snowmelt timing through increasing temperatures and increased variability in precipitation. Rising temperatures cause increased snowpack sublimation and earlier melt, causing shifts in both the magnitude and timing of the spring pulse. Transitional watersheds near freezing are particularly susceptible to the effects of increased temperatures as snow shifts to rain at higher and higher elevations (Hay et al, 2010; Miller et al, 2003; Stewart, 2009). Predicted changes in precipitation are much more variable, with both increases and decreases expected due to complex atmospheric mechanisms (Nijssen et al, 2001). Potential increases of precipitation in certain regions may supplement snowpack lost to increasing temperatures in the coldest watersheds (Stewart, 2009). In contrast, Miller et al (2003) found that future snow accumulation decreased under all modeling scenarios regardless of whether precipitation increased or decreased. Either way, precipitation cannot be expected to bolster snow loss for much longer if temperatures continue to rise.

Both historical and predicted changes in streamflow timing trend towards an earlier spring pulse in the U.S. Mountain West (Clow, 2009; Dudley et al, 2017) and around the world (Moran-Tejeda et al, 2014). This has been largely linked to higher winter and spring air temperatures that cause snowpack to melt earlier than historically seen (Dudley et al, 2017; Stewart et al, 2005). A significant part of that variability spans the Pacific Decadal Oscillations, indicating that these changes are due to temperature increases beyond normal climatic variations (Stewart et al, 2005). As with snowpack, streamflow in lower-elevation and transitional watersheds that lie near freezing are and will be particularly affected (Dudley et al, 2017). Assuming no change in overall streamflow volume, this can be partially mitigated by creating sufficient storage. However, this will not work in all cases and neglects the impact of earlier snowmelt on other natural processes. Changes in magnitude are less certain than those in timing, but in general, decreases in streamflow will be seen due to weaker snowpacks caused by decreased precipitation; higher evapotranspiration and sublimation due to increased temperatures (Hay et al, 2010; Udall and Overpeck, 2017); and a shift from snow to rain (Feng and Hu, 2007). This is true for the U.S. Mountain West (Fyfe et al, 2017; Milly et al, 2005) and for major basins around the world (Nijssen et al, 2001). However, increased precipitation in certain regions has the potential to increase streamflow in the short term, particularly at very high elevations where this precipitation continues to fall as snow, increasing the winter snowpack (Stewart, 2009).

Water supply prediction is a crucial tool for city planners and water infrastructure managers, among others, to prepare for the coming water year. This is done through a variety of statistical methods that include modeling of physical processes as well as statistical calculations like snow depletion curves. These methods depend on a snowpack measurement known as snow water equivalent (SWE), or the amount of water that would be released from the snowpack if it were to melt. This is also known as snow water content. SWE can be measured using a variety of methods, both automatic and manual.

SNOTEL snow monitoring stations in the U.S. track hourly SWE using snow pillows that weigh the snow and calculate the water content based on density. These measurements allow for a detailed picture of the snowpack at a specific location, but their network is limited due to the logistical and financial obstacles in setting up new stations in mountainous terrain. Thus, these stations may or may not be representative of an entire watershed and interpolating their data to the spatial domain is difficult and error prone. Furthermore, snow water equivalent data is scarce or non-existent in many of the world's most snow-dependent regions, such as in the Hindu-Kush-Himalayas, due to a lack of expansive snow monitoring systems.

Satellite-based measurements, such as snow cover extent (SCE), are often used in snowmelt runoff modeling to supplement SWE in defining snowpack-streamflow dynamics for a watershed. SCE, sometimes known as snow covered area or snow areal extent, measures the proportion of a given area that is covered in snow. It gives a broad view of the snow conditions in a watershed at the sacrifice of detailed data such as depth and water content. Snow cover products derived from the Moderate Resolution Imaging Spectroradiometer (MODIS) sensors mounted on National Aeronautics and Space Administration (NASA) satellites reports the presence of snow daily at a 500m spatial resolution with near-global coverage and is free to the public. This allows researchers to study greater spatial extents and more remote regions to gain new insights into snowpack-streamflow dynamics. SCE has been used in a variety of snowpack-streamflow analyses attempting to characterize the relationship between SCE, SWE, streamflow, and climate variables (Immerzeel et al, 2009; Tahir et al, 2011; Yang et al, 2003; Yang et al, 2007).

Like all satellite-based products, SCE struggles with cloud cover, which obscures the landscape and sends a reflectance signal similar to that of snow. Methods such as compositing and smoothing can help lessen this constraint, but certain regions that experience persistent cloud cover, such as the U.S. Pacific Northwest, may require more advanced cloud filling techniques or may not be suitable for research using SCE. SCE also experiences saturation near its upper boundary of 1.0, which represents full coverage of the watershed. SCE may stay near this value for most of the snow season in high-elevation watersheds, causing a loss in predictive capacity. Derivative metrics focused on the timing of key inflections in SCE, such as the start and end of snow melt, have previously been used to circumvent this challenge (Reed et al, 2009).

Many procedures have been created to transform SCE into SWE with mixed results (Martinec and Rango, 1981; Molotch and Margulis, 2008) due to the complex topographical and climatic variables that factor into snow accumulation and ablation. However, few studies have examined how SCE may be used apart from SWE to characterize the snowpack-streamflow dynamics of a watershed. Even fewer have examined how these dynamics change between watersheds and how those changes are reflected in SCE. At the time of this study, no previous work was found that put forth a methodology and concrete examples for using SCE to analyze inter- and intra-watershed relationships to characterize and differentiate between watersheds. This would allow researchers to explore snowpack-streamflow dynamics in watersheds without snowpack monitoring systems either as the main analysis or to assist in watershed selection and preliminary analysis.

The goal of this study is to assess and demonstrate the suitability of snow cover extent for characterization and analysis of snowpack-streamflow dynamics of mountain watersheds. This goal is met by assessing the ability of SCE and SCE-based metrics to (a) capture inter-watershed variability with respect to climate, SWE, and streamflow; (b) capture intra-watershed patterns with respect to SWE and streamflow; and (c) characterize and differentiate between the snowpack-streamflow dynamics of hydrologically distinct watersheds in the U.S. Mountain West.

2. Methodology and Data Sources

The methodology for this study uses spatial and temporal aggregation to transform datasets with disparate spatial and temporal resolutions into a series of comparable text files and metrics, as summarized in Figure 1. Snow cover extent (SCE) (Section 2.2) is calculated for designated watersheds (Section 2.1) from spatial snow cover data to produce a singular measurement that can be compared to streamflow. Similarly, daily streamflow (Section 2.3) is temporally aggregated to match the 8-day period of the snow cover extent. The SCE and streamflow for an average water year (Section 2.4) are then calculated from the 8-day SCE and streamflow for water years 2001 to 2016. Information on the cloud cover, streamflow record, and maximum SCE are then used to filter the original watersheds for the analysis (Section 2.5).

Snow season characterization (Section 2.6) is performed using a series of thresholds to pinpoint key inflections in the snow season based on SCE. These are the start of the snow season (SOS), the start of snow melt (SOMelt), and the end of the snow season (EOS). Average SCE (AvgSCE) for the entire average water year is also calculated to capture the shape of the SCE curve. The main foundation for the remainder of the analysis consists of (a) these SCE-based metrics, (b) the SCE and streamflow for all water years, and (c) the SCE and streamflow for the average water year.

Additional data sources are used to describe the snow water equivalent (SWE), climate, and elevation of the study watersheds. SWE is handled similarly to streamflow where daily values are aggregated into 8-day periods and then into an average water year (Section 2.7.1). Climate data are used to generate average annual precipitation and temperature for each watershed over the study period (Section 2.7.2). Elevation metrics are derived from a hydrologically-accurate digital elevation model (Section 2.7.3).

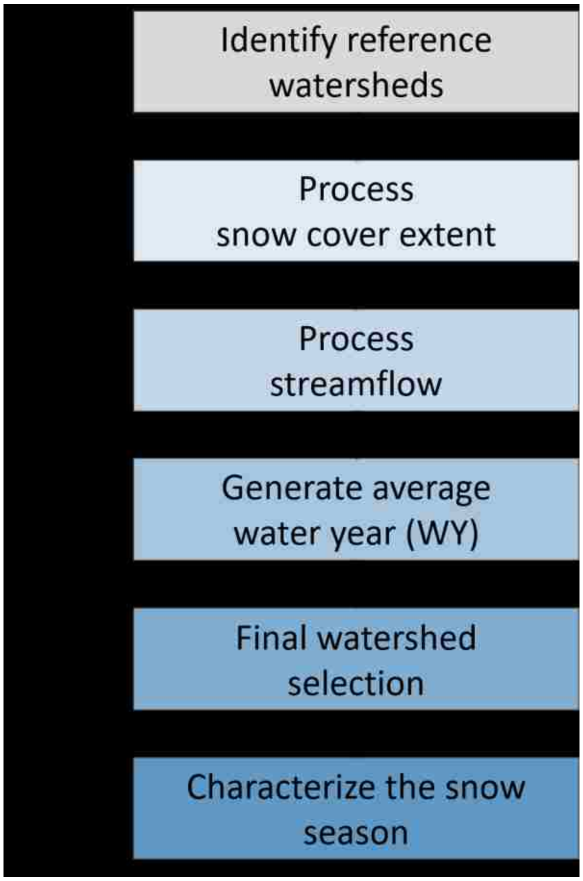
Identify reference watersheds
Process snow cover extent
Process streamflow
Generate average water year (WY)
Final watershed selection
Characterize the snow season

Figure 1: Data processing flow diagram for main data sources.

2.1 Initial watershed selection

The Geospatial Attributes for Gages for Evaluating Streamflow (version II) (https://water.usgs.gov/GIS/metadata/usgswrd/XML/gagesII_Sept2011.xml) (Falcone, 2011), or GAGES II, provides watershed delineation and geospatial attributes for stream gages maintained by the U.S. Geological Survey (USGS). This data set also classifies each gage’s watershed as reference (minimal human impact) or non-reference and labels each one with the appropriate ecological classification. This research used GAGES II to identify watersheds that met the following criteria: (1) reference watershed; (2) located in the Mountain West region of the U.S. and (3) has 20 years of data since 1990. 193 gages of the 9322 total gages and 2057 reference gages met these standards.

2.2 Snow cover extent

Remotely-sensed snow cover products have been generated by the National Ice and Snow Data Center (NISDC) using data from Moderate Resolution Imaging Spectroradiometer (MODIS) sensors on-board NASA’s Aqua and Terra satellites (https://nsidc.org/data/modis/index.html) (Hall et al, 2002). MODIS-derived snow cover extent has been used in a variety of snowmelt-runoff modeling studies (Immerzeel et al, 2009; Reed et al, 2009; Tekeli et al, 2005). Snow cover mapping algorithms used by the NISDC employ the Normalized Difference Snow Index (NDSI) using surface reflectance values from MODIS bands 4 (0.545-0.565 μm) and 6 (1.628-1.652 μm) (Eq. 1) (Hall et al, 1995). Additional quality control measures are applied to account for dense canopies and errant snow pixels in areas with temperatures that cannot sustain snow, among other sources of error. Pixels are classified as snow, land, inland water, ocean, or cloud or are labeled with one of several different error codes.

$$NDSI = \frac{(Band\ 4 - Band\ 6)}{(Band\ 4 + Band\ 6)} \tag{1}$$

MOD10A2 (*http://nsidc.org/data/MOD10A2*) is an 8-day composite snow cover product at 500m spatial resolution from the MODIS sensors aboard NASA’s Terra satellite (Hall et al, 2002). This product marks a pixel as *snow* if snow was detected within a pixel for any day during the 8-day period, meaning that it represents the maximum snow cover during the composite period. A pixel is marked as *cloud* only if clouds were present in the pixel for *every* day in the period. The composite method helps limit the negative effects of cloud cover on snow detection, increasing accuracy at the expense of temporal resolution (Zhou et al, 2005). Accuracy of the lower-level products used to generate MOD10A2 were shown to have an accuracy of ~93% when compared with snow cover at Snow Telemetry (SNOTEL) monitoring stations (Hall and Riggs, 2007).

MOD10A2 files were downloaded for every 8-day period from September 29, 2000 to September 28, 2016 to cover water years 2001 to 2016. These files were projected into USA Contiguous Albers Equal Area and mosaiced together using the MODIS Reprojection Tool. Using the ArcGIS ArcPy module for Python, the projected files for each 8-day period were clipped to each of the watersheds in this study, creating a new raster for each period for each gage ID. Each period was classified with a number that signified its position in the water year where 1 represents the first 8-day period at the beginning of October and 46 represents the last 8-day period at the end of September of the next year. This is referred to as the *period of the water year* for the remainder of this study.

Snow cover extent (SCE) (Eq. 2) and cloud cover extent (CCE) (Eq. 3) were defined as the proportion of the pixels in a watershed marked as *snow* or *cloud*, respectively. ArcPy was used to extract SCE and CCE from each raster and generate a file for each watershed containing the SCE and CCE for each 8-day period.

$$SCE = \frac{Number\ of\ \text{snow}\ pixels}{Total\ pixels} \tag{2}$$

$$CCE = \frac{Number\ of\ \text{cloud}\ pixels}{Total\ pixels} \tag{3}$$

A smoothing algorithm was developed to further alleviate the effects of cloud cover under certain circumstances. This algorithm was aimed at watersheds that experienced short-term cloud cover that corresponded to a sharp drop in SCE, indicating that cloud cover was obscuring snow, as demonstrated in Reed et al, 2009. These gaps were filled using linear interpolation, and the change in SCE was limited by the amount of cloud cover as that is the maximum amount of the watershed that could be covered in obscured snow. Any interpolated SCE value that was less than the original one was thrown out in favor of the original to preserve data. Several watersheds across different climate types were visually inspected to ensure accurate smoothing results. The smoothed SCE values were used for the remainder of the analysis. See Appendix B for details.

2.3 Streamflow

The United States Geological Survey (USGS) maintains streamflow gages throughout the United States and its territories, providing data through the National Water Information System (NWIS) (https://waterdata.usgs.gov/nwis/sw) (USGS, 2016). This study uses historical daily mean streamflow from September 29, 2000 to September

28, 2016 to cover water years 2001 to 2016. Daily values were aggregated to match the MODIS 8-day periods using the average streamflow for the period as demonstrated in Zhou et al (2005). A linear regression analysis revealed a strong positive logarithmic correlation between peak streamflow and watershed drainage area as shown in Figure 2a. This reflects that larger watersheds generally collect more water and represent higher-order rivers with larger streamflows. Streamflow was normalized by the drainage area to allow for analysis of underlying relationships with other variables. Figure 2b shows that the normalization was highly effective at eliminating the relationship between peak streamflow and drainage area. This normalized streamflow was used for the remainder of the analysis.

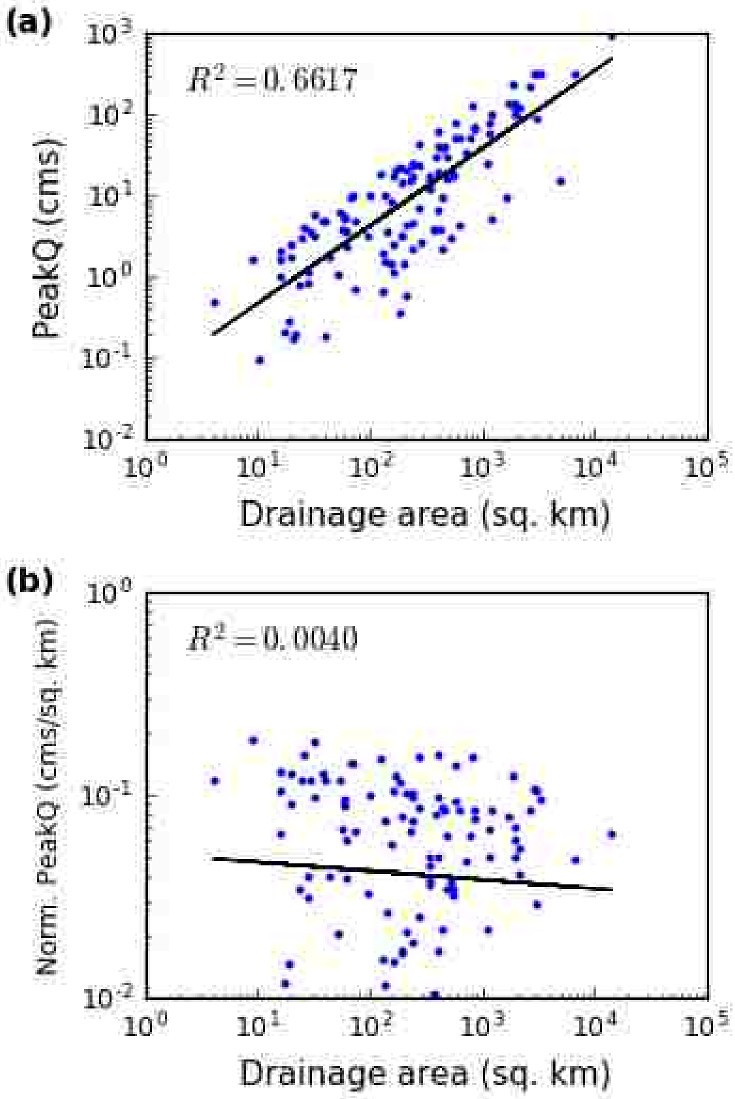

Figure 2: Logarithmic regression of drainage area with (a) peak Q and (b) peak Q normalized by drainage area.

2.4 Average water year

The concept of an *average water year* was used during this research to generate a concise description of “typical” watershed behavior to allow for efficient analysis of and comparisons between watersheds. It is calculated for a specific variable by generating the

16-year average for each 8-day period, thus producing a statistical portrait of the watershed. Previous research has employed this concept in a limited capacity using terms such as “average seasonal snow cycle” (Immerzeel et al, 2009), “seasonal cycle of SWE” (Yang et al, 2003; Yang et al, 2007), and “average snow-covered area over [a time] period” (Tahir et al, 2011). This study goes further and utilizes the average water year as a core concept for characterizing a watershed based on its average SCE, SWE, streamflow, temperature, and precipitation. Watersheds can then be described and compared based on their typical behavior for each indicator.

2.5 Final watershed selection

Once cloud cover extent, smoothed snow cover extent, and normalized streamflow were processed for the 193 initial watersheds (Section 2.1), a series of filters using these variables were applied to ensure data quality for the remainder of the analysis.

Streamflow

GAGES II only accounts for data continuity through 2010 so current streamflow data from USGS were used to filter out watersheds with incomplete stream gage records. Eight watersheds were eliminated under this criterion.

Cloud cover

MODIS SCE, like other satellite data sets, is limited by cloud cover that prohibits sensors from getting an accurate picture of the ground. To account for this, a cloud ratio was generated for each watershed based on the average water year *after* smoothing (Eq. 4). This ratio reflects the average amount of cloud coverage with respect to SCE, indicating the persistency of cloud cover as well as the compatibility of cloud-SCE co-occurrence patterns with the smoothing algorithm. Watersheds with limited cloud cover or with ephemeral cloud cover that corresponds to a similar drop in SCE will have low cloud ratios. Watersheds with high cloud cover that occurs over extended periods of time and does not correlate well with decreases in SCE will have high cloud ratios. These watersheds are unsuitable for this type of analysis without more rigorous cloud removal processes.

$$cloud\ ratio = \frac{average\ CCE}{average\ smoothed\ SCE} \tag{4}$$

Watersheds with a cloud ratio greater than 0.5 were eliminated from the final dataset, leaving 127 watersheds for analysis. As expected, most of the watersheds with high cloud ratios were in the Pacific Northwest where cloudy skies persist throughout the winter season, hindering satellite readings.

Snow cover extent

The final filter removed any watersheds with an average annual peak SCE less than 30%, or those with consistently low snow coverage even at the height of the snow season. Only six watersheds were eliminated based on this criterion. These watersheds were eliminated as they interfered with algorithms used to classify the snow season.

A total of 121 watersheds were found suitable for further analysis (see Figure 3). These watersheds had drainage areas ranging from 4.03 to 14,267 km^2 that skewed towards smaller basins with a mean of 706 km^2 and a median of 236 km^2. This skew is caused by the necessary restriction of the study area to reference, or natural, watersheds. Mean elevations (Section 2.7.3) of the study watersheds are normally distributed, ranging from 277 to 3626 m with a mean of 2220 m and a median of 2268 m. Average annual temperatures (Section 2.7.2) are also normally distributed, ranging from -0.63 to 13 °C with a mean of 5.35 °C and a median of 5.45 °C. Precipitation is skewed to the left due to the relatively few study watersheds on the Pacific coast where precipitation magnitudes are generally higher. Average annual precipitation (Section 2.7.2) ranges from 35 to 252 mm with a mean of 84.8 mm and a median of 69.6 mm.

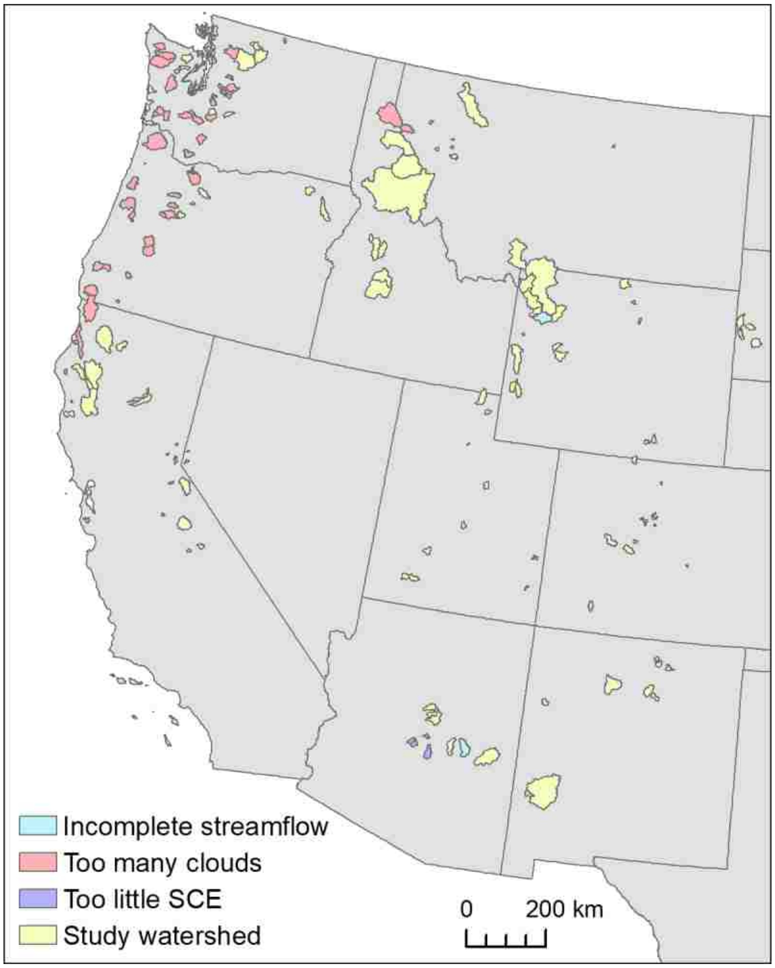
Incomplete streamflow
Too many clouds
Too little SCE
Study watershed
0
200 km

Figure 3: Initial GAGESII reference watersheds in the Mountain West characterized by their status after final watershed selection. Study watersheds represent the final watershed selection for this study.

2.6 Snow season characterization

Snow cover extent, by definition, has a maximum of 1.0 at which the watershed is completely covered in snow. This leads to saturation of the variable as shown in Figure 4. During the middle of the snow season, most high-altitude watersheds remain at an SCE near 1.0 for months, rendering SCE useless for direct comparison with other hydrological variables such as snow water equivalent and streamflow. However, a temporal classification of the key inflections of the snow season using SCE mitigates the effects of this saturation and allows for further analysis.

Studies that classify the snow season based on SCE are limited, and no studies were found that used that classification to assess the dynamics of watershed hydrology. However, this type of classification makes sense given how important the timing of snow melt can be to streamflow and snow depth (Rango, 1997). A similar method was used by Reed et al (2009) to classify the start and end of the snow season based on MODIS SCE to assess the relationship of snow season timing to vegetation greenness during the growing season, which inadvertently measures some aspects of snowpack-streamflow dynamics. Inspiration was also taken from Trujillo et al (2009) who classified snow water equivalent curves based on the timing and slopes of the accumulation and ablation seasons.

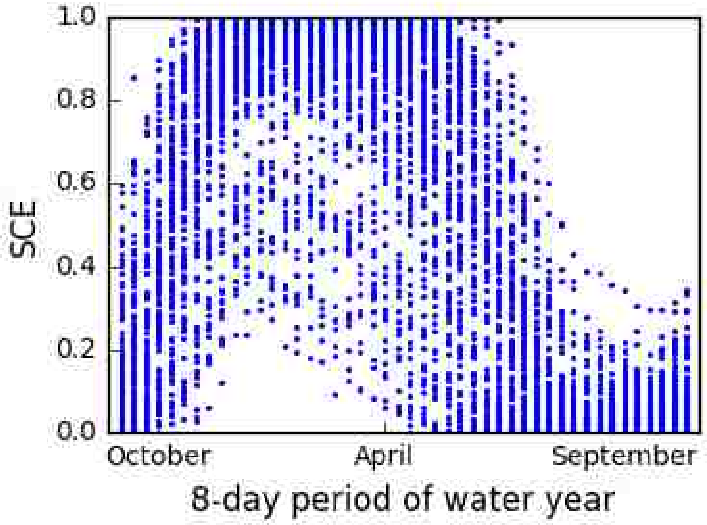

Figure 4: SCE distribution for all study watersheds with respect to the 8-day period in the average water year.

Snow season metrics were derived for each watershed from the SCE for an average water year using a series of thresholds. Thresholds were determined by starting with those from Reed et al (2009) and refining them through experimentation and visual analysis. An absolute threshold was quickly determined to be insufficient to handle the variability of snowpack dynamics captured by the study watersheds. Rather than defining static thresholds for each geographic area, as in Reed et al (2009), thresholds were defined by equations that were then calibrated to each individual watershed. The first threshold defines the start and end of the snow season, or SOS and EOS, respectively, and is set at *minimum SCE + (10% of peak SCE)*. SOS is defined as the period when the SCE crosses this threshold in the upward direction, and EOS is defined as the period when the SCE once again falls below this threshold. This threshold was allowed to begin before the start of the water year, indicated by negative SOS values, as many watersheds in the upper Rockies experience a snow season that begins before October 1. The second threshold defines the start and end of the main snow season, or the plateau caused by the saturation of SCE, and is set at *80% of peak SCE*. The end of the main snow season is defined as the start of snowmelt, or SOMelt, and signifies a transition from snow accumulation to snow ablation. SOMelt is defined as the period when SCE falls back below the main season threshold. See Appendix C for more details.

These metrics divide the season into three segments: accumulation, ablation, and off-season, as shown in Figure 5. Accumulation occurs from SOS to (SOMelt – 1); ablation occurs from SOMelt to (EOS – 1); and the off-season occurs from EOS to (SOS – 1), as the average water year is cyclical.

Average snow cover extent (AvgSCE) for the average water year was also calculated as a proxy for the overall shape of the SCE curve (see Figure 5). AvgSCE serves to complement the timing metrics described above. Its value is influenced by the peak SCE; how long the watershed remains in the main snow season, or plateau, before snow melt; how long the entire snow seasons lasts; and how quickly SCE moves to and from saturation near the maximum SCE. Peak snow cover extent was also explored as a potential metric but was discarded because it did not adequately capture inter-watershed snow season variability as many watersheds achieve approximately the same maximum SCE due to the saturation effect.

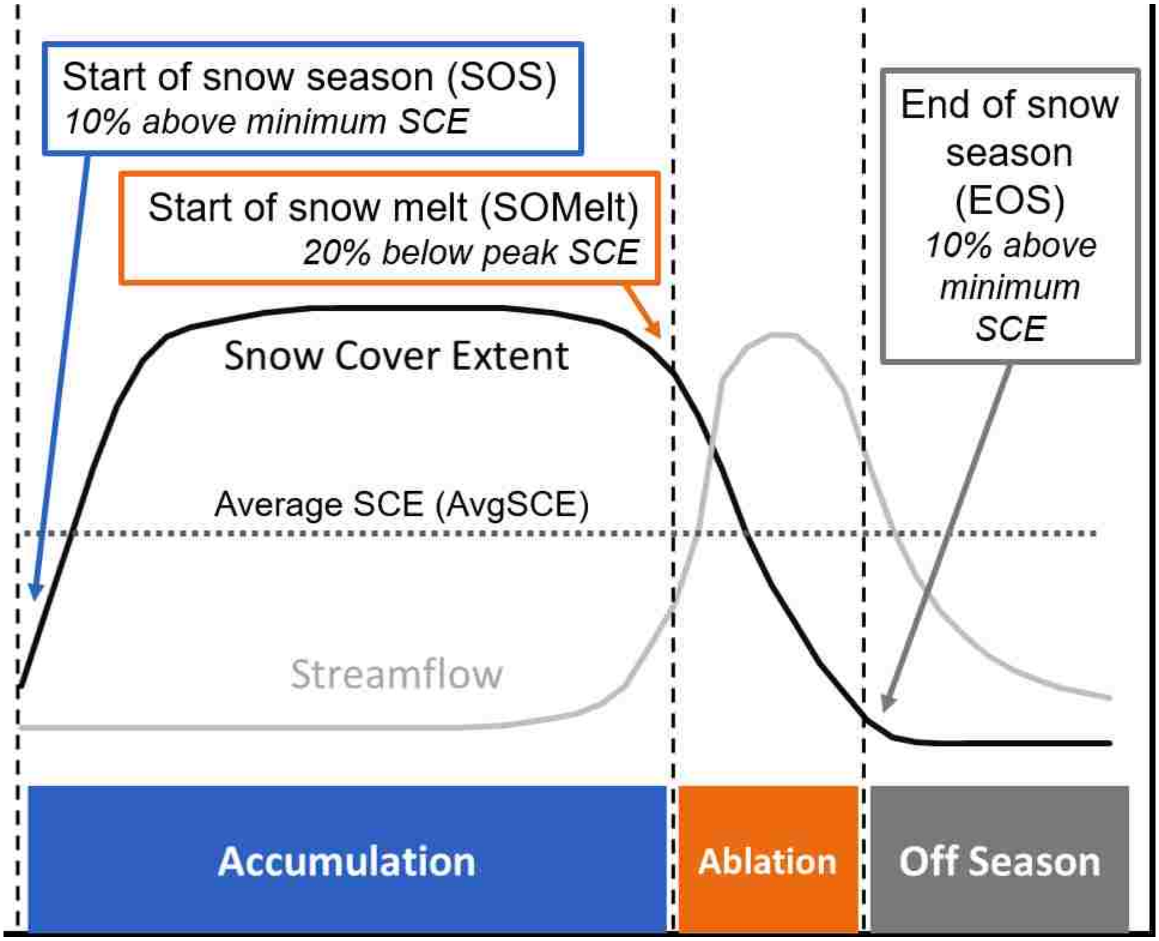
Start of snow season (SOS)
10% above minimum SCE
Start of snow melt (SOMelt)
20% below peak SCE
End of snow season (EOS)
10% above minimum SCE
Snow Cover Extent
Average SCE (AvgSCE)
Streamflow
Accumulation
Ablation
Off Season

Figure 5: Characterization of the snow season using a threshold method for SCE to identify the start of the snow season, start of snow melt, and end of the snow season.

2.7 Additional Data sources

2.7.1 Snow water equivalent

The National Resources Conservation Center's Snow Telemetry (SNOTEL) (https://www.wcc.nrcs.usda.gov/snow) network consists of 800 automated data collection sites in high mountain watersheds that collect data on precipitation, temperature, wind, snowpack, and other hydro-meteorological variables. Each station includes a snow pillow, which weighs the snowpack and calculates the snow water equivalent (SWE), or the amount of water that the snow would produce if it were to melt. See Serreze et al (1999) for a comprehensive description of the SNOTEL network and the resulting snowpack data.

Of the 121 watersheds in this study, 41 of them were found to contain one or more SNOTEL stations for a total of 78 stations. Daily SWE readings from each of these stations was downloaded for the same time period as the MODIS SCE data, September 29, 2000 to September 28, 2016. Not all SNOTEL stations contained the full record, but no stations were eliminated as it was not necessary to have the entire 16 years of SWE for the purposes of this portion of the analysis.

This data was aggregated to match the MODIS 8-day periods by extracting the maximum SWE reading for each period. The SWE for an average water year for each station was then calculated from the aggregated data using however many years were available (see Section 2.4). Average water year SWE for watersheds with more than one station were averaged before being attributed to that watershed. This eliminated issues with statistical normality during analysis between SCE and SWE stemming from duplicate SCE data due to the one-to-many relationship. It also ameliorated the effects of the elevation-dependence of snowpack within a watershed.

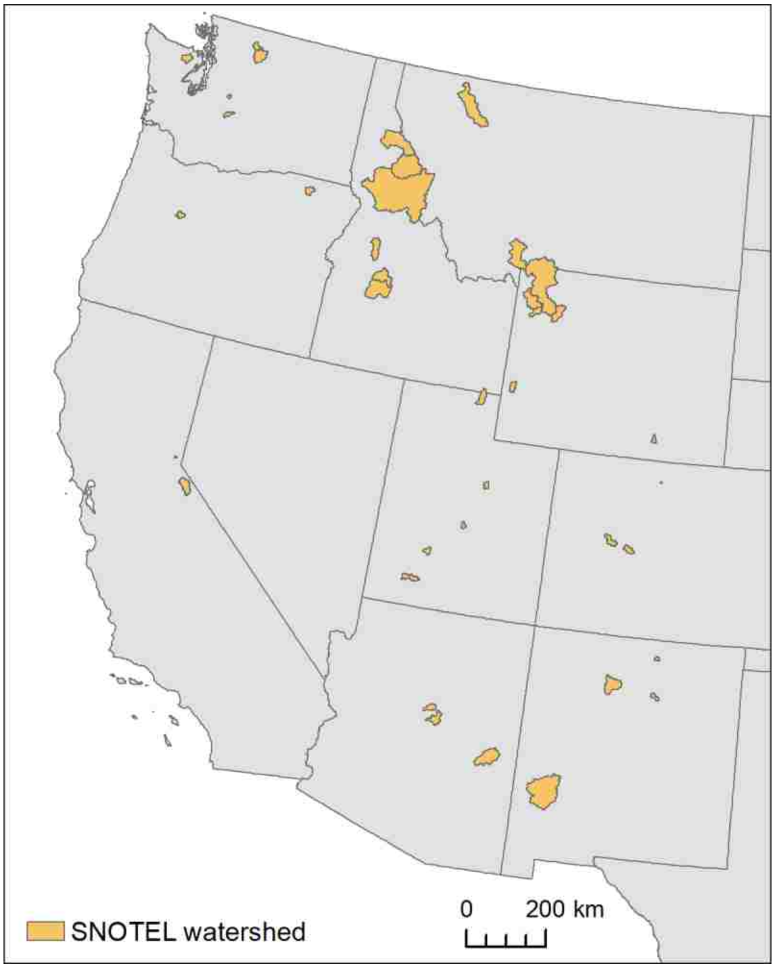

Figure 6: Map of study watersheds containing one or more SNOTEL stations.

2.7.2 Climate

PRISM (parameter-elevation regressions on independent slopes model) datasets (http://www.prism.oregonstate.edu/) were used to generate precipitation and temperature data for each of the study watersheds. The PRISM Climate Group produces and maintains these datasets using a variety of monitoring networks and modeling techniques to create historical spatial climate records (Daly et al, 2002). The variables used in this research are precipitation, minimum temperature, maximum temperature, and mean temperature.

Monthly 4km datasets were downloaded for October 2000 to October 2016; projected to U.S. Contiguous Albers Equal Area; resampled to match the 500km MODIS dataset; and clipped to the study watersheds. For each variable, the average for each watershed and each period were calculated and then aggregated into mean annual values over the 16 water years as well as the following seasonal values: mean for December to March, mean for April to July, and mean for August to November. Snow and rain could not be accurately separated using monthly datasets.

2.7.3 Elevation

Hydro1K (https://lta.cr.usgs.gov/HYDRO1K) is derived from the USGS GTOPO30 dataset (https://lta.cr.usgs.gov/GTOPO30) and is designed to provide a hydrologically correct digital elevation model (DEM) for hydrological analysis (Verdin, 2011). It has a spatial resolution of 30 arc-seconds (~1km). This dataset was projected to U.S. Contiguous Albers Equal Area and resampled to match the 500km MODIS dataset. ArcPy was used to clip the DEM to each study watershed and extract the following metrics: minimum elevation, maximum elevation, mean elevation, and range of elevations.

3. Results

The goal of this study is to assess and demonstrate the suitability of snow cover extent for characterization and analysis of snowpack-streamflow dynamics of mountain watersheds. This is accomplished through statistical analysis of the ability of SCE and SCE-based metrics to capture hydro-climatological differences between watersheds (Section 3.1) and hydrological dynamics within a watershed (Section 3.2) as well as their ability to characterize and differentiate between the snowpack-streamflow dynamics of hydrologically distinct watersheds in the U.S. Mountain West (Section 3.3).

3.1 Inter-watershed variability

The ability of snow cover extent to capture snowpack-streamflow dynamics between watersheds was explored using SCE-based metrics (Section 2.6) for all 121 study watersheds. A preliminary correlation analysis was conducted between a large group of metrics to identify and remove those metrics which were redundant or insignificant. For example, annual precipitation and temperature were determined to be sufficient for a robust climatological analysis, leading to the removal of annual minimum and maximum temperatures as well as seasonal classifications of temperature and precipitation. See Appendix D for more details.

Final metrics chosen for the analysis of inter-watershed variability are mean annual temperature (AvgAnnualTemp), mean annual precipitation (AvgAnnualPPT), maximum SWE (PeakSWE), and maximum streamflow (PeakQ). First, climatological variance with respect to SCE is assessed using AvgAnnualTemp and AvgAnnualPPT to ensure that SCE captures the impact of climate on snowpack (Section 3.1.1). Next, PeakSWE is used to assess how well SCE and SWE correlate as well as to determine how the differences between SCE and SWE express themselves and what this may mean for the application of SCE (Section 3.1.2). Finally, relationships between SCE-based metrics and PeakQ help determine SCE's ability to capture snowpack-streamflow dynamics between watersheds (Section 3.1.3).

3.1.1 Climatological variance

A correlational analysis was performed between the SCE-based metrics and the two climatic variables – average annual temperature (°C) (AvgAnnualTemp) and average annual precipitation (mm) (AvgAnnualPPT) (Section 2.7.2). This was first performed without any transformations to assess normality of the regressions. SOS, SOMelt, EOS, and AvgSCE all had significant linear relationships with AvgAnnualTemp with $p<0.005$ (see Table 1). Linear regression of each variable with AvgAnnualTemp revealed normal distributions of the residuals with skewness between -0.7 and +0.7. Thus, no further data transformations were applied to allow for straight-forward interpretation of the results. As shown in Figure 7, AvgSCE had the strongest correlation with an R^2 of 0.7944 followed closely by SOMelt with an R^2 of 0.6983, SOS with an R^2 of 0.6763, and EOS with an R^2 of 0.4277. SOS was the only variable with a positive correlation to AvgAnnualTemp while all other variables had a negative correlation. The opposing correlations of SOS and EOS indicate that the snow season contracts in warmer climates rather than simply shifting earlier.

Table 1: R^2, R, and p values for the correlational analysis between AvgAnnualTMean and each of SOS, EOS, SOMelt, and AvgSCE.

	R^2	R	p
SOS*	0.6763	0.8224	6.28E-31
EOS*	0.4277	0.6540	4.18E-16
SOMelt*	0.6983	0.8356	9.43E-33
AvgSCE*	0.7944	0.8913	1.09E-42

* Significant correlation with $p<0.005$.

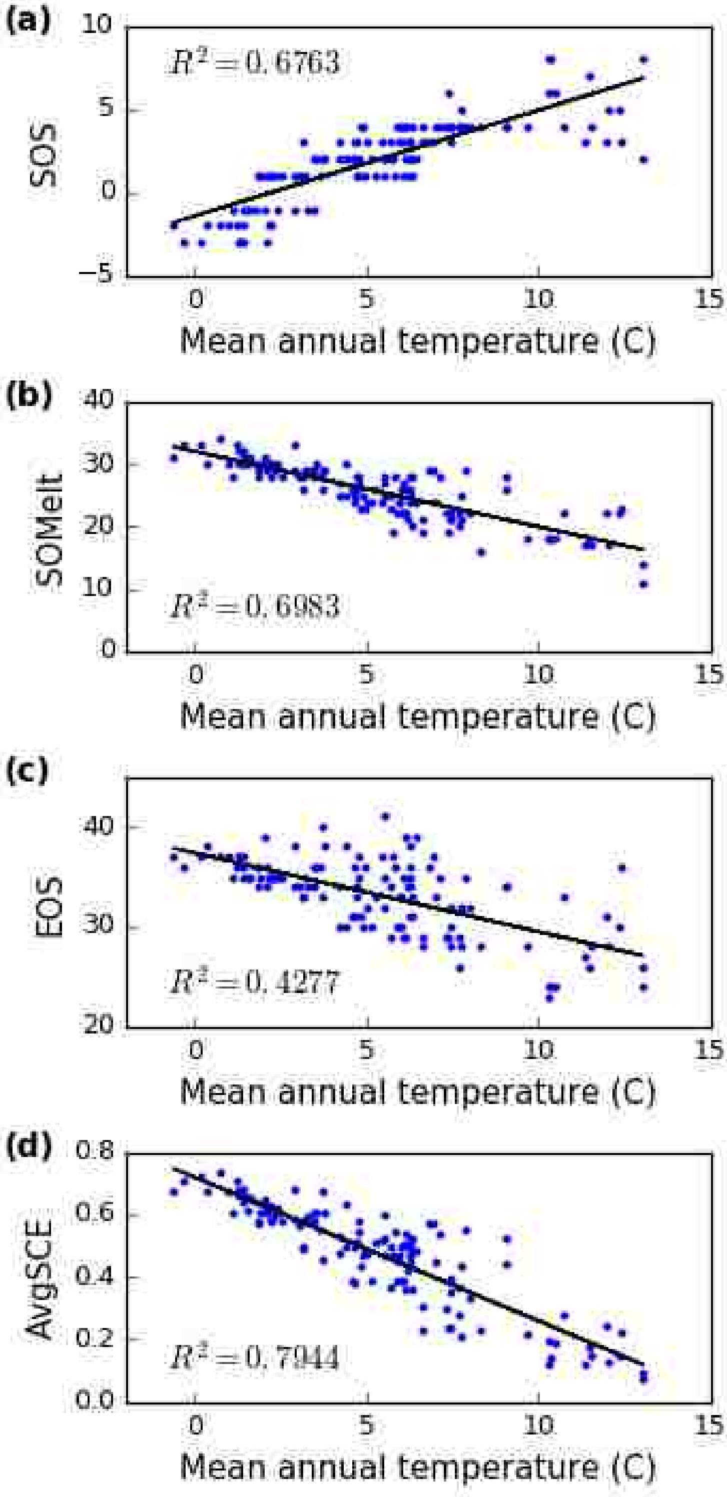

Figure 7: Linear regression of (a) SOS, (b) SOMelt, (c) EOS, and (d) AvgSCE against the mean annual temperature from PRISM for all study watersheds.

For precipitation, only EOS had a significant linear relationship with AvgAnnualPPT with $p<0.005$. However, a linear regression of EOS against AvgAnnualPPT revealed non-normal distributions of the residuals with skewness > 0.7, indicating that transformations were necessary. AvgAnnualPPT was determined to be highly skewed to the left. It was transformed to normality using the inverse square root, henceforth written as INVSQRT(AvgAnnualPPT), and the analysis was repeated. This is not done in Section 3.1.3 during the multiple linear regression with AvgSCE, SQRT(PeakQ), and AvgAnnualPPT since our residuals were normal in that instance.

Using INVSQRT(AvgAnnualPPT), EOS was still the only metric with a significant linear relationship with $p<0.005$ (see Table 2). A linear regression of the two variables revealed a normal distribution of the residuals with skewness between -0.7 and +0.7. Thus, no further data transformations were applied. EOS has a positive correlation to INVSQRT(AvgAnnualPPT) with an R^2 of 0.3137 (see Figure 8).

Table 2: R^2, R, and p values for the correlational analysis between INVSQRT(AvgAnnualPPT) and each of SOS, EOS, SOMelt, and AvgSCE.

	R^2	R	p
SOS	0.0066	0.0810	0.377
EOS*	0.3137	0.5601	2.41E-11
SOMelt	0.0412	0.2030	0.0255
AvgSCE	0.0555	0.2356	0.00928

* Significant correlation with $p<0.005$.

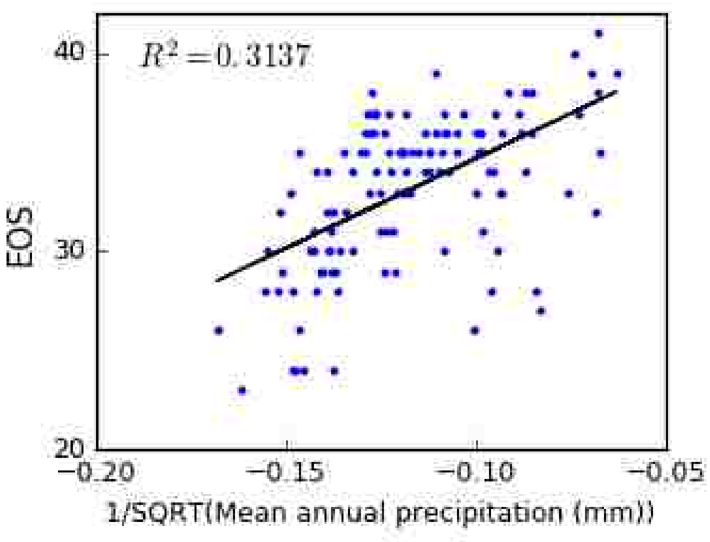

Figure 8: Linear regression of EOS against the inverse square root of mean annual precipitation from PRISM for all study watersheds.

3.1.2 Snow water equivalent

A correlational analysis was then performed between the SCE-based metrics and maximum snow water equivalent (mm) (PeakSWE). This was first performed without any transformations to assess normality of the regressions. SOMelt, EOS, and AvgSCE all had linear relationships with PeakSWE with a $p<0.005$. SOS was not significantly related to PeakSWE. However, linear regression of each variable with PeakSWE revealed non-normal distributions of the residuals with skewness > 0.7, indicating that transformations were necessary. PeakSWE was then transformed to normality using the square root, henceforth written as SQRT(PeakSWE), and the analysis was repeated.

Using SQRT(PeakSWE), SOMelt, EOS, and AvgSCE all still had significant linear relationships with $p<0.005$ while SOS was still not significant despite being normally distributed (see Table 3). A linear regression analysis was then performed again between each of the significant SCE metrics – SOMelt, EOS, and AvgSCE – and SQRT(PeakSWE) as shown in Figure 9. The linear regressions revealed normal distributions of the residuals with skewness between -0.7 and +0.7. Thus, no further data transformations were applied to allow for straight-forward interpretation of the results. EOS had the strongest linear relationship with SQRT(PeakSWE) with an R^2 of 0.4662 followed by AvgSCE with an R^2 of 0.3756 and SOMelt with an R^2 of 0.3455.

Table 3: R^2, R, and p values for the correlational analysis between each of the SCE metrics – SOS, EOS, SOMelt, and AvgSCE – and SQRT(PeakSWE).

	R^2	R	p
SOS	0.1598	0.3997	0.00962
EOS*	0.4662	0.6838	8.73E-07
SOMelt*	0.3455	0.5878	5.32E-05
AvgSCE*	0.3756	0.6128	2.05E-05

* Significant correlation with $p<0.005$.

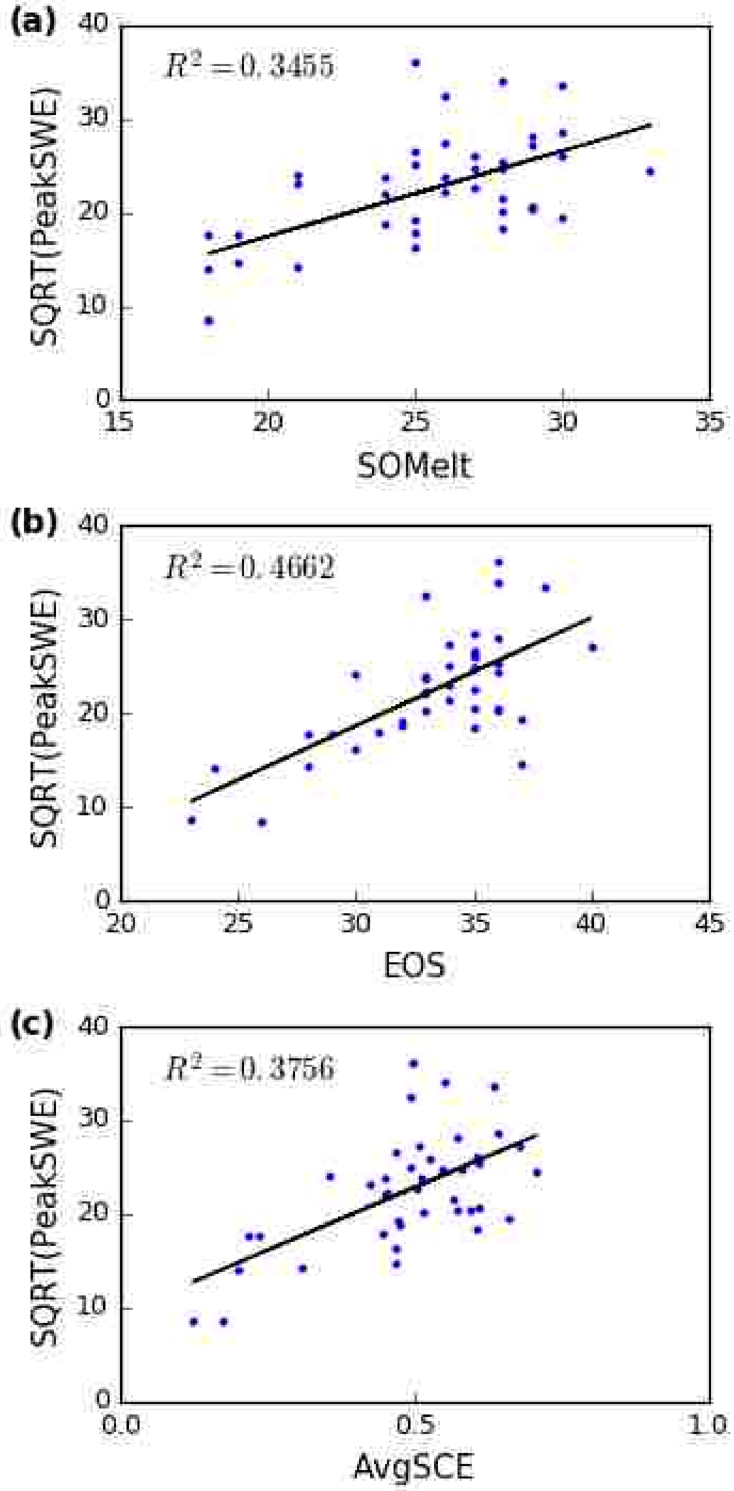

Figure 9: Linear regression of SQRT(PeakSWE) against (a) SOMelt, (b) EOS, and (c) AvgSCE for watersheds containing one or more SNOTEL stations. Metrics for watersheds with multiple stations were averaged.

An additional factor to consider is how the elevation of the SNOTEL station affects the relationship between the SCE-based metrics and SWE. The impact of including elevation was assessed for all metrics through a multiple linear regression analysis. The R^2 values for SOS, SOMelt, and AvgSCE were all improved with both the SCE-based metric and elevation coefficients found to be statistically greater than zero with $p<0.005$ (see Figure 10 (right)). Graphs on the left-hand side of Figure 10 visually demonstrate how including elevation introduces more variability within PeakSWE values for the same value of the SCE-based metric. Although EOS also showed an improvement in R^2, elevation was found to be insignificant with $p=0.117$. When combined with elevation, SOMelt has the strongest linear relationship with R^2 of 0.5336, up from 0.3455, followed by AvgSCE with R^2 of 0.4942, up from 0.3756, and SOS with R^2 of 0.3723, which was made significant by the inclusion of elevation.

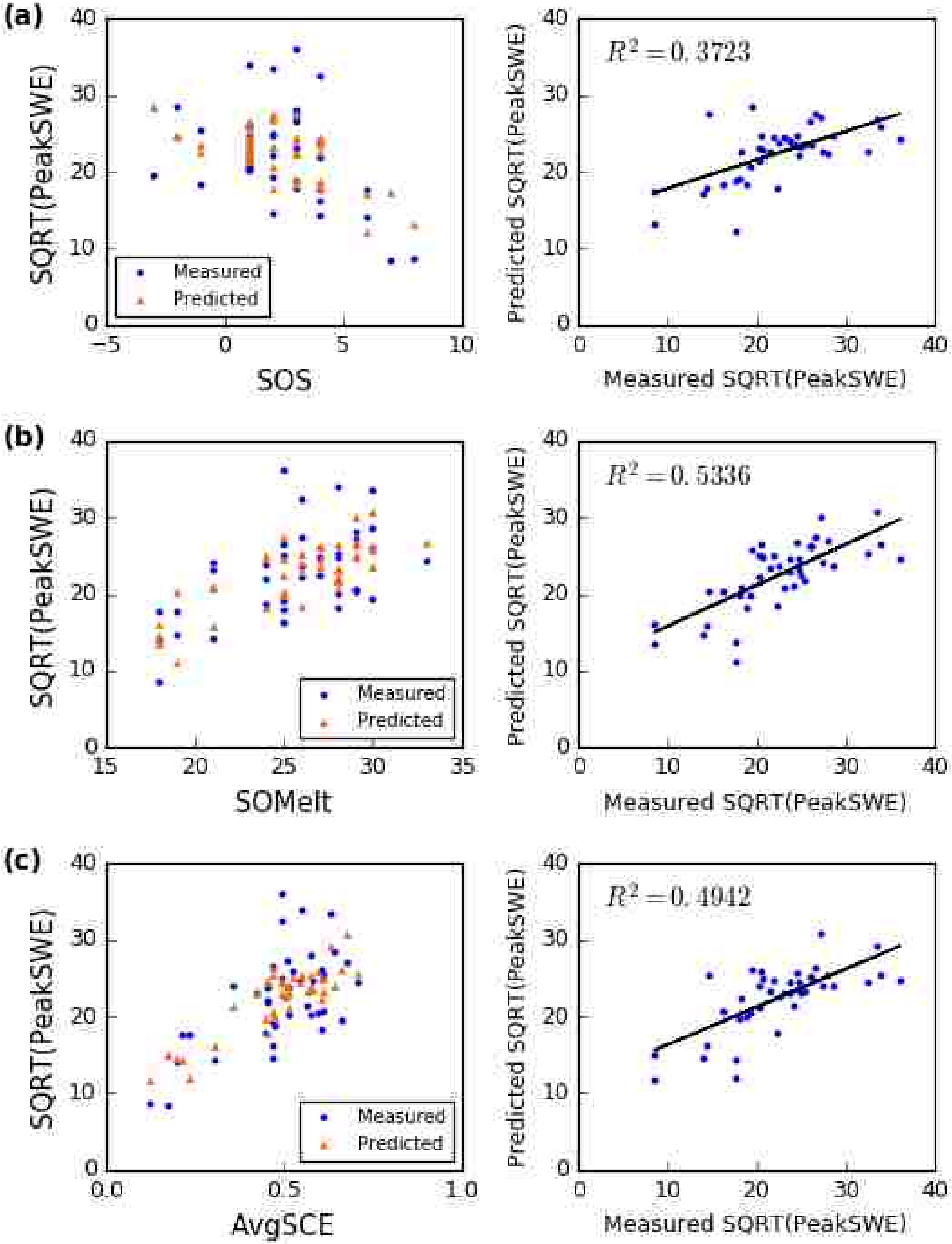

Figure 10: Multiple linear regression of SQRT(PeakSWE) using elevation and (a) SOS, (b) SOMelt, and (c) AvgSCE for watersheds containing one or more SNOTEL stations. Overlaid measured vs. predicted SQRT(PeakSWE) against each metric are on the left. The linear regressions of measured vs. predicted SQRT(PeakSWE) are on the right. Metrics for watersheds with multiple stations were averaged.

3.1.3 Streamflow

A correlational analysis was performed between the SCE-based metrics and maximum normalized streamflow (cms/km^2) (PeakQ) (Section 2.3). This was first performed without any transformations to assess normality of the regressions. SOS, SOMelt, EOS, and AvgSCE all had linear relationships with PeakQ with a $p<0.005$. However, linear regression of each variable with PeakQ revealed non-normal distributions of the residuals with skewness > 0.7, indicating that transformations were necessary. PeakQ was then transformed to normality using the square root, henceforth written as SQRT(PeakQ), and the analysis was repeated.

Using SQRT(PeakQ), SOS, SOMelt, EOS, and AvgSCE all still had significant linear relationships with $p<0.005$ (see Table 4). A linear regression analysis was then performed between each of the SCE-based metrics and SQRT(PeakQ) as shown in Figure 11. The linear regressions revealed normal distributions of the residuals with skewness between -0.7 and +0.7. Thus, no further data transformations were applied. EOS had the strongest linear relationship with SQRT(PeakQ) with an R^2 of 0.5308 followed by AvgSCE with an R^2 of 0.3101, SOMelt with an R^2 of 0.3047, and SOS with an R^2 of 0.1941. SOS and EOS have a negative and positive relationship, respectively, indicating that the contraction of the snow season relates negatively to streamflow.

Table 4: R^2, R, and p values for the correlational analysis between each of the SCE metrics – SOS, EOS, SOMelt, and AvgSCE – and SQRT(PeakQ).

	R^2	R	p
SOS*	0.1941	0.4405	4.27E-07
EOS*	0.5308	0.7285	2.79E-21
SOMelt*	0.3047	0.5520	5.28E-11
AvgSCE*	0.3101	0.5569	3.29E-11

* Significant correlation with $p<0.005$.

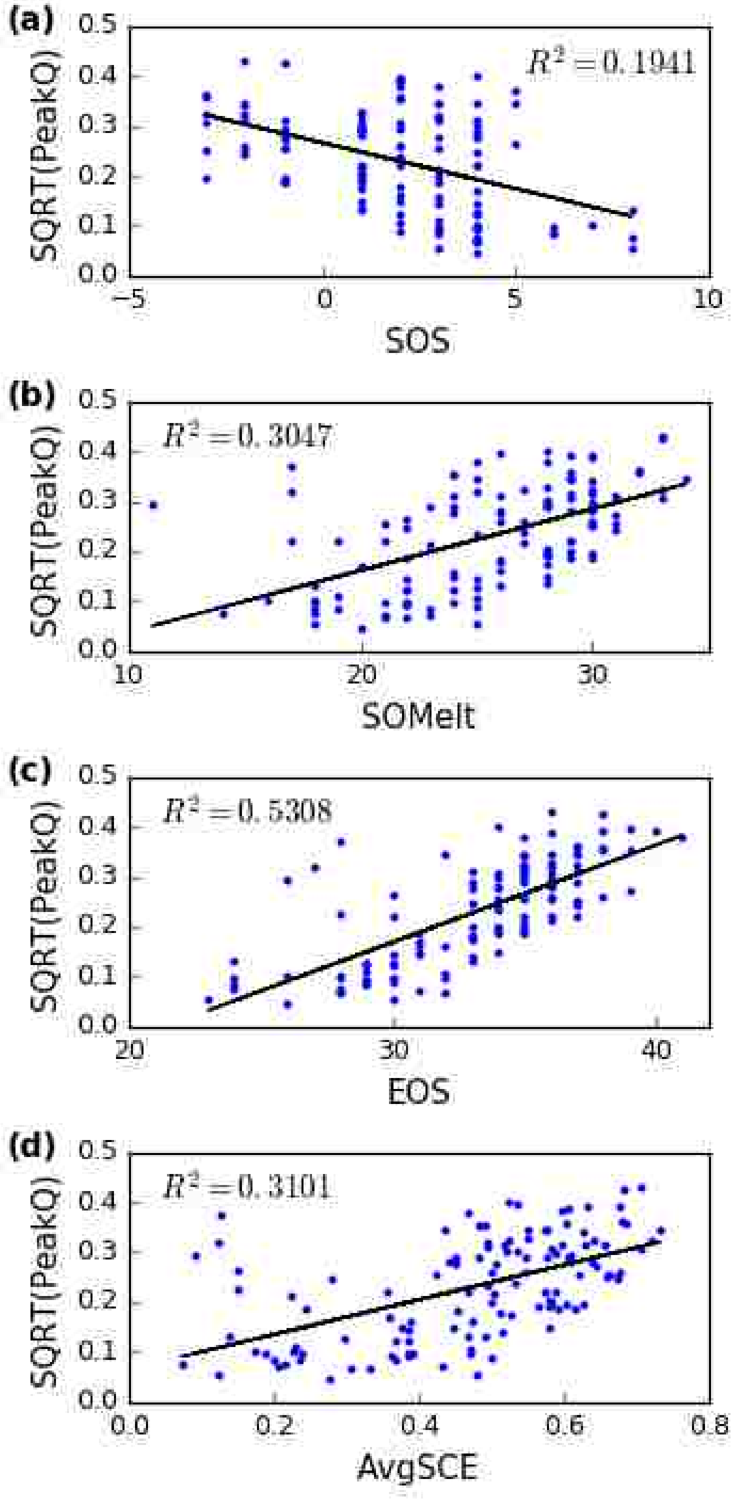

Figure 11: Linear regression of SQRT(PeakQ) against (a) SOS, (b) SOMelt, (c) EOS, and (d) AvgSCE for watersheds containing one or more SNOTEL stations. Metrics for watersheds with multiple stations were averaged.

Although AvgSCE and SQRT(PeakQ) have a significant linear relationship, there are several outliers of concern (see Figure 11d). Of particular concern are the outliers in the upper-left quadrant that come from the coastal region of California that experiences low SCEs and high PeakQs. This indicates that factors such as non-frozen winter precipitation may be confounding the relationship.

To explore this phenomenon, a multiple linear regression was performed using AvgSCE and average annual precipitation (mm) (AvgAnnualPPT) to predict SQRT(PeakQ). AvgAnnualPPT does not display a normal distribution, but the residuals of the linear regression model are normally distributed with a skewness of 0.325, so the model is considered to be successful. Including precipitation in our model brings the R^2 up from 0.3101 with AvgSCE alone in Figure 11d to 0.7048 in Figure 12 (right). Both variables have $p < 0.005$, indicating that the regression coefficients are statistically greater than zero. Although this model provides a much better fit, it still has trouble capturing low-SCE, high-flow points on the left-hand side and moderate-SCE, low-flow points on in the lower middle region. However, the results are promising for both the SCE-metrics alone and a multiple linear regression model that incorporates precipitation.

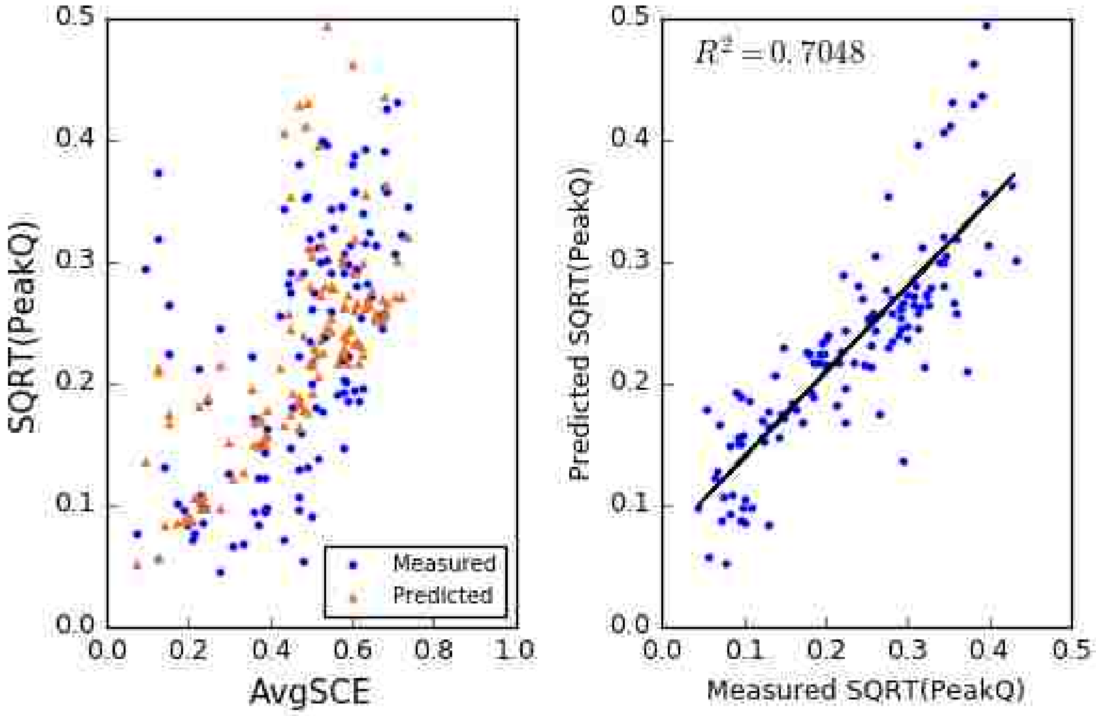

Figure 12: Multiple linear regression of SQRT(PeakQ) using AvgSCE and precipitation. Overlaid measured vs. predicted SQRT(PeakQ) against AvgSCE are on the left. The linear regressions of measured vs. predicted SQRT(PeakQ) are on the right.

3.2 Intra-watershed patterns

The ability of snow cover extent to capture snowpack-streamflow dynamics within a watershed was explored using the 8-day average water year values (Section 2.4) for SCE, SWE, and streamflow for all 121 study watersheds. The relationship between SCE and SWE within all watersheds is examined to find intra-watershed patterns that shed light on the complex dynamics between the two variables. The same analysis is then performed on a single watershed to better demonstrate the pattern (Section 3.2.1). The relationship between SCE and streamflow within all watersheds is then examined to find intra-watershed patterns that illustrate the snowpack-streamflow dynamics of the study watersheds. Again, the same analysis is also performed on a single watershed to better demonstrate the pattern (Section 3.2.2). Assessment of SCE's ability to express climatological variance within an individual watershed was not within the scope of this study, but analysis of SCE and climate indicators by elevation band provides an opportunity for future research.

3.2.1 Snow water equivalent

Plotting 8-day SCE against 8-day SWE for all watersheds containing SNOTEL stations (see Figure 13) results in a display of the hysteretic behavior shown in Magand et al (2013) who found the same pattern between SCE and snow depth. SCE increases rapidly with respect to SWE during accumulation (blue) and decreases more slowly and with greater variability during ablation (orange). Figure 13 also demonstrates the saturation of SCE near 1.0 at the right side of the figure with high SCE values associated with a wide range of SWE values. High altitude SNOTEL stations and permanent snowpacks cause several points in the off-season to have high SWE values, but overall, off-season values hover near the origin.

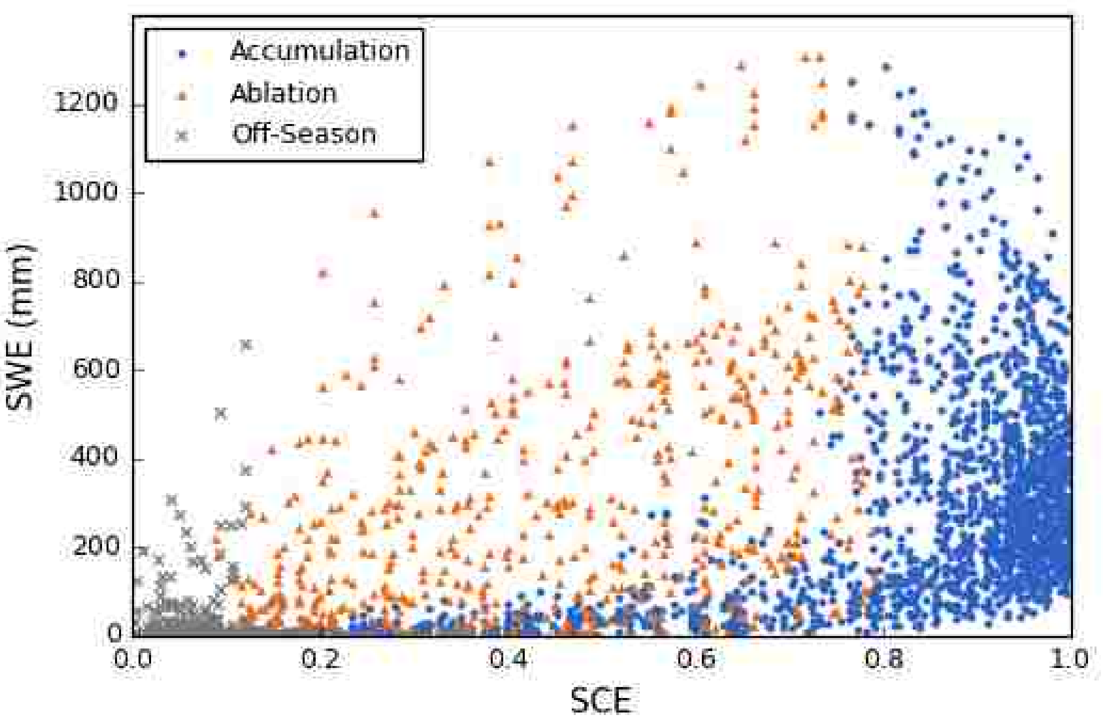

Figure 13: 8-day SCE vs SWE from the average water year for every study watershed containing one or more SNOTEL stations. Metrics for watersheds with multiple stations were averaged.

Another way to explore the relationship between SCE and SWE is by analyzing how they change with respect to each other. Graphs of the changes in SCE versus the changes in SWE for each portion of the snow season, as shown in Figure 14, illuminate how the relationship between these two variables differs between accumulation and ablation as well as on *how* accumulation and ablation are defined. This type of figure, regardless of the variables used, will henceforth be known as a *delta graph*. Figure 14 shows the distribution of SCE and SWE during accumulation, ablation, and the off-season for the average water year for all 121 study watersheds.

Figure 14a validates the definition of SOS and SOMelt and their ability to delineate the accumulation season using only SCE. Accumulation can be loosely defined from this delta graph as any point at which SWE is increasing or stable. Points with a SWE below 0.0 indicate difficulties in snow season characterization using SCE. However, this behavior is expected to some extent given the nature of the threshold method used to define SOMelt. Furthermore, we expect to see increases in SWE met with both negative and positive changes in SCE due to the saturation of the SCE curve and transient melt at lower elevation while snow is still accumulating at higher elevations. Figure 14a shows that 90.9% of accumulation points fall in the upper quadrants, as expected, and only 9.1% of points have a negative SWE, indicating good delineation of the accumulation season. Of the points in the upper quadrants, 62.9% have non-negative SCE values and 27.1% have negative SCE values. Thus, despite the variability in the accumulation season, a majority of points still show an agreement between SCE and SWE in terms of sign.

Similarly, Figure 14b validates the definition of SOMelt and EOS and their ability to delineate the ablation season using only SCE. Ablation can be defined from Figure 14b as any point at which SWE is decreasing or stable. As with accumulation, SWE values that do not fit this criterion indicate difficulties in snow season characterization using SCE. The delta graph shows that 88.7% of ablation points fall in the lower-left quadrant, as expected, and only 11.3% of points have a positive SWE. Just 2% of points have a positive change in SCE, indicating that the SCE-based metrics can properly delineate the ablation season.

The off-season delta graph in Figure 14c is of less interest but has been provided to show that there are no unexpected behaviors. A lack of major increases in SWE indicate that the transition between the off-season and the accumulation season is well-defined. Points in the lower-left quadrant are capturing the remainder of snowmelt after the EOS threshold has been met, including points on the negative x-axis that represent continued snowmelt after snow at the SNOTEL station has completely melted. Points on the positive x-axis with increases in SCE without increases in SWE are likely snow events at high elevations early in the season before the SOS threshold has been met.

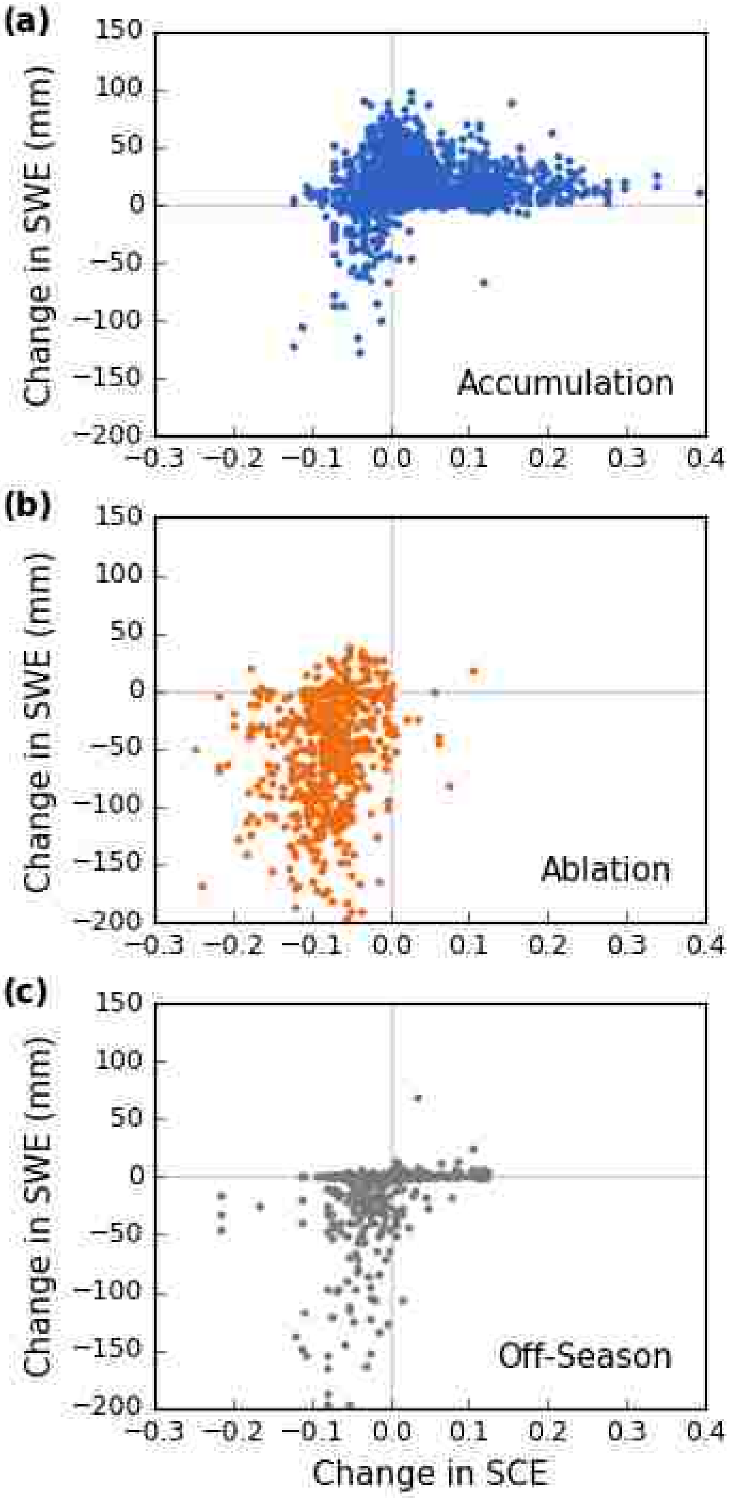

Figure 14: Delta graphs of 8-day SCE vs 8-day SWE from the average water year for every study watershed containing at least one SNOTEL station for the (a) accumulation season, (b) ablation season, and (c) off-season. Metrics for watersheds with multiple stations were averaged.

Case Study

Plotting 8-day SCE vs 8-day SWE for the Yellowstone River Watershed (GAGESII ID 06191500) gives us snow distribution curves for the lowest and highest elevation SNOTEL stations in the basin with elevations of 7350ft and 9400ft, respectively (see Figure 15). This was done for all 16 water years as well as for the average water year. There are five SNOTEL stations in this watershed, but only two are presented here as they demonstrate the range of variability in the watershed's SCE-SWE relationship.

Both SNOTEL stations in the Yellowstone River Watershed display the distinct hysteretic behavior found by Magand et al (2013) and illustrated by 8-day SCE and SWE in the study watersheds in Figure 13. Importantly, the shape of this behavior is preserved when the data is aggregated to the average water year (see Figure 16 (right)), demonstrating the applicability of this portion of the methodology (Section 2.4). As the elevation increases from one station to another, the ablation leg appears to swell at a much higher rate than the accumulation leg, creating a more open triangle at the higher elevation and indicating that ablation behavior changes much more rapidly with elevation than does accumulation behavior.

Although there are many important variables for snowpack dynamics missing in this analysis, including aspect, shading, and slope, SCE metrics can still capture the key temporal inflection points in the snow season, namely the start of accumulation, the start of ablation, and the end of the snow season. Discrepancies in how well SCE metrics define the different seasons can be seen in how well SOS captures when the blue dots start to rise off the x-axis (gray to blue), how well SOMelt captures the peak of the loop (blue to orange), and how well EOS captures the moment where points converge back near zero (orange to gray). These metrics appear to do a better job of capturing the snow season inflection points at the higher elevation station in this watershed, although they are still sufficiently captured in the lower elevation station. Points change from blue to orange right at the peak of the triangle meaning that the start of snow melt, as defined by SCE, matches that indicated by the first major decrease in SWE. Points then change from orange to grey near the convergence back to zero meaning that EOS successfully captures the true end of the snow season at this station. These metrics are based on the SCE across the entire watershed, so lower elevation stations may melt out more quickly than the metrics indicate. Once again, the importance of SNOTEL placement and elevation is highlighted.

The delta graph for all 16 years in Yellowstone River Watershed in Figure 16 (left) maintain the overall patterns found in Figure 14, and these patterns remain coherent in the average water year in Figure 16 (right), again demonstrating its usefulness as a simplifying concept. Accumulation points present mainly in the upper quadrants and the lower-left quadrant. It is captured more accurately in the higher elevation station where only two points fall just barely outside of the upper quadrants as opposed to the lower elevation where significant melt happens during the tail end of the identified accumulation season. Ablation presents mainly in the lower-left quadrant. In the lower elevation watershed, ablation points near the negative x-axis indicate a loss of SCE at higher elevations after all snow at this station has melted. In the average water year, all ablation points for the higher elevation station fall in the lower-left quadrant, as expected. Off-season patterns for this watershed are more well-defined than in Figure 14. The majority of off-season points fall tightly around the y-axis, indicating no more snowmelt after the end of the ablation season. This may indicate how well these SNOTEL stations represent the overall behavior of the watershed.

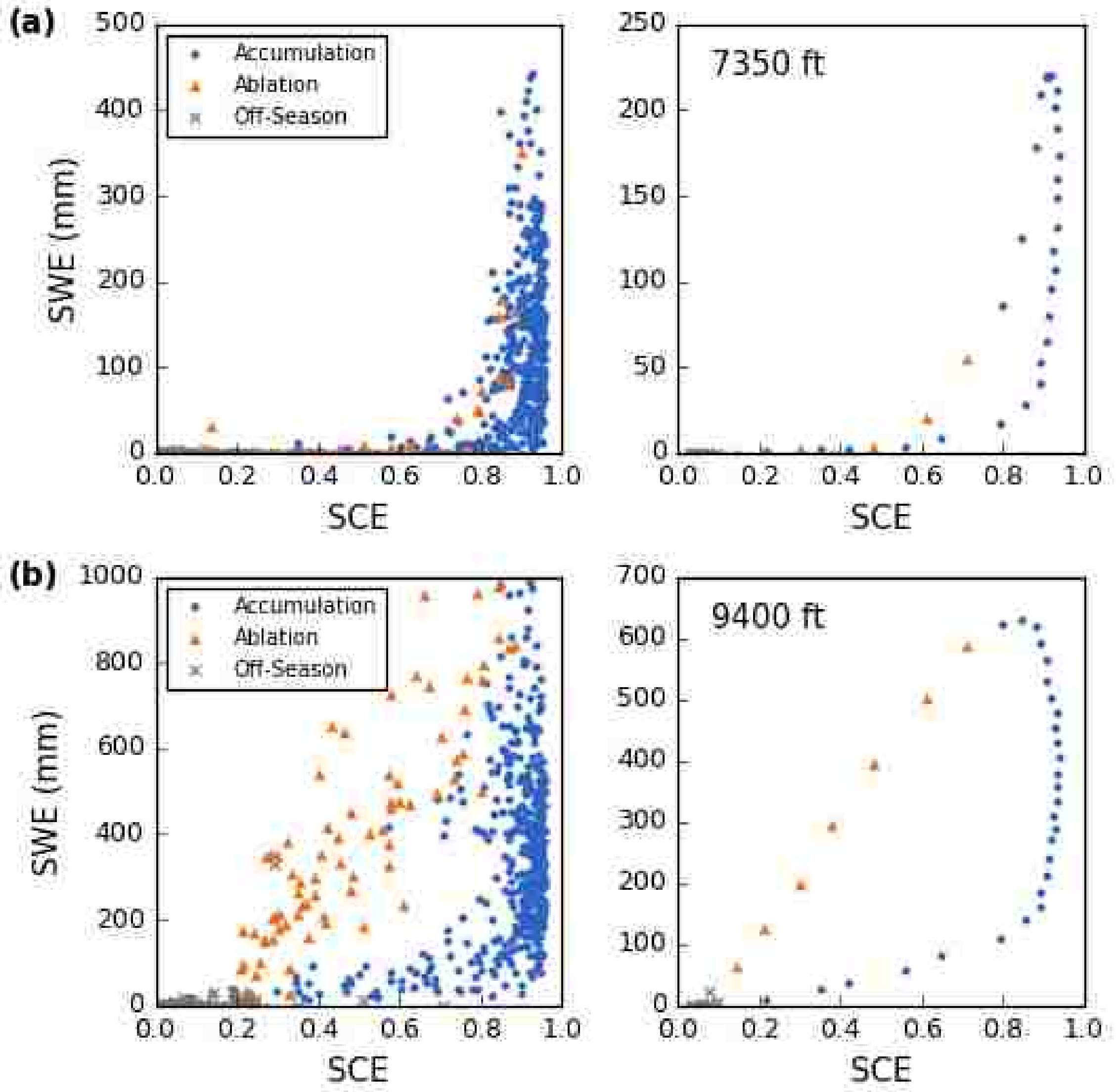

Figure 15: MODIS SCE versus SNOTEL SWE for the Yellowstone River Watershed for each 8-day period (left) and average 8-day period (right) using SNOTEL station (a) 670 and (b) 683.

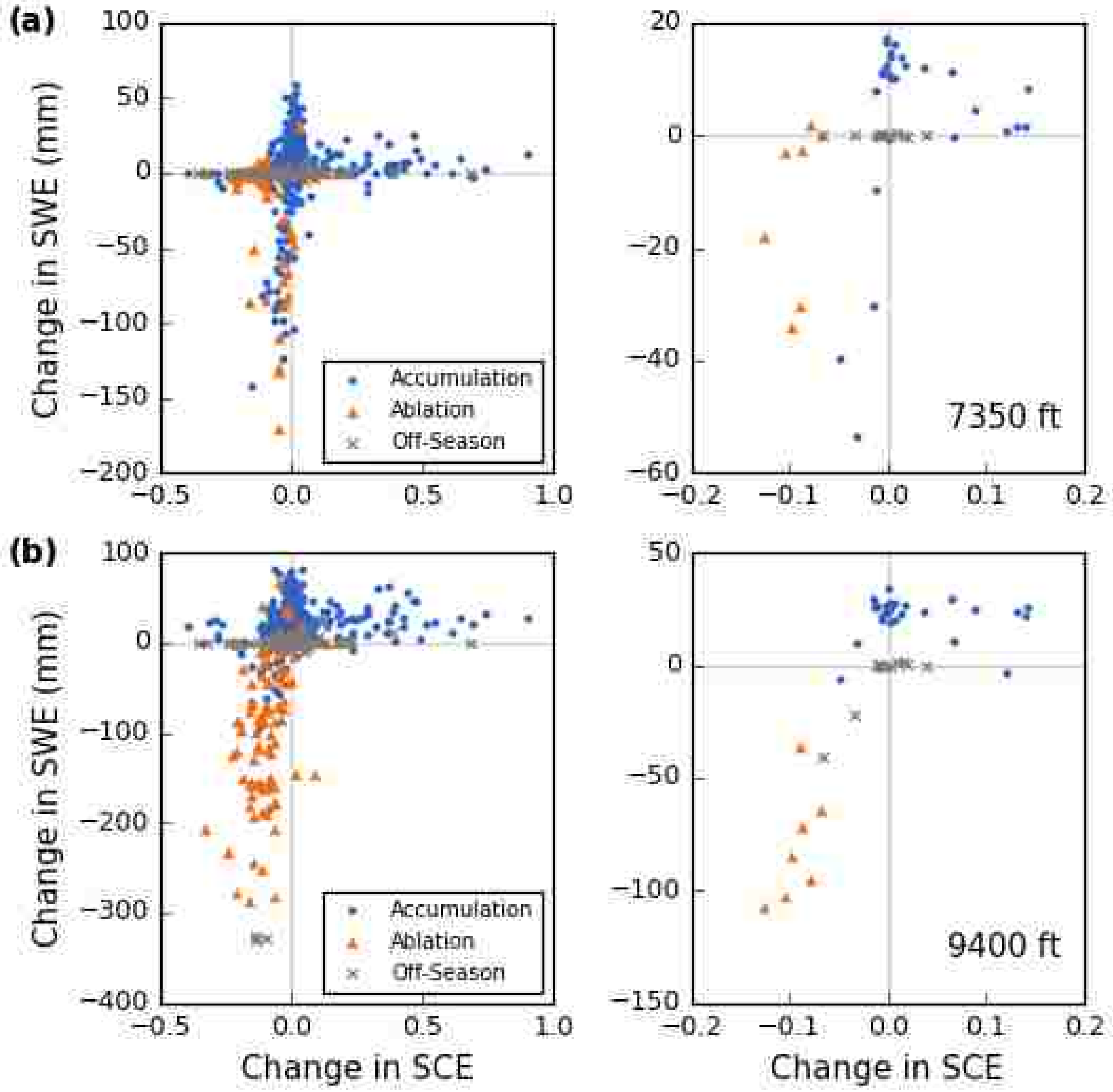

Figure 16: Delta graphs of 8-day SCE versus 8-day SWE for all 16 water years (left) and the average water year (right) in Yellowstone River Watershed for SNOTEL stations (a) 670 and (b) 683.

3.2.2 Streamflow

Plotting 8-day SCE against 8-day streamflow for all watersheds demonstrates yet another example of hysteretic behavior between SCE and a hydrological indicator (see Figure 17). As with SWE, the differences are still associated with whether the watershed is experiencing accumulation or ablation, but the relationship is notably different. Although the wide range of streamflows and peak SCE values across the 121 watersheds obscures some of the pattern, even after streamflow normalization, we can still characterize much of the accumulation season as low flow with higher flows happening on the right-hand side as snow begins to melt at lower elevations. As the snow melts during the ablation season, we begin to see streamflows spike and hit their maximums before attenuating. The off-season points hover around the lower-left corner, although summer rain and early ephemeral snow cause significant spikes in some watersheds. The shape of this response is henceforth referred to as a hysteresis loop in this study as it exhibits behaviors similar to hysteresis loops in other disciplines, such as that of soil water retention curves during wetting and drying cycles (Sławiński, 2011). The shape and size of the loop changes from watershed to watershed and shows great potential for watershed analysis using remotely-sensed snow cover.

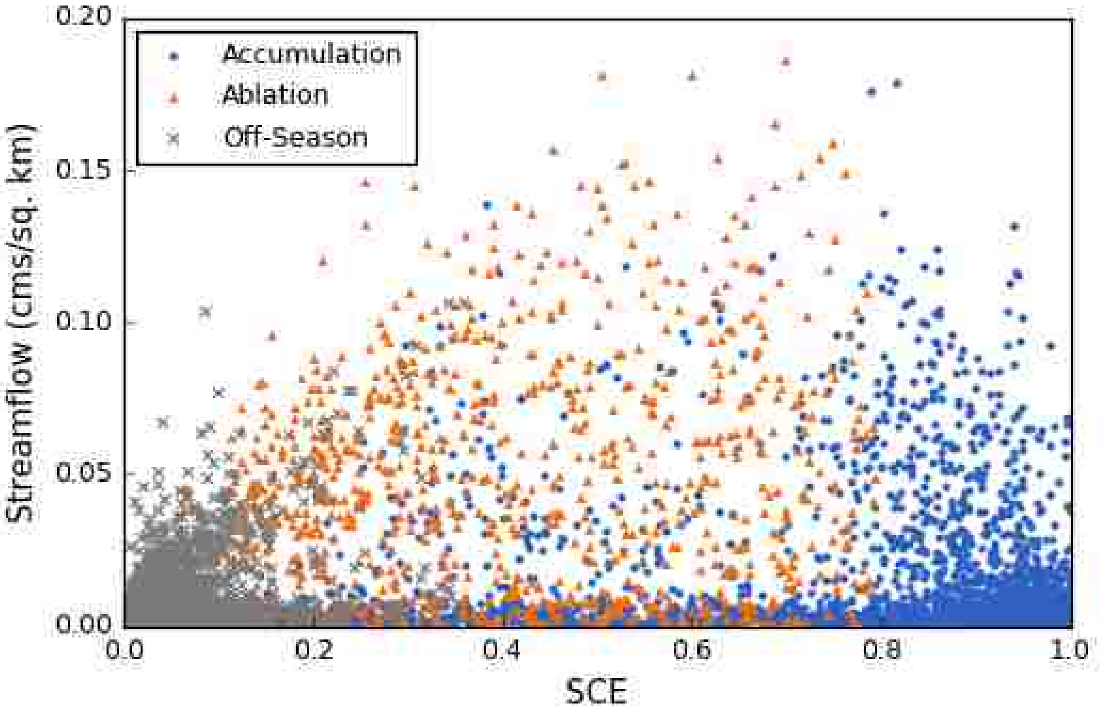

Figure 17: SCE vs normalized streamflow for every 8-day period in the average water year for each study watershed. The snow season for each watershed was characterized to determine the timings of the accumulation, ablation, and off seasons.

As with SWE, the delta graphs of SCE and streamflow are generated to gain further insight into the temporal and physical relationships between the two variables. Figure 18 demonstrates the behavioral differences between the accumulation and ablation seasons. During accumulation, we expect to see increases in SCE corresponding to either no change or a decrease in streamflow as the spring snowmelt pulse and summer rains work their way through the watershed. However, the relationship is ill-defined with 53.5% of points having a positive change in streamflow. 27.8% of all points lie in the upper-right quadrant with positive changes in SCE and streamflow, indicating mid-season melt events or winter storms that dump rain at lower elevations. However, only

4.06% of all points gave a change in streamflow greater than one positive standard deviation of 0.00642, implying that many streamflow fluctuations may be minor. 25.7% of all points fall in the upper-left quadrant and represent issues with the threshold method of pinpointing SOMelt that misattributes the beginning of the ablation season. Only 1.19% of points have a negative change in SCE that corresponds to a negative change in streamflow greater in magnitude than one standard deviation. These points in the lower-left quadrant may capture mid-season melt events where sublimation, rather than melt into a nearby stream, is the primary driver of snowpack loss.

The ablation season shows a much stronger pattern between SCE and streamflow. Almost all points (94.8%) fall in the left quadrants, as we would expect since snow should be melting during this portion of the snow season. Decreases in SCE are met by both increases (54.3%) and decreases (40.4%) in streamflow, demonstrating the rise and attenuation of the spring snowmelt pulse. Streamflow increases until peak streamflow is attained and then decreases even though snowmelt is likely still contributing to the overall streamflow. The off-season captures the remaining spring pulse attenuation that occurs after the snow has melted, with 78.7% of points demonstrating a decrease in streamflow.

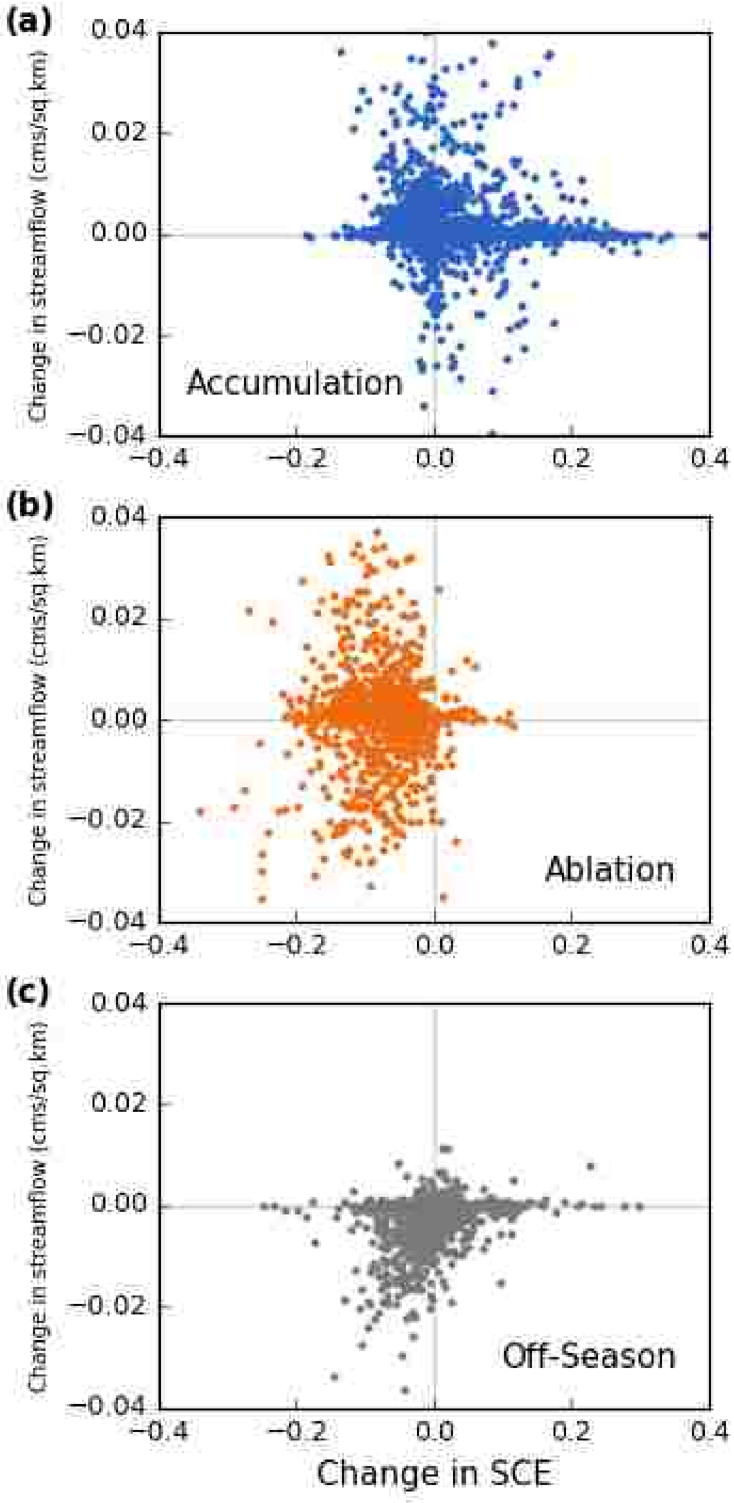

Figure 18: Delta graphs of 8-day SCE vs 8-day streamflow from the average water year for every study watershed for the (a) accumulation season, (b) ablation season, and (c) off-season.

Case Study

Plotting 8-day SCE vs 8-day streamflow for the average water year for the Yellowstone River Watershed (GAGESII ID 06191500) gives better insight into how the relationship looks for a single, snow-dependent watershed (see Figure 19). For a single watershed, the shape of the SCE-streamflow response is more defined and provides a clear view of how the relationship changes throughout the seasons. During accumulation, the points are associated with a base streamflow for the watershed. Only during the end of the accumulation season does the streamflow increase due to the challenges of setting thresholds to characterize the season. During ablation, the streamflow steadily increases before reaching its peak and then attenuating. The off season is associated with decreases in streamflow from further attenuation of the spring pulse that then settles back near the base flow.

The delta graph for this watershed in Figure 20 displays a much clearer relationship than for all watersheds in Figure 18, and that relationship is maintained in the average water year. Accumulation points lie almost entirely on the x-axis indicating no change in streamflow as the snowpack grows. This indicates that this watershed experiences little to no mid-season melt events on average, perhaps due to its low temperatures and inland location away from warm, ocean-powered storms. Ablation points lie in both quadrants on the left showing the rising and falling limbs of the spring pulse as SCE decreases and snow melts. The off-season captures the remaining streamflow attenuation before falling back to the base flow (i.e. no change in streamflow).

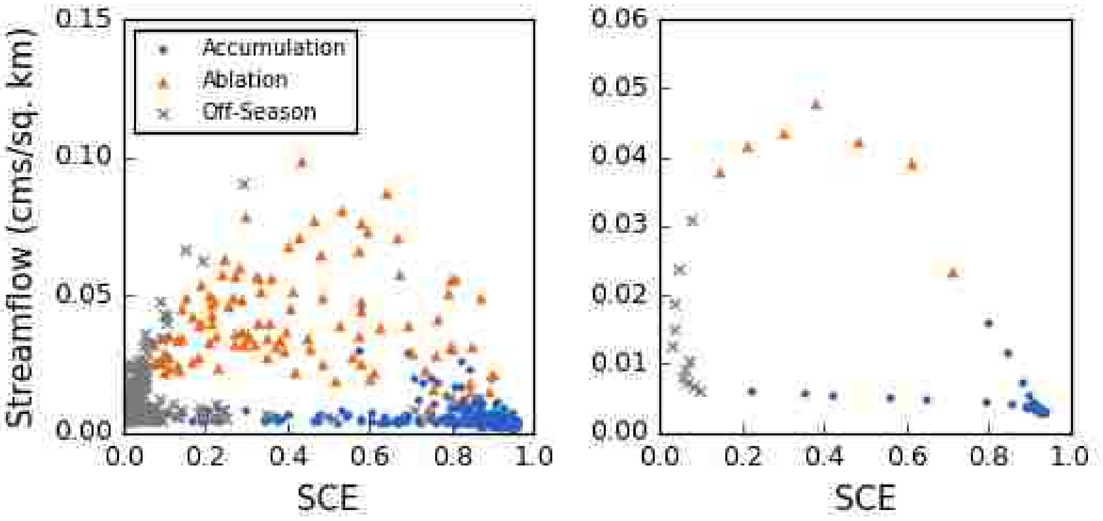

Figure 19: SCE versus streamflow for the Yellowstone River Watershed for each 8-day period (left) and average 8-day period (right).

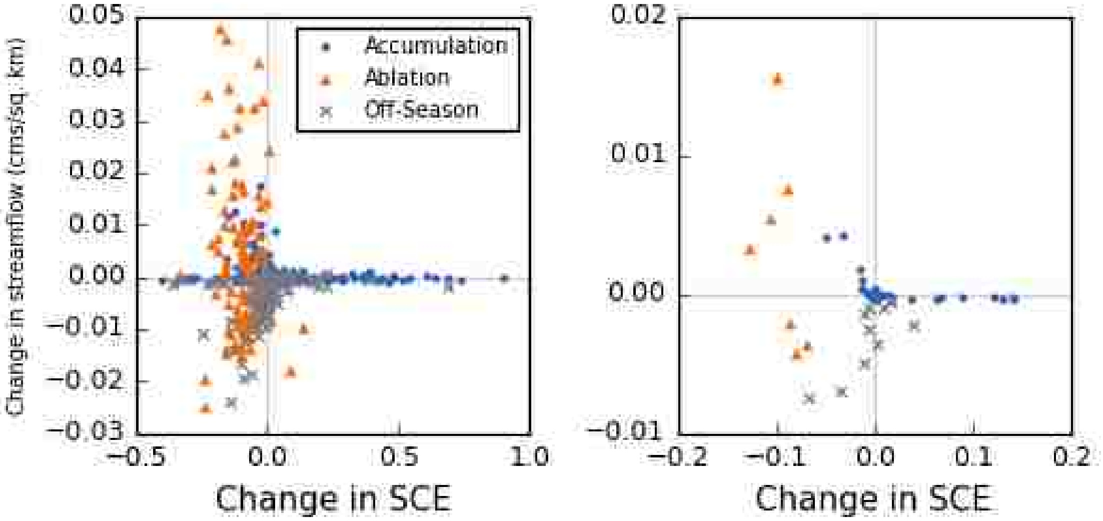

Figure 20: Delta graphs for 8-day SCE vs. 8-day streamflow for all 16 water years (left) and the average water year (right) of the Yellowstone River Watershed.

3.3 Snowpack-streamflow dynamics in hydrologically distinct watersheds

The following case study of three hydrologically distinct watersheds in the U.S. Mountain West demonstrates how SCE and SCE-based metrics can be used to assess the snowpack-streamflow dynamics both between and within watersheds. Section 3.3.1 provides a brief description of each watershed. Section 3.3.2 outlines the initial analysis involving characterization and comparison of watersheds through examination of their climate profiles, the relationships between SCE and streamflow and the relationship, and the variability of SCE and streamflow during the study period. This analysis is then done using only the hysteresis loops and delta graphs for each watershed to demonstrate the power of this study's methodology in assessing snowpack-streamflow dynamics, as shown in Section 3.3.3.

3.3.1 Watershed descriptions

The Yellowstone River Watershed (GAGESII ID 06191500) is in northwestern Wyoming in the upper Rockies. It drains to the north with its outlet in southwestern Montana. It is the largest of the three watersheds, and one of the larger ones in this study, with a drainage area of 6783 km^2. It is a high elevation watershed with elevations ranging from 1615 to 3609 m. According to the snow regimes classified by Trujillo and Molotch (2014), Yellowstone is a Continental watershed, meaning that its winter precipitation is dominated by storm fronts with below-freezing temperatures, and that it experiences a longer accumulation season with lower intensity precipitation and a later ablation (Serreze et al, 1999).

The Gila River Watershed (GAGESII ID 09430500) is in southwestern New Mexico in the arid Gila Wilderness Area near the borders of Arizona and Mexico and drains toward the southwest. It spans an especially large range of elevations, from 462 to 3213 m, and has a drainage area of 4805 km^2. The Gila is classified as an intermountain watershed by Trujillo and Molotch (2014). Intermountain watersheds exhibit temperature and precipitation trends in between those of wet, warm Pacific Coast watersheds and cold, dry Continental watersheds. According to Serreze et al (1999), Arizona/New Mexico watersheds experience a lower ratio of SWE to precipitation with a significant amount of precipitation falling outside of the snow season. The snow accumulation in any given year is highly dependent on temperature.

The Upper Van Duzen River Watershed (GAGESII ID 11478500) is in northern California in the North Coast Range with its streamflow gage located roughly 40 km from the Pacific Ocean on the northwestern corner of the basin. It is a small, low elevation, transitional watershed with elevations ranging from 218 to 1695 m and a drainage area of only 572 km^2. The Upper Van Duzen exhibits strong Maritime patterns according to Trujillo and Molotch (2014). Snow accumulation is dominated by short, high precipitation winter storms caused by Atmospheric Rivers interacting with coastal mountains, allowing deep snowpacks to form over shorter accumulation seasons (Guan et al, 2010). Due to higher temperatures and spring rainfall, ablation happens earlier in Maritime watersheds.

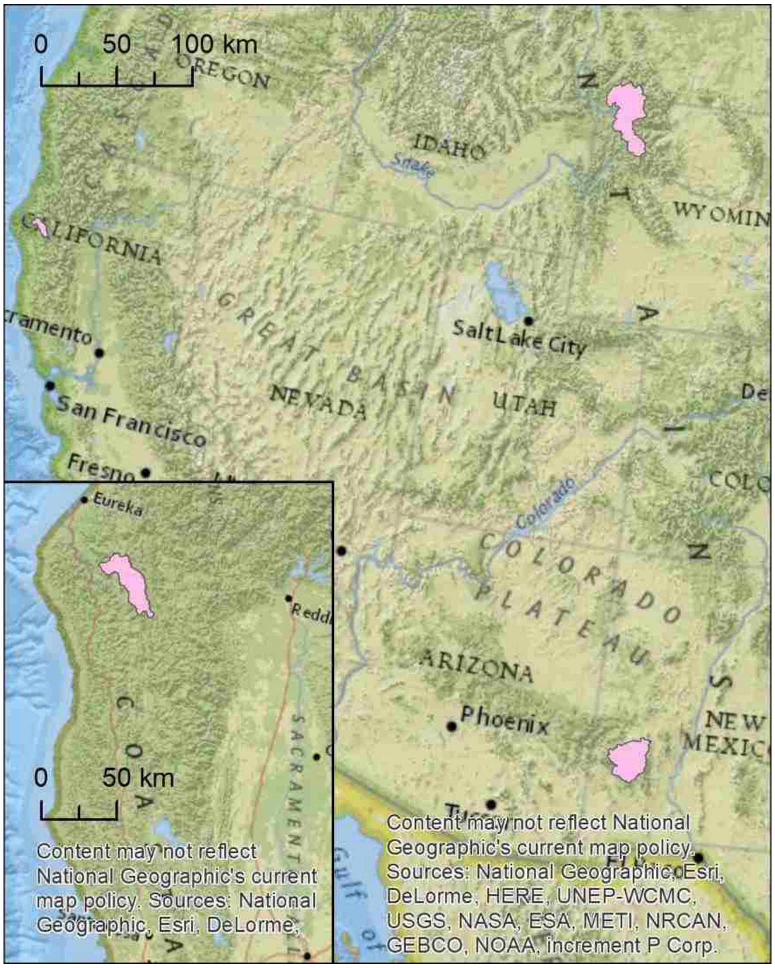
0 50 100 km
OREGON
IDAHO
Snake
WYOMIN
CALIFORNIA
Sacramento
San Francisco
Fresno
GREAT BASIN
NEVADA
UTAH
Salt Lake City
Colorado
COLORADO PLATEAU
ARIZONA
Phoenix
NEW MEXICO
Gulf of
Eureka
Redd
SACRAMENTO
COAST
0 50 km
Content may not reflect National Geographic's current map policy. Sources: National Geographic, Esri, DeLorme,
Content may not reflect National Geographic's current map policy. Sources: National Geographic, Esri, DeLorme, HERE, UNEP-WCMC, USGS, NASA, ESA, METI, NRCAN, GEBCO, NOAA, increment P Corp.

Figure 21: Map of the three watersheds in this case study. Yellowstone River Watershed is in the upper-right corner in northwestern Wyoming. Gila River Watershed is in the lower-right corner in southwest New Mexico. Upper Van Duzen Watershed is in the upper-left corner in northern California with a more detailed view in the inset in the lower-left corner.

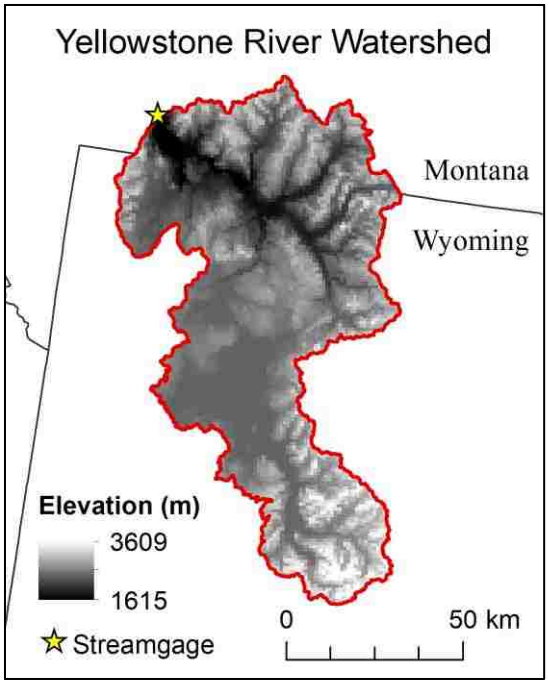
Yellowstone River Watershed
Montana
Wyoming
Elevation (m)
3609
1615
Streamgage
0
50 km

Figure 22: Basin delineation and elevation for the Yellowstone River Watershed (GAGESII ID 06191500). The location of the U.S.G.S. streamgage is indicated by with a star.

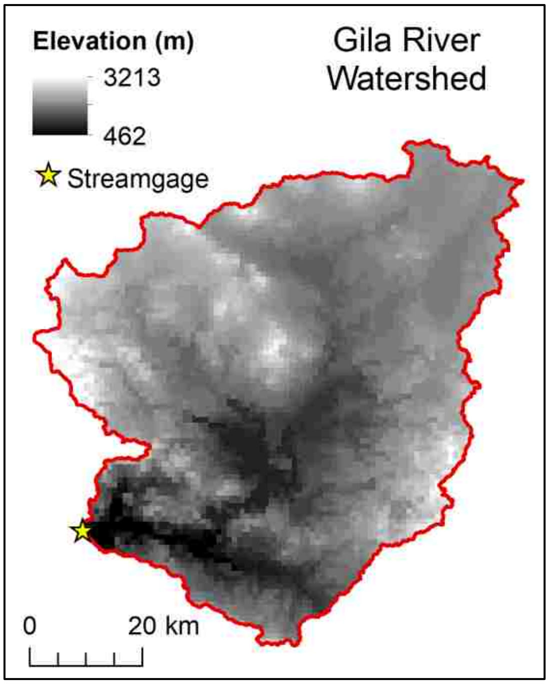
Elevation (m)
3213
462
Streamgage
Gila River Watershed
0
20 km

Figure 23: Basin delineation and elevation for the Gila River Watershed (GAGESII ID 09430500). The location of the U.S.G.S. streamgage is indicated by a star.

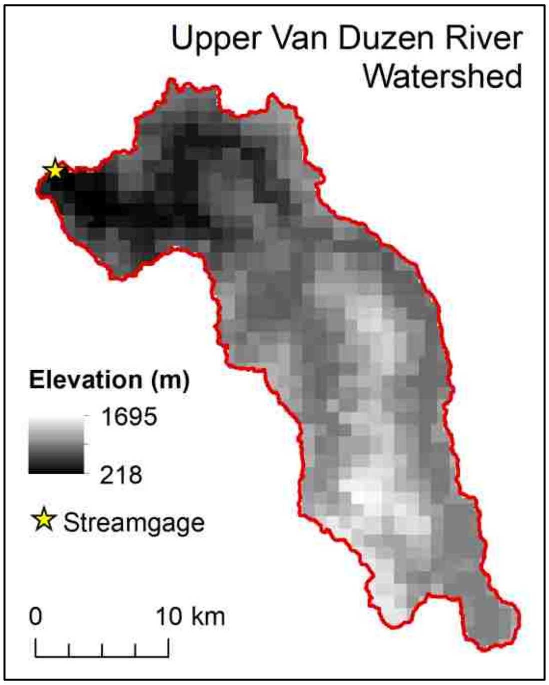
Upper Van Duzen River Watershed
Elevation (m)
1695
218
☆ Streamgage
0
10 km

Figure 24: Basin delineation and elevation for the Upper Van Duzen River Watershed (GAGESII ID 11478500). The location of the U.S.G.S. streamgage is indicated by a star.

3.3.2 Initial analysis of snowpack-streamflow dynamics

These watersheds represent three distinct climate profiles with unique relationships between temperature and precipitation, as shown in Figure 25 and as indicated by the snow regimes in Trujillo and Molotch, 2014. All three temperature curves have a similar S-shape, signifying the general temperature trends of a temperate climate. However, on average, only the Yellowstone River Watershed experiences sub-zero temperatures. In Yellowstone, the temperature falls below 0 °C for roughly half of the year, as is typical of a Continental watershed (Trujillo and Molotch, 2014). The Gila and Upper Van Duzen have a very similar temperature curve, although the Upper Van Duzen experiences higher temperatures for most months, especially during the winter from October to April. In the Gila, the average temperature never falls below 0 °C, although individual years and certain elevations certainly experience sub-zero temperatures periodically throughout the winter. Summer temperatures peak at nearly 20°C in July. The Upper Van Duzen River Watershed has winter temperatures hovering between 5 and 10 °C with a peak just over 20°C in July.

Despite their similar temperature curves, the Gila and the Upper Van Duzen experience very different precipitation patterns, in terms of both magnitude and timing, that ultimately differentiate their vastly different climates and snow regimes. The Gila receives only 458 mm of total precipitation in the average water year as compared to 1705 mm in the Upper Van Duzen, reflecting the significantly wetter climate of the U.S. Pacific Coast. In the Gila, the majority of precipitation (~ 55%) falls between July and September as rain during the Southwest’s monsoon season. Less than 10% of the total precipitation falls in any month between October and April. In contrast, the Upper Van

Duzen experiences the majority of its precipitation (~ 78%) from November to March. However, the average winter temperatures indicate that not all of that precipitation falls as snow, which is expected of a transitional watershed where only the higher elevations receive snowfall. Only a total of 1.56% of precipitation falls from July to September when the Gila is experiencing high precipitation. The Yellowstone River Watershed sees steady precipitation from October to June, receiving an average of 9.34% of precipitation per month over that period. Precipitation decreases by roughly half from July to September during the warmest months with an average of 5.3% of precipitation per month. Total precipitation for the average water year is 747 mm. This moderate and steady precipitation is indicative of Yellowstone’s classification as a Continental watershed where snow accumulates slowly over a longer period.

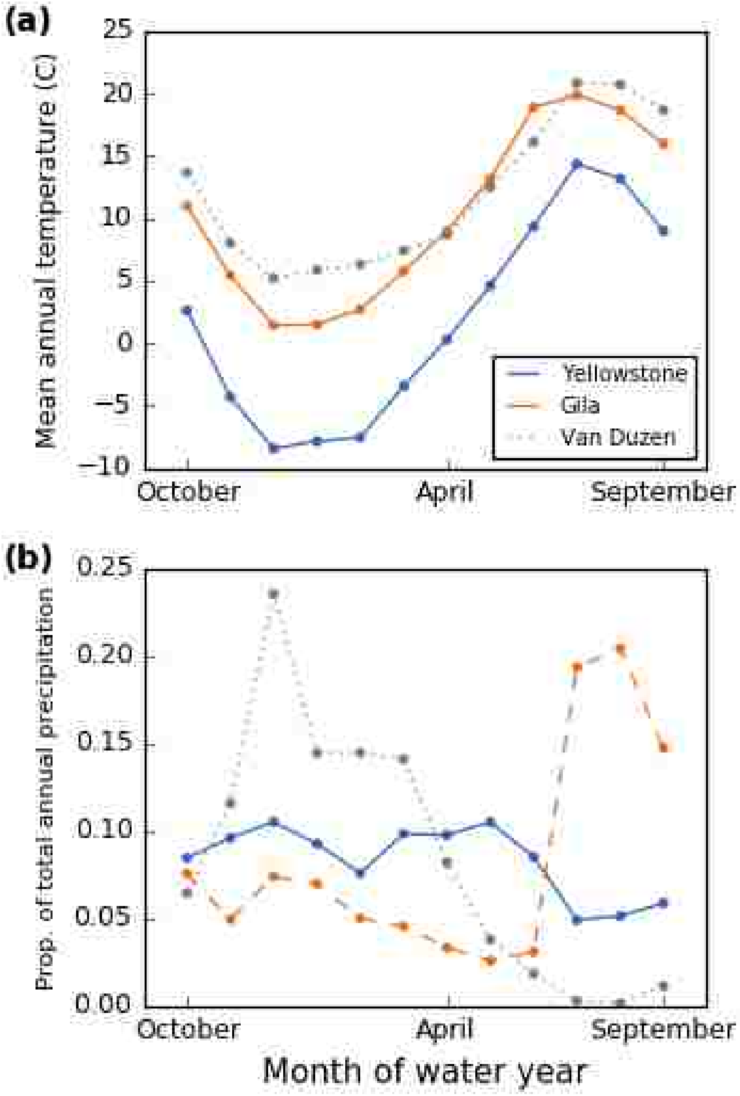

Figure 25: Monthly (a) mean annual temperature (°C) and (b) proportion of total annual precipitation for the average water year for the Yellowstone River, Gila River, and Upper Van Duzen River Watersheds. The total annual precipitations for the average water year for Yellowstone, Gila, and Upper Van Duzen are 747 mm, 458 mm, and 1705 mm, respectively.

As expected from their unique climate profiles, these watersheds also experience distinctly different relationships between SCE and streamflow and differing amounts of inter-annual variability within SCE and streamflow, as illustrated by Figure 26 and Figure 27. Figure 26 and Figure 27 show the distribution of SCE and streamflow, respectively, throughout the water year for water years 2001 to 2016 along with mean SCE and mean streamflow. Looking at the mean SCE and streamflow alone, these three watersheds present three unique snowpack-streamflow relationships. Yellowstone's SCE increases rapidly to a plateau for the remainder of the season before starting to melt in early-May. Its streamflow indicates a typical spring pulse with streamflow increases beginning in late-April, reaching a peak of 0.048 cms/km^2 in early June, and attenuating into the next accumulation season. Meanwhile, the Gila displays a mild, ill-defined spring pulse in February with a peak of 0.0023 cms/km^2. A much bigger peak of 0.0031 cms/km^2 occurs in late September, corresponding to the summer monsoon. SCE during the main snow season appears bimodal with peaks in late-December and early-February with maximums of 0.52 and 0.43, respectively. SCE and streamflow in the Upper Van Duzen appear to move together with coinciding increases and decreases. As in the Gila, SCE is bimodal with peaks in late-December and early- to mid-March with values of 0.39 and 0.30, respectively. Similarly, streamflow is bimodal with a large peak of 0.14 cms/km^2 and a smaller peak of 0.088 cms/km^2. The first streamflow spike occurs in the same 8-day period as the first SCE peak, and the second occurs just one 8-day period after the second SCE peak, making a strong case for an elevation-dependent precipitation that falls as rain at lower elevations and snow at higher ones. Streamflow remains near zero from June to October, indicating little to no summer precipitation in this region.

The 16-year distributions of SCE in Figure 26 and streamflow in Figure 27 provide additional insight into hydrological variability in each of the watersheds. Yellowstone displays consistent SCE and streamflow values throughout the year. The highest SCE variability occurs during the end of the off-season and the beginning of the accumulation season due to early storms that cause the start of the snow season to fluctuate. Streamflow varies most during the ablation and off-season portions of the spring pulse, indicating differences in snowpack SWE between years. The Gila and Upper Van Duzen present similar SCE profiles with high variability during the accumulation and ablation seasons and low variability during the off-season with some noticeable, large rainfall events in the Gila. However, their streamflow distributions demonstrate very different hydrological dynamics. Upper Van Duzen experiences significant winter streamflow events throughout the accumulation and ablation seasons The Gila experiences occasional increases in streamflow throughout the water year with a notably consistent dry spell from late-May to mid-July before increased variability during the summer monsoon.

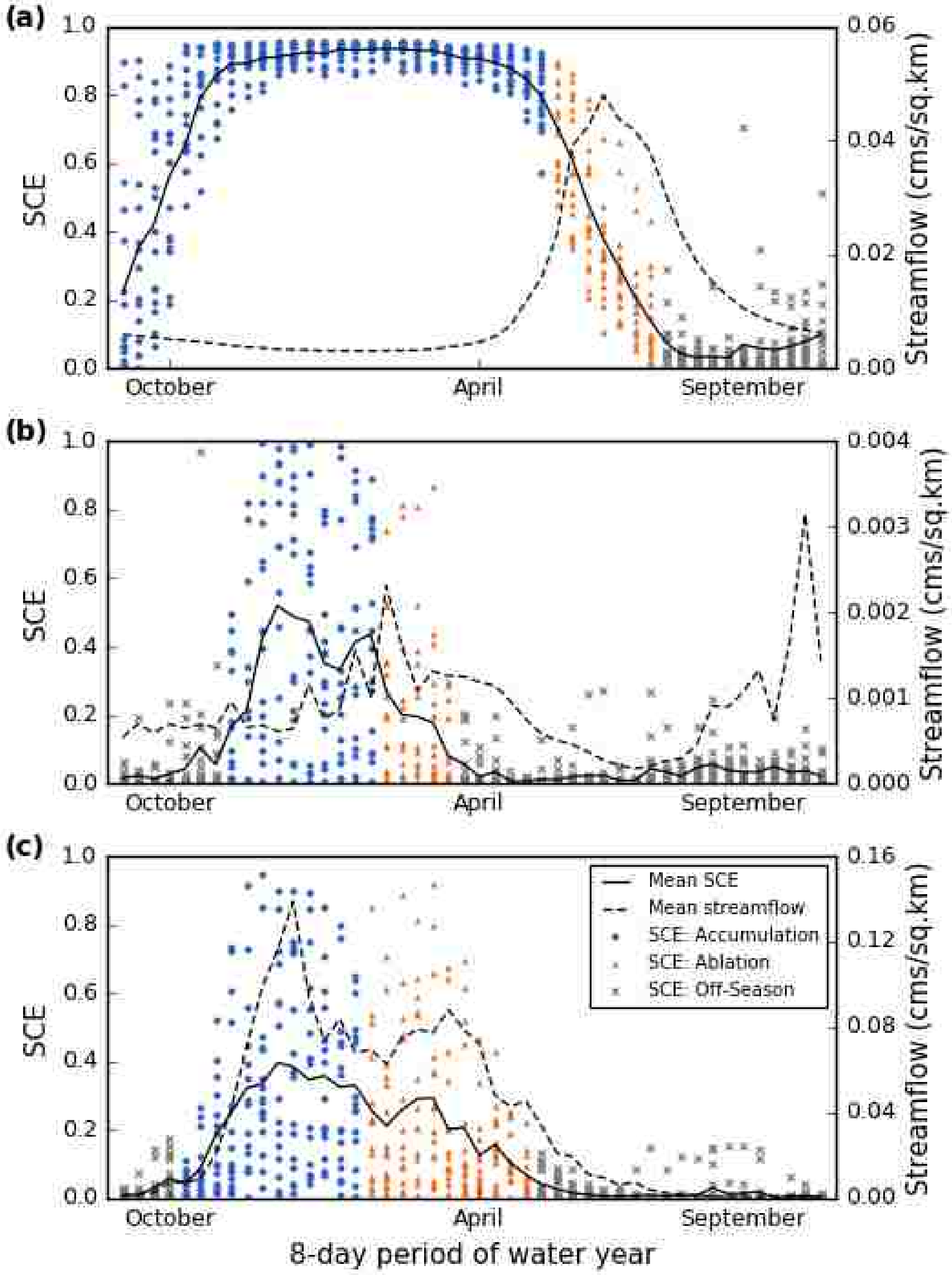

Figure 26: Distribution of SCE for the 8-day periods of all 16 water years divided by season along with the SCE and streamflow for the average water year for (a) Yellowstone River Watershed, (b) Gila River Watershed, and (c) Upper Van Duzen Watershed.

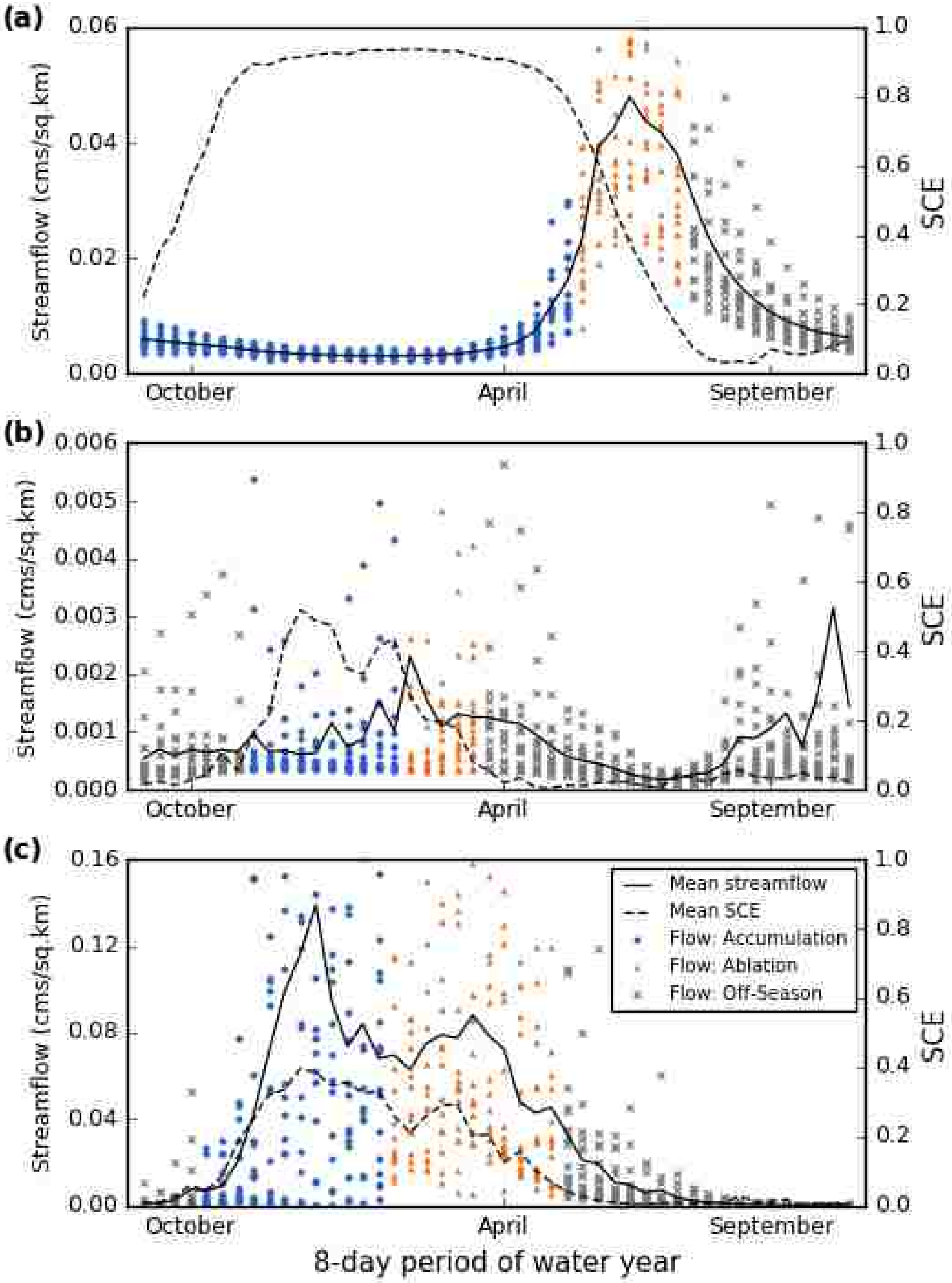

Figure 27: Streamflow for every 8-day period from 2000 to 2016 mapped against the period of the water year for the (a) Yellowstone River Watershed, (b) Gila River Watershed, and (c) Upper Van Duzen Watershed.

3.3.3 Compact analysis using hysteresis loops and delta graphs

The hysteresis loop for Yellowstone, as explored in Section 3.2.2, is well-defined with an open structure that transitions smoothly between accumulation, ablation, and the off-season. Streamflow remains near base flow during accumulation and then begins to contribute significantly to the streamflow during ablation before attenuating back down to the base flow in the off-season. In contrast, the loops for the Gila and Upper Van Duzen are chaotic and do not form actual loop structures, although points still follow a general pattern of accumulation points on the bottom and right, ablation points on the top, and off-season points on the left. In the Gila, accumulation points mostly remain below ablation points, indicating the presence of a mild spring pulse as snow melts. Off-season points remain near zero SCE, but they cover a wide range of streamflows, including the peak streamflow, illustrating the impacts of the summer monsoon. The Upper Van Duzen River Watershed, displays yet another distinct pattern of snowpack-streamflow dynamics. Accumulation points quickly rise off the x-axis, indicating storms that contribute small increases in SCE at higher elevations and large amounts of rain at lower elevations that cause streamflow to increase instantaneously. In opposition to the ablation seasons in Yellowstone and the Gila, ablation points in the Upper Van Duzen do not contain a peak or represent any kind of spring pulse. Off-season points remain near the origin, indicating a dry summer with little to no remaining streamflow attenuation.

The delta graph for Yellowstone, as also explored in Section 3.2.2, shows clear functional differences between accumulation, ablation, and the off-season. It closely follows the trends found for all watersheds in Figure 18, although the accumulation season is better defined due to a lack of winter rain, shown by the proximity of the accumulation points to the x-axis. Ablation points lie in both quadrants on the left, as in Figure 18, showing the rising and falling limbs of the spring pulse as SCE disappears. The off-season captures the remaining streamflow attenuation in the lower-left quadrant before falling back to base flow, as indicated by points near the origin that indicate limited summer rain. The Gila and Upper Van Duzen show how watersheds that do not depend as heavily on winter snow present in a delta graph. The accumulation points for both are scattered across all four quadrants with changes in streamflow happening through the season, rather than just near the end. Ablation points for the Gila fall mostly in the lower-left quadrant, as expected, indicating a slight spring pulse. Ablation points for the Upper Van Duzen, however, are once again scattered throughout all four quadrants demonstrating a lack of a spring pulse and therefore a weak snowpack-streamflow connection. Off-season points in the Gila fall along the y-axis with several large increases and decreases capturing the significant rainfall from the summer monsoon. Off-season points in the Upper Van Duzen fall close to the origin reflecting its dry summer.

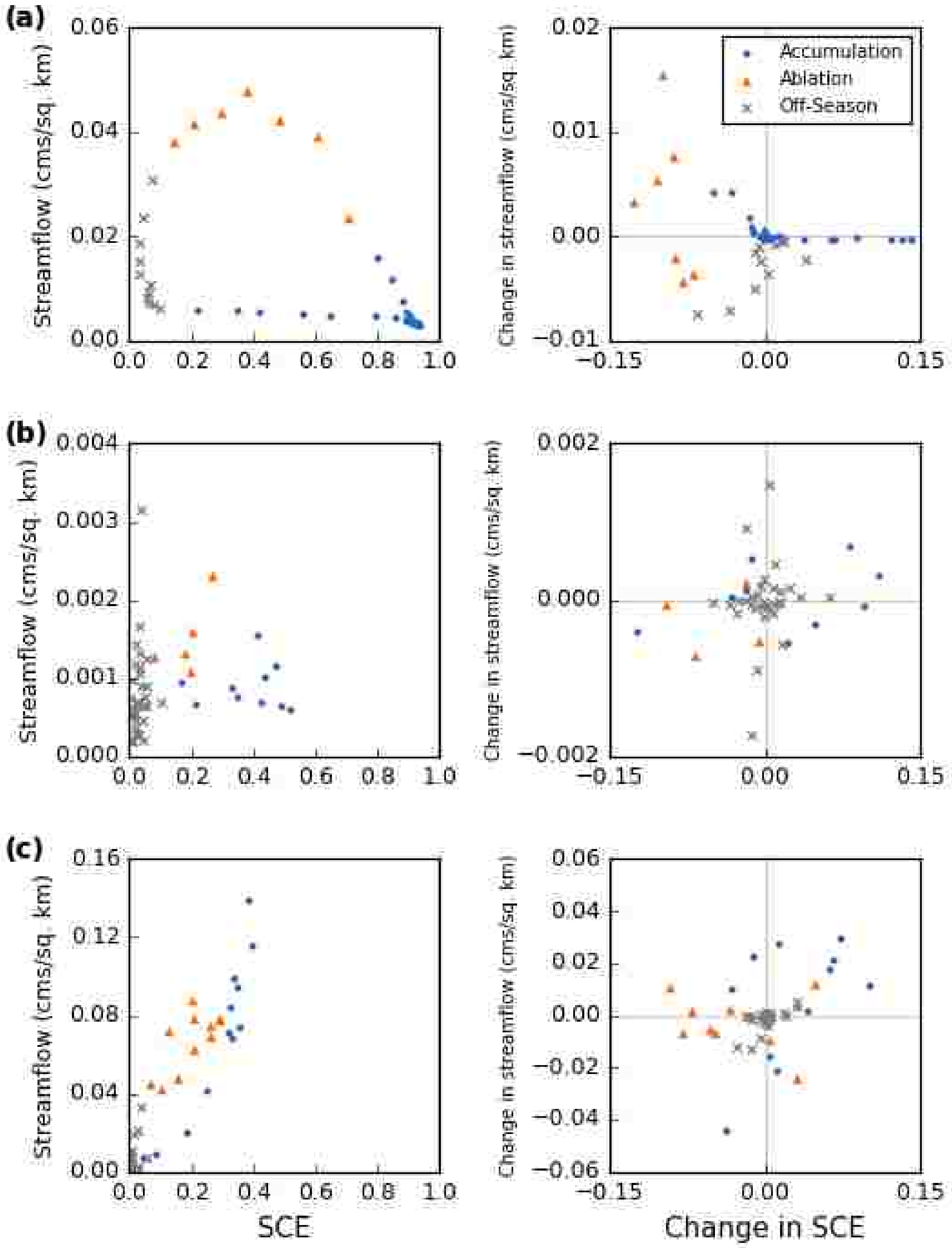

Figure 28: Hysteresis loops (left) and delta graphs (right) for (a) Yellowstone River Watershed, (b) Gila River Watershed, and (c) Upper Van Duzen Watershed.

4. Discussion

4.1 SCE and inter-watershed variability

To explore the potential of SCE for characterizing the snowpack-streamflow dynamics of mountain watersheds, SCE-based metrics compared to key climate, snowpack, and streamflow variables. These metrics were generated for each watershed from the SCE curve for the average water year to capture key temporal inflection points (SOS, SOMelt, and EOS) and the overall shape of the curve (AvgSCE).

SCE-based metrics showed strong correlations to the average annual temperature, demonstrating that they capture hydro-climatological variations between watersheds. AvgAnnualTemp had a significant linear relationship with all four SCE-based metrics. This is evidence that SCE metrics may provide valid insight into how snowpack-streamflow dynamics change between watershed, supporting the remainder of the analysis in this study. Higher temperatures correlated to an earlier SOMelt and EOS and a later SOS, meaning that the snow season contracts in warmer climates as found in previous research (Musselman et al, 2017; Yang et al, 2007). Conversely, the snow season expands in watersheds with lower average temperatures. Because both the start and end of the snow season are affected by warmer temperatures, this amplifies their impact on mountain watersheds. Higher temperatures are also correlated with decreasing AvgSCE, indicating less overall snowpack in warmer climates. These trends could potentially be seen within a single watershed with SCE-metrics calculated for two different time periods. This type of analysis could be used to explore the impacts of climate change on watershed dynamics. Precipitation has a weak relationship with EOS and no significant relationship with other SCE-based metrics as supported by Yang et al, 2007 who found that SWE was not significantly related to precipitation.

Snow cover extent had a complex relationship with snow water equivalent that highlights the key differences between spatial and point measurements. Significant linear relationships between SQRT(PeakSWE) and the following SCE-based metrics – SOMelt, EOS, and AvgSCE – indicate that SCE may be useful in inter-watershed analysis of snowpack dynamics. Although the strength of this relationship was only moderate, it was more than anticipated given that SCE measures the presence of snow over a large spatial extent while SWE measures snow water content at a single point. Additional discrepancies between SCE and SWE were partially accounted for by including elevation into the regression analysis to represent its role in the spatial variability of SWE across a watershed. Introducing elevation into the regression increased the strength of the relationships for SOMelt and AvgSCE and brought SOS into significance. However, it did not improve the model fit for EOS, suggesting that the end of the season may not respond to the same drivers as the other metrics or at least not respond in the same way. Differences in snowpack depth and water content between watersheds due to climate patterns likely account for a large portion of the remaining variability in the models. Further analysis is needed to assess how much of the effect of adding elevation into the analysis is due to the elevation-dependence of snowpack versus the impact of distinct climates that occur at different elevation ranges due to the topographical patterns of the Western U.S. The effect of SNOTEL placement on the SCE-SWE relationship is another key avenue for further research to better understand their complex connection.

SCE-based metrics also had a significant inter-watershed relationship with peak streamflow (PeakQ) that supports the use of SCE in characterizing and analyzing snowpack-streamflow dynamics. SQRT(PeakQ), transformed for normality, had a significant linear relationship with all four SCE-based metrics, implying that a longer snow season and later melt correspond to higher PeakQ values, as seen in Yang et al, 2003. The results indicate that SCE captures important snowpack dynamics in terms of both timing (SOS, SOMelt, and EOS) and magnitude (AvgSCE) that contribute to streamflow. Including precipitation into the analysis of AvgSCE increased the model fit by more than double. AvgAnnualPPT captures a significant portion of the inter-watershed variability of SWE that leads to differences in streamflow, perhaps serving to differentiate between deep and shallow snowpacks. In warmer watersheds, AvgAnnualPPT may also be capturing low elevation rainfall that causes streamflow peaks outside of a spring pulse, such as in the Upper Van Duzen River Watershed. This indicates that precipitation from climate models and monitoring networks shows promise in supplementing SCE in the analysis of snowpack-streamflow dynamics in watersheds without detailed in-situ snowpack data.

4.2 SCE and intra-watershed patterns

Based on the results from inter-watershed variability, snow water equivalent and streamflow were further analyzed to determine their potential for capturing hydrological patterns within a watershed. Climate variables were not used for this portion of the analysis as the temporal resolution of the PRISM dataset was too coarse to allow for further examination. Future work could include the daily PRISM data to further examine the impact of temperature on SCE for an average water year.

SCE displayed a distinct seasonal hysteresis with SWE that mimics that found in Magand et al (2013) using snowpack depth. During accumulation, SCE and SWE reveal a logarithmic relationship with quick increases in SCE that saturate near 1.0 leading to asymptotic behavior. During ablation, SCE decreases more slowly and with greater variability, with every SCE value associated with a much larger range of SWE values than during accumulation. Magand et al (2013) attributes this hysteresis to the fact that snow accumulation tends to happen more uniformly over a watershed while snow ablation is preferential and affected more by topographic variations such as aspect and shading. In addition, shallow snow during the early accumulation season means that a high SCE may occur during a relatively low SWE. Discrepancies between shallow and deep snowpacks are also dampened during accumulation due to saturation of SCE near 1.0, which is not the case during ablation. This pattern is better demonstrated by the Yellowstone River Watershed, which displays a pronounced hysteresis and shows how ablation is affected by elevation across SNOTEL stations.

The delta graphs of SCE and SWE more clearly illustrate the differences between these two measurements as snowpack indicators. If SCE and SWE were perfectly related and the snow season was perfectly characterized, then all accumulation points would lie in the upper-right quadrant and all ablation points would lie in the lower-left quadrant. Put differently, all increases in SCE would be met with increases in SWE and would be classified as accumulation points. Similarly, all decreases in SCE would be met with decreases in SWE and would be classified as ablation points. Several factors prevent this from occurring. First, determining the start of snow melt from SCE alone is prone to errors due to data irregularities, system complexity, and spatial heterogeneity of snow melt timing. Therefore, the start of snowmelt, as determined by SCE, may not line up with the start of snow melt of a specific SNOTEL station at a specific elevation. This elevation-dependence is demonstrated in Figure 16 using two SNOTEL stations at different elevations in the Yellowstone River Watershed. This source of error manifests as accumulation points that exhibit ablation behavior and vice versa. In addition, intermittent snow cover loss may occur at lower elevations throughout the season. Thus, moderate decreases in SCE may occur due to melt at lower elevations later in the season while the high elevation SNOTEL stations are still receiving snowfall. This discrepancy manifests as accumulation points in the upper-left quadrant where SCE and SWE are seemingly at odds over the current state of the snow season.

Despite these idiosyncrasies, the delta graphs of SCE and SWE demonstrate that all three seasons are well-defined with distinct relationships. The majority of accumulation (~ 91%) and ablation (~ 89%) points, as defined using SCE and the methods in Section 2.6, correspond to positive and negative SWE values, respectively. Therefore, although changes in SCE and SWE may not always correspond in magnitude, they are well-correlated with regards to sign. Furthermore, each season displays a unique SCE-SWE relationship that can be used to better understand the dynamics between these two snowpack measurements and to develop better methods for using SCE. Further refinements in the snow season characterization methods outlined in Section 2.6 can be evaluated by assessing how well they improve the outliers in the current delta graphs.

The hysteretic nature of the SCE-SWE relationship highlights the challenges faced by comparing spatial and point measurements of the same variable. Although complex, the relationship between SCE and SWE is much stronger than anticipated with a clear temporal component as exhibited by the seasonal trends displayed in Figure 13 and Figure 14. This must be accounted for in hydrological studies that aim to integrate snow cover extent into their models.

As with SWE, the SCE-streamflow relationship also displays hysteretic behavior that captures the fundamental differences between the accumulation and ablation seasons. During accumulation, streamflow is generally low, although watersheds with significant hydrological inputs other than snowmelt may display higher streamflow. This streamflow increases during the latter part of the accumulation season as snow begins to melt (Yang et al, 2003; Yang et al, 2007). The biggest spikes in streamflow can be seen during the ablation season as snowmelt makes its way to the rivers and then attenuates. This study refers to this pattern as a hysteresis loop after similar patterns in soil water retention curves (Sławiński, 2011). A look at the hysteresis loop for Yellowstone River Watershed makes the SCE-streamflow relationship for snow-dependent watersheds more obvious with a flat slope during accumulation and then rising and falling limbs to match the spring pulse during ablation.

The delta graphs for SCE and streamflow demonstrate volatility during the accumulation season and a much clearer relationship during ablation. Over half of the accumulation points (53.5%) demonstrate an increase in streamflow, implying that the relationship between SCE and streamflow during accumulation is complex and varies widely between watersheds and climates. Lower elevation rain and mid-season melt events obscure the connection between the snowpack and streamflow. This connection is also greatly affected by the threshold method of snow season characterization which necessarily labels the first few periods of the ablation season as accumulation. The delta graph for Yellowstone River Watershed in Figure 20 shows what an accumulation pattern looks like for a snow-dependent watershed with no outside streamflow sources. Future improvements should be focused at better identification of the start of snow melt, which will require grappling with disparate SCE-curves across watersheds. In contrast to accumulation, the SCE-streamflow relationship is especially well-defined during the ablation season. This is promising as ablation is the most essential season for assessing how and when snowmelt reaches our rivers. Further streamflow attenuation occurs in the off-season. Integrating streamflow into the snow season characterization process may allow for better delineation of the spring pulse. However, early attempts at this showed that this method struggled with signals from winter rainfall and summer monsoons in watersheds without a defined spring pulse. This was not pursued further in this study as the focus was on the ability of SCE to characterize the season alone.

4.3 Snowpack-streamflow dynamics in hydrologically distinct watersheds

The analysis of three watersheds with distinct climate profiles and hydrological behaviors illustrates how these differences are expressed in the relationship between SCE and streamflow. Yellowstone River Watershed displays the quintessential behavior of a snowmelt-dependent watershed in the inner United States with low inter-annual variability. SCE increases rapidly until it reaches and maintains saturation from late-November to mid-April before melting into a classic spring pulse that peaks and then retreats to base flow. In contrast, the Gila River Watershed demonstrates how SCE and streamflow look for a warm, dry Southwestern basin with a strong summer monsoon signal. SCE only covers half of the watershed at its peak, quickly melts, and is associated with only a moderate spring pulse. A large peak in streamflow in September captures the relative influence of the summer monsoon as compared to water from the winter snowpack. The warm climate and uncertain winters create a large amount of interannual variability in both SCE and streamflow. The Upper Van Duzen River Watershed represents a warm, coastal basin with a winter precipitation that does not reliably fall as snow. The SCE-streamflow relationship indicates that winter storms that increase SCE also increase streamflow as rain falls at lower elevation. No real spring pulse is discernable, and the summer months are extremely dry, in stark contrast to the Gila.

The compact analysis demonstrates how methods developed in this study can be used to quickly and robustly classify the snowpack-streamflow dynamics of a watershed. The distinct hydrological behaviors identified in Section 3.3.2 through a more rigorous analysis can be derived in a compact and visually-descriptive way using hysteresis loops and delta graphs as shown in Figure 28. Although delta graphs are simply a permutation of the hysteresis loop, they provide a unique view of the data dynamics. The snow-dependent, consistent Yellowstone River Watershed presents as a clear, open hysteresis loop, and its delta graph displays well-defined seasonal behaviors. The monsoon-dependent Gila River Watershed with high interannual variability and moderate spring pulse presents as a collapsed loop with high streamflows during the off-season. Its delta graph shows an ill-defined accumulation pattern with an ablation pattern that vaguely captures the spring pulse and an off-season that clearly shows the effects of monsoon events. The Upper Van Duzen Watershed, with its winter rains and lack of clear spring pulse, creates a collapsed loop that shoots out at a diagonal from the origin with the winter rain made clear by the accumulation points rising from the x-axis. The disconnect between snow and streamflow is apparent in the delta graph where the accumulation and ablation seasons lack any meaningful relationships while the off-season simply reflects the area's dry summers.

Notably absent from the compact analysis is the inter-annual variability found in the initial analysis, but this can be hypothesized from the regularity of the loop. A classic loop structure as seen in Yellowstone implies consistent snow seasons while the lack of a clear loop in both the Gila and Upper Van Duzen indicate higher variability that comes with an inconsistent snow season. A strong snow season stabilizes a watershed, providing consistent water every year around the same time. Transitional watersheds like the Gila and Upper Van Duzen, in contrast, are highly variable with both rain and snow and an unstable relationship between snow and streamflow from year to year.

These compact methods can be used to quickly characterize and classify watersheds for further hydrological study. For example, watersheds with distinct hydrological behaviors can be identified by comparing their hysteresis loops and delta graphs as in Section 3.3.2. The inverse may also be done for those seeking hydrologically similar watersheds to control for hydrology in ecological, biological, and similar studies.

These two visualizations also provide a solid foundation for generating future hypotheses about the impacts of climate change. The Upper Van Duzen shows an extreme disconnect between the water supply (rainy winter) and the water demand (dry summer) with the majority of streamflow occurring during the winter and fully attenuating before the dry season. Therefore, the effects of climate change on water supply may be mitigated with the construction of water reservoirs for human use during the summer. The Gila’s dependence on the summer monsoon indicates that its resources would be most at risk from climate change effects that impact that monsoon. Due to its high interannual variability, small increases in temperature could also cause a substantial decrease in its snowpack reserves, devastating ecosystems that depend on that moderate spring pulse. Similarly, decreased snowpacks under higher temperatures could greatly affect the dynamics of the Yellowstone River Watershed. Since watersheds like Yellowstone currently provide a consistent water supply, changes in their snowpack-streamflow dynamics could have profound and unanticipated ramifications.

4.4 Guidelines for the use of snow cover extent

SCE as a representation of snowpack works best in climates with intermittent cloud cover that allows the MOD10A2 compositing algorithm to capture at least one clear image every eight days. Smoothing algorithms can help in areas where cloud cover is intermittent, short-lasting, and does not occur consistently in any given time frame every year. Analysis using the *average water year* concept as outlined in Section 2.4 also helps to limit yearly cloud cover effects.

Although SCE saturates in watersheds with heavy, consistent snowpack, SCE metrics like those used in this study can be used to accurately capture snow season dynamics and characterize watersheds for comparison. However, saturation may hinder analyses that require a high degree of differentiation of during peak season or depend on knowledge of the depth or water content of the snowpack.

5. Conclusion

The goal of this study was to assess and demonstrate the suitability of snow cover extent for characterization and analysis of snowpack-streamflow dynamics of mountain watersheds. This goal was met by assessing the ability of SCE and SCE-based metrics to (a) capture inter-watershed variability with respect to climate, SWE, and streamflow; (b) capture intra-watershed patterns with respect to SWE and streamflow; and (c) characterize and differentiate between the snowpack-streamflow dynamics of hydrologically distinct watersheds in the U.S. Mountain West. Metrics for describing the critical temporal inflections in the SCE curve (SOS, SOMelt, and EOS) as well as the overall shape of the curve (AvgSCE) were developed to allow for the characterization of the snow season using only remotely-sensed snow cover extent, as described in Section 2. Snow cover, snow water extent, streamflow, and climate data from October 2000 to September 2016 were processed and compressed into an average water year (see Section 2.4) for each of the 121 study watersheds.

Analysis of SCE-based metrics between watersheds revealed significant relationships between SCE and climate variables, SWE, and streamflow. A strong relationship between average annual temperature and all SCE-based metrics showed SCE's ability to capture the effects of climate on snowpack and prompted further analysis. Correlations between PeakSWE and three of the SCE-based metrics demonstrated that SCE also captured much of the behavior measured by the more commonly used, but more difficult to acquire, snow water equivalent. Similar correlations between peak streamflow and SCE-based metrics supported further exploration of SCE in characterizing and analyzing watershed snowpack-streamflow dynamics within a watershed.

Analysis of the intra-watershed patterns of SCE, SWE, and streamflow further demonstrated the ability of SCE and SCE-based metrics to capture snowpack-streamflow dynamics at the watershed level. These analyses revealed significant hysteresis in both the SCE-SWE and SCE-streamflow relationships, providing a visual representation of the fundamental differences between snowpack dynamics in the accumulation and ablation seasons. The SCE-SWE hysteresis serves to illuminate the complex relationship between point and spatial measurements, such as the saturation of the spatial domain that can occur in SCE. The hysteresis in the SCE-streamflow relationship serves to delineate seasonal dynamics and is harnessed as an analytical tool for the next portion of the analysis.

The power of hysteresis loops and delta graphs for the analysis of watershed dynamics is demonstrated in Section 3.3 by characterizing and comparing three hydrologically and climatologically distinct watersheds. Yellowstone River Watershed represents a snowpack-dependent, consistent, inner-continental basin; Gila River Watershed represents a monsoon-dependent, warm, Southwest basin with a relatively dry winter; and Upper Van Duzen River Watershed represents a coastal, transitional basin with a dry summer and wet, rainy winter. Background research and initial analysis using SCE and streamflow were done to develop a comprehensive profile for each watershed. Compact analysis using hysteresis loops and delta graphs were then executed and were able to illustrate the differences in their snowpack-streamflow dynamics in a visually-compelling and unique way. These two analytical tools provide an opportunity for researchers to perform more efficient watershed selection and preliminary analysis as well as to develop new hypotheses related to climate change, ecology, and other water-related disciplines.

This study demonstrated that SCE is capable of accurately capturing snowpack-streamflow dynamics at the watershed level. SCE and SCE-based metrics provide a unique opportunity for studying remote and unmonitored regions and for approaching snowpack-streamflow analysis from a unique perspective in watersheds with existing snowpack monitoring systems. Future work should include better cloud removal and further investigation of the complex relationship between SCE and SWE to increase the applicability of SCE-based metrics. Furthermore, refinement of the methodology for obtaining those metrics would improve the ability of the hysteresis loops and delta graphs to communicate snowpack-streamflow dynamics. Expanding analysis to mountain ranges on different continents and in varying climates would aid in this refinement as well as expand understanding of the full range of possible hydrological responses in mountain watersheds. SCE-based metrics can also be used to set a reference point to which future changes in snowpack can be compared to analyze the impact of climate change on the world’s water supply.

Appendices

Appendix A: Term definitions

Term	Definition
SOS	Start of the snow season. This marks the beginning of the accumulation season as snow begins to fall.
SOMelt	Start of snow melt. This marks the beginning of the ablation season as the snowpack begins to melt and make its way to the streams.
EOS	End of the snow season. This marks the end of the ablation season when almost all the snowpack has melted.
AvgSCE	Average SCE. This captures some portion of the overall shape of the SCE curve.
POWY	Period of the water year. This is the 8-day period as a function of the water year so 1 marks the first period in October and 46 marks the last period in September.
AvgAnnualTemp	Average annual temperature. This value is derived from the mean temperature datasets from PRISM.
AvgAnnualPPT	Average annual precipitation. This value is derived from the mean precipitation datasets from PRISM.
PeakSWE	Peak snow water equivalent. This value is the maximum SWE for the average water year of a watershed.
PeakQ	Peak streamflow. This value is the maximum streamflow for the average water year of a watershed.

Appendix B: SCE smoothing algorithm

A smoothing algorithm was developed and applied to the original 8-day SCE data for water years 2001 to 2016. The snow cover extent (SCE) and cloud cover extent (CCE) for the average water year was generated from this smoothed data. Note that CCE is unaffected by the smoothing process and represents the original CCE. To better demonstrate the abilities and results of this algorithm, two watersheds are compared below, one of which has a snow-cloud relationship amenable to simple smoothing and one which does not. Note that the figures below represent the average water years *after* smoothing, but the smoothing algorithm was applied to the full 16-year period.

Figure 29 and Figure 30 show the effect of the smoothing algorithm for watershed 06191500 in the Upper Rockies and watershed 12035000 in the Pacific Northwest, respectively. Watershed 06191500 was retained for the remainder of the analysis based on its low cloud ratio of 0.1843. Watershed 12035000 was rejected based its high cloud ratio of 1.193. The cloud ratio and final watershed selection is described in Section 2.5. Watershed 06191500 worked well with the smoothing algorithm as increases in cloud cover generally corresponded to similar decreases in SCE, as demonstrated in Figure 29. Smoothing led to a nice even plateau during the main snow season that more accurately captures the snowpack dynamics of the watershed. In contrast, watershed 12035000 shows no relationship between changes in cloud cover and snow cover, as illustrated in Figure 30, that allow it to be accurately smoothed using the current method. Its high CCE, low SCE, and its incompatibility with the smoothing algorithm lead to its high cloud ratio.

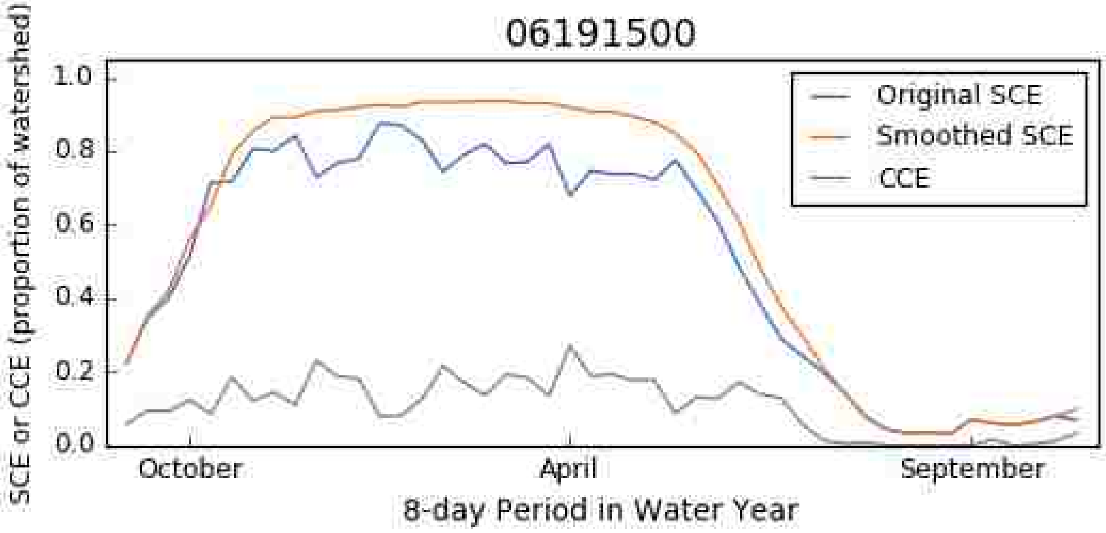

Figure 29: Snow cover extent (SCE) before and after smoothing along with the cloud cover extent (CCE) for watershed 06191500 in the Upper Rockies. The cloud ratio is 0.1842.

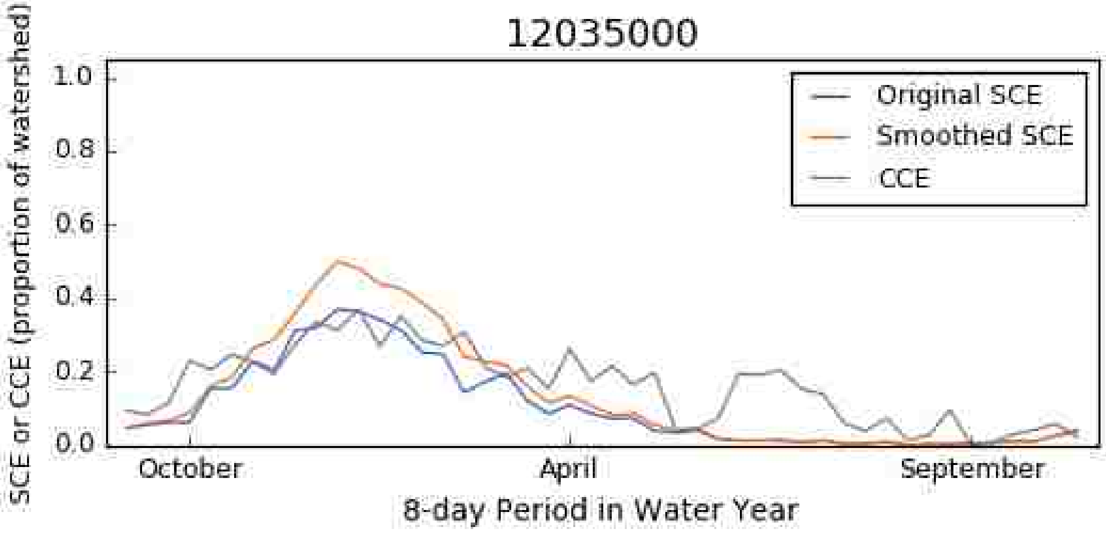

Figure 30: Snow cover extent (SCE) before and after smoothing along with the cloud cover extent (CCE) for watershed 12035000 in the Pacific Northwest. The cloud ratio is 1.193.

The following Python script was used to smooth the original SCE data for every 8-day period for water years 2001 to 2016 as detailed in Section 2.2.

```python
import re
import csv
import os
import sys

###########################################
### Input: text file with gage ID's for each basin. These gage IDs are used to get the appropriate
### CSV from "../Results_SCE_Unsmoothed/" that contains 8-day SCE data to be smoothed.
###
### Output: (1) CSV file for entire time period with SCE-percent for each 8-day period. The data will
### now be smoothed by determining which days experience simulataneous high cloud cover and a sudden drop in
### snow cover. These gaps will be filled by interpolation.
### (2) CSV file for 16-year average using smoothed 8-day values.
###########################################

### Define the workspace (but NOT the arcpy.env.workspace)
workspace = "D:/Thesis/"

### Get the text file of gage ID's from the command line.
if len(sys.argv) != 2:
    print "Need this form: python modis-sce-smooth.py <gage_IDs.txt>"
    print sys.argv
    sys.exit()

gageFilename = sys.argv[1]

### Open the gage ID file and create a list of the gage IDs.
gageFile = open(gageFilename, 'r+')
reader = csv.reader(gageFile, delimiter=',')

gages = []
for row in reader:
    # QC for row format
    if len(row) != 1:
        print "Improper text file format. One gageID per row: %s" % row
        sys.exit()

    # Get the gage ID and add it to the "gages" list.
    gages.append(row[0])

#############
### Main. ###
#############
for gageID in gages:

    print "Processing gage %s" % gageID

    ### Locate the SCE file name "sce-weekly-<gageID>.csv".
    sceFilename = os.path.join(workspace, "Results_SCE_Unsmoothed/sce-weekly-%s.csv" % gageID)
    if not os.path.exists(sceFilename):
        print "The snow directory does not exist: %s" % sceFilename
        sys.exit()


    ######################################
    ### Read in the SCE and Cloud data ###
    ######################################
    periodInWY = []
    sceOrig = []
    cloudOrig = []
    beforeRows = []
    afterRows = []

    sceFile = open(sceFilename, 'r+')
    sceReader = csv.reader(sceFile, delimiter=',')

    # Save the header for writing out.
    header = sceReader.next()

    # Get period in WY, sce, and cloud %.
    # Save the rest of the row for writing to file.
    for row in sceReader:
        beforeRows.append(row[0:4])
        periodInWY.append(float(row[2]))
        sceOrig.append(float(row[4]))
        cloudOrig.append(float(row[5]))
        afterRows.append(row[6:])

    # Set record length, N.
    N = len(sceOrig)
    if len(cloudOrig) != N:
        print "SCE and Cloud arrays have different lengths: %d != %d" % (N, len(cloudOrig))
        sys.exit()

    ######################################################################
    ### Initialize a data dictionary to calculate averages at the end. ###
    ######################################################################

    dataDictionary = {}
    cloudDictionary = {}
    for i in range(1, 47):
        dataDictionary[i] = []
        cloudDictionary[i] = []


    ##################################
    ### Process SCE and Cloud data ###
    ##################################

           ### Loop through the SCE data.
           isSnowSeason = False
           sceFilled = [sceOrig[0]]
           dataDictionary[1].append(sceOrig[0]) # Add first entry to data dictionary.
           buffer = []
           for i in range(1, N):

               sce = sceOrig[i]
               cloud = cloudOrig[i]
```

```

            ### Check if isSnowSeason needs to change.
            if sce >= 0.1 and not isSnowSeason:
                isSnowSeason = True
            elif sce < 0.1 and cloud < 0.1 and isSnowSeason:
                isSnowSeason = False

            ### If we're in the snow season, add the index to the buffer to
            ### be smoothed through linear interpolation.
            if isSnowSeason and cloud >= 0.1 and i > 0:

                # Add the index to the buffer.
                buffer.append(i)

            elif len(buffer) > 0:

                ### Process the records in the buffer using linear
                ### interpolation across the span of the records.
                gapLength = len(buffer)
                beforeIndex = buffer[0] - 1
                afterIndex = buffer[gapLength-1] + 1

                beforeSCE = sceOrig[beforeIndex]
                afterSCE = sceOrig[afterIndex]


                ### Fill in all gaps, to create a linear change between the
                ### good (i.e. low cloud cover) records on either side.
                deltaGap = (afterSCE - beforeSCE) / (gapLength + 1)
                for j in range(gapLength):
                    gapIndex = buffer[j]
                    newSCE = beforeSCE + deltaGap * (j + 1)

                    cloudCurr = cloudOrig[beforeIndex + j + 1]
                    sceCurr = sceOrig[beforeIndex + j + 1]
                    cloudSCE = cloudCurr + sceCurr

                    if newSCE > cloudSCE:
                        newSCE = cloudSCE


                    ### Keep the original SCE if it's larger than the interpolated one.
                    origSCE = sceOrig[gapIndex]
                    if newSCE < origSCE:
                        newSCE = origSCE

                    sceFilled.append(newSCE)
                    dataDictionary[periodInWY[gapIndex]].append(newSCE)

                    ### Add clouds to appropriate period in cloudDictionary.

                    cloudCurr = cloudOrig[gapIndex]
                    cloudDictionary[periodInWY[gapIndex]].append(cloudCurr)



                ### Reset buffer.
                buffer = []

                ### Append the afterSCE to sceFilled.
                sceFilled.append(afterSCE)
                dataDictionary[periodInWY[afterIndex]].append(newSCE)

                ### Add the clouds to appropriate period in cloudDictionary.
                cloudCurr = cloudOrig[afterIndex]
                cloudDictionary[periodInWY[afterIndex]].append(cloudCurr)

            else:
                ### Add the SCE to the filled data.
                sceFilled.append(sce)

                ### Add the SCE to the appropriate period in dataDictionary.
                dataDictionary[periodInWY[i]].append(sce)

                ### Add the clouds to appropriate period in cloudDictionary.
                cloudCurr = cloudOrig[i]
                cloudDictionary[periodInWY[i]].append(cloudCurr)


            ### Increment i.
            i = i + 1


        ##################################
        ### Write out the filled data. ###
        ##################################

        ### Open the output file and write the header.
        outfileName = os.path.join(workspace, "Results_SCE/sce-weekly-%s.csv" % gageID)
        outfile = open(outfileName, 'wb')
        writer = csv.writer(outfile, delimiter=',')
        writer.writerow(header)

        for i in range(N):
            outRow = beforeRows[i]
            outRow.append(sceFilled[i])
            outRow.append(cloudOrig[i])
            outRow.extend(afterRows[i])

            writer.writerow(outRow)

        ### Close the output file.
        outfile.close()


        #######################################################
        ### Calculate and write out the long-term averages. ###
        #######################################################

        ### Open a new file to write out the long-term averages.
        outfileName = os.path.join(workspace, "Results_SCE/sce-averages-%s.csv" % gageID)
        outfile = open(outfileName, 'wb')
        writer = csv.writer(outfile, delimiter=',')
        writer.writerow(['Period in WY', '% Snow', '% Cloud'])

        # Calculate and write out average percentages for each category.
        for period in range(1, 47):
            sceData = dataDictionary[period]
            cloudData = cloudDictionary[period]

            # Calculate the average for sce and cloud.
            avgSCE = sum(sceData)/len(sceData)
            avgCloud = sum(cloudData)/len(cloudData)

            # Write out to file.
            outrow = [period, avgSCE, avgCloud]
            writer.writerow(outrow)

        # Close the output file.
        outfile.close()

    print "Done!"
```

Appendix C: Snow season characterization

The figures below show the SCE (solid blue line) and streamflow (dashed orange line) curves for the average water year of each watershed. Each figure is labeled with the primary metrics used in this analysis – SOS, SOMelt, EOS, and AvgSCE. AvgSCE is represented by the dotted horizontal line and the remaining metrics are represented by solid horizontal lines.

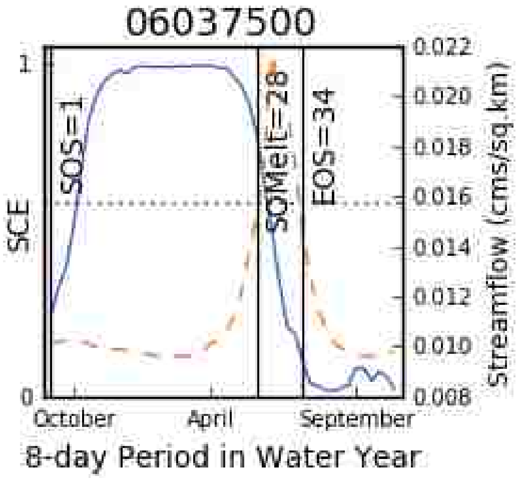

06037500

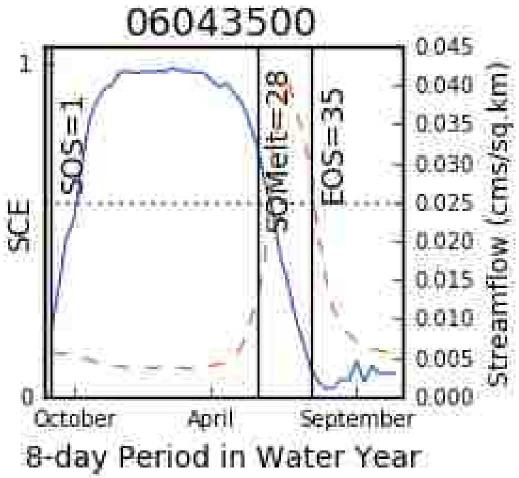

06043500

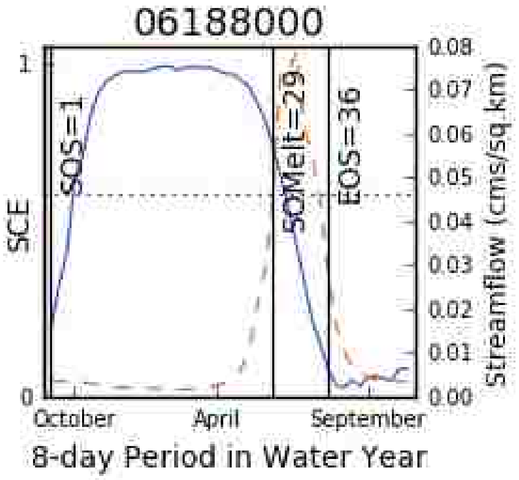

06188000

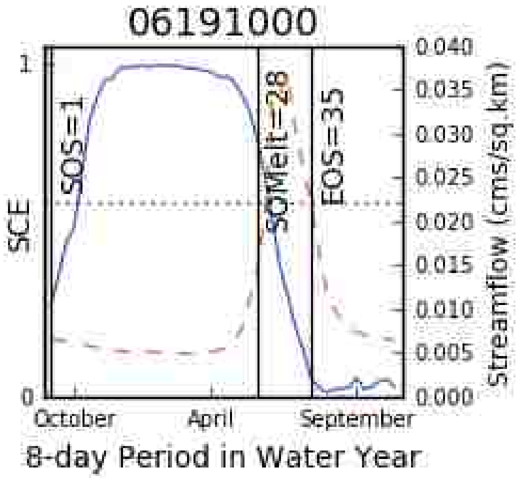

06191000

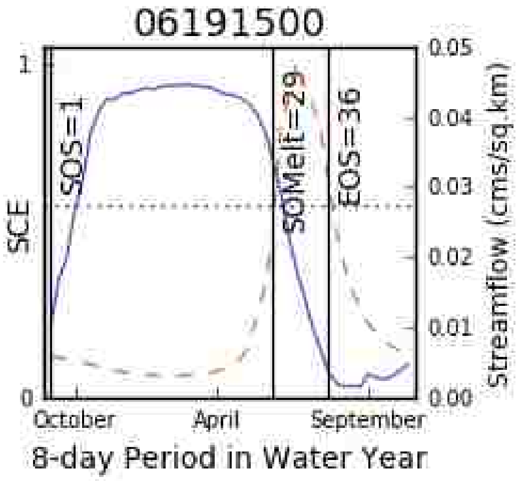

06191500

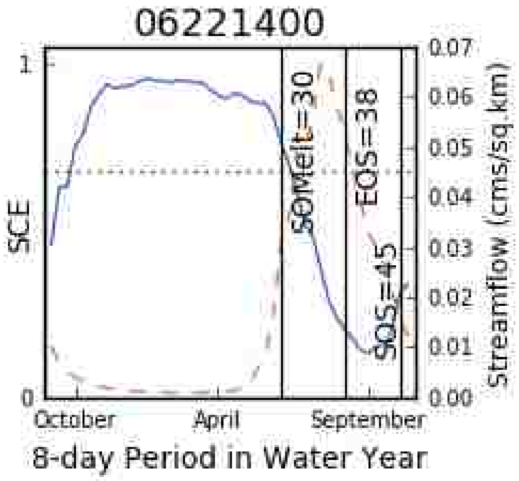

06221400

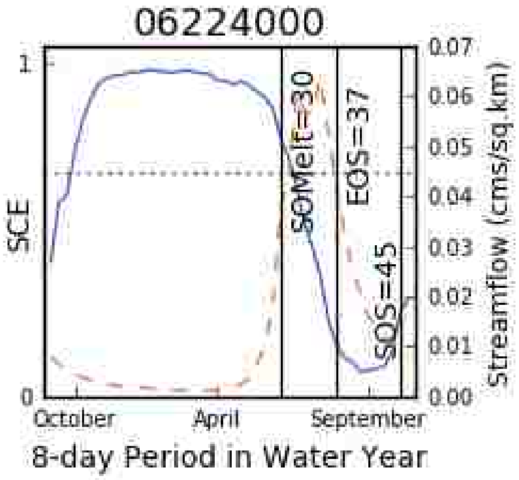
06224000
SCE
1
0
October
April
September
8-day Period in Water Year
0.07
0.06
0.05
0.04
0.03
0.02
0.01
0.00
Streamflow (cms/sq.km)
SOMelt=30
EOS=37
SOS=45

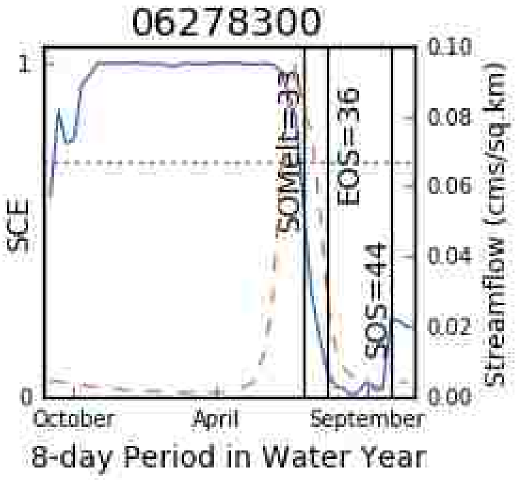
06278300
SCE
1
0
October
April
September
8-day Period in Water Year
0.10
0.08
0.06
0.04
0.02
0.00
Streamflow (cms/sq.km)
SOMelt=33
EOS=36
SOS=44

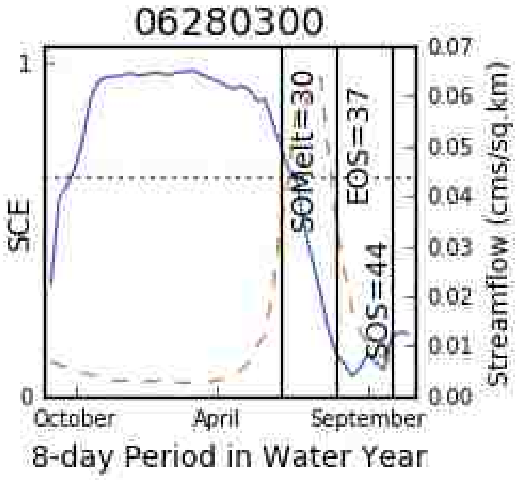
06280300
SCE
1
0
October
April
September
8-day Period in Water Year
0.07
0.06
0.05
0.04
0.03
0.02
0.01
0.00
Streamflow (cms/sq.km)
SOMelt=30
EOS=37
SOS=44

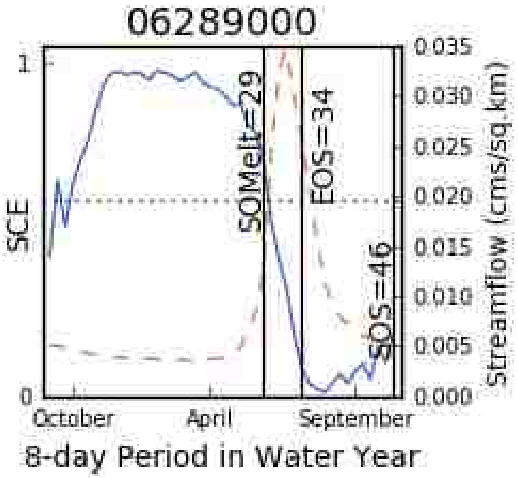
06289000
SCE
1
0
October
April
September
8-day Period in Water Year
0.035
0.030
0.025
0.020
0.015
0.010
0.005
0.000
Streamflow (cms/sq.km)
SOMelt=29
EOS=34
SOS=46

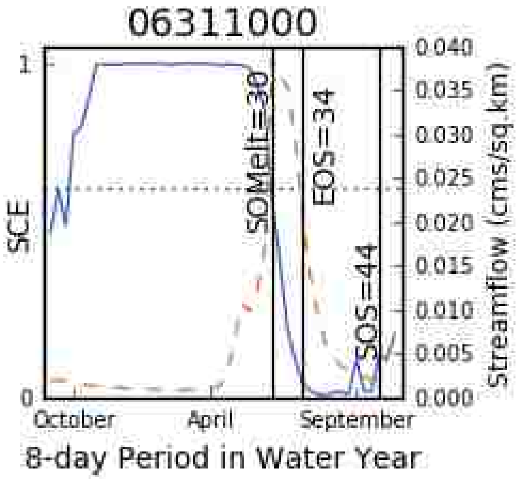
06311000
SCE
1
0
October
April
September
8-day Period in Water Year
0.040
0.035
0.030
0.025
0.020
0.015
0.010
0.005
0.000
Streamflow (cms/sq.km)
SOMelt=30
EOS=34
SOS=44

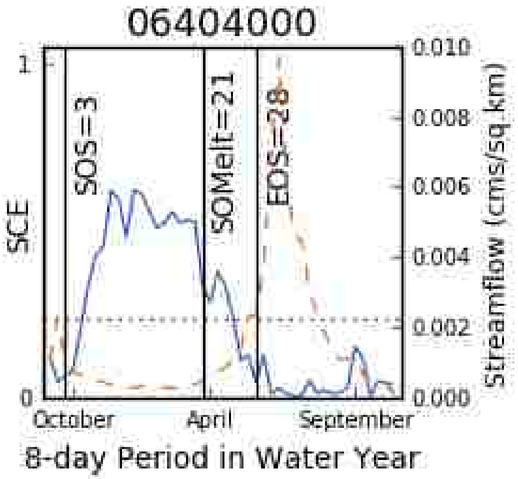
06404000
SCE
1
0
October
April
September
8-day Period in Water Year
0.010
0.008
0.006
0.004
0.002
0.000
Streamflow (cms/sq.km)
SOS=3
SOMelt=21
EOS=28

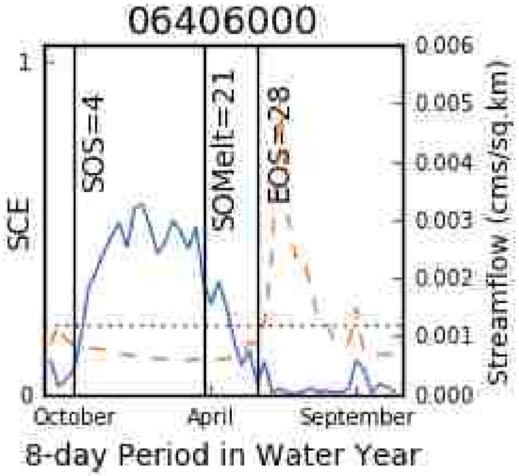
06406000
SCE
1
0
SOS=4
SOMelt=21
EOS=28
0.006
0.005
0.004
0.003
0.002
0.001
0.000
Streamflow (cms/sq.km)
October
April
September
8-day Period in Water Year

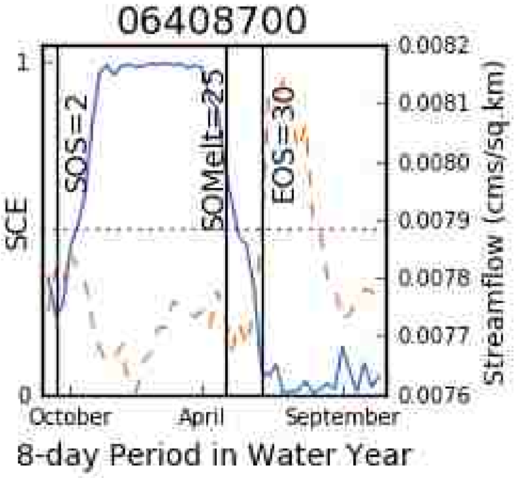
06408700
SCE
1
0
SOS=2
SOMelt=25
EOS=30
0.0082
0.0081
0.0080
0.0079
0.0078
0.0077
0.0076
Streamflow (cms/sq.km)
October
April
September
8-day Period in Water Year

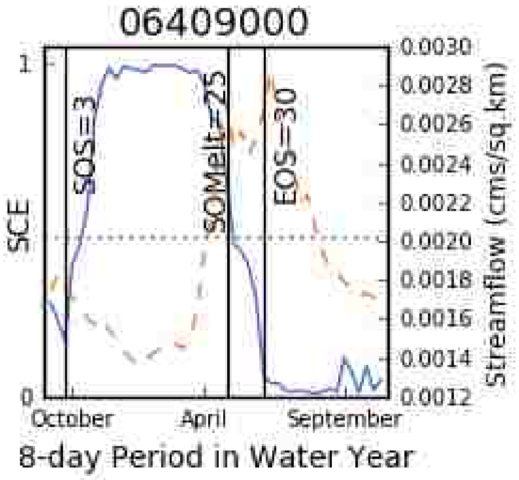
06409000
SCE
1
0
SOS=3
SOMelt=25
EOS=30
0.0030
0.0028
0.0026
0.0024
0.0022
0.0020
0.0018
0.0016
0.0014
0.0012
Streamflow (cms/sq.km)
October
April
September
8-day Period in Water Year

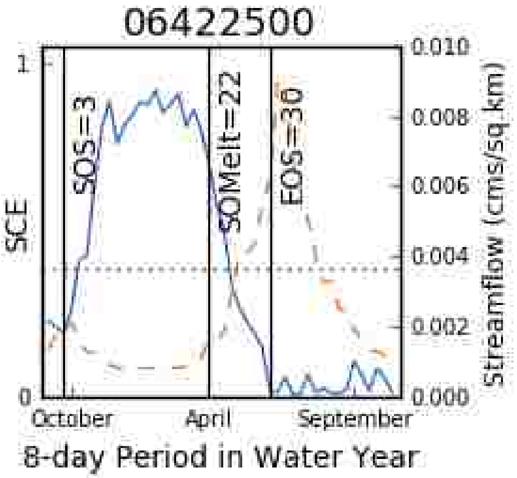
06422500
SCE
1
0
SOS=3
SOMelt=22
EOS=30
0.010
0.008
0.006
0.004
0.002
0.000
Streamflow (cms/sq.km)
October
April
September
8-day Period in Water Year

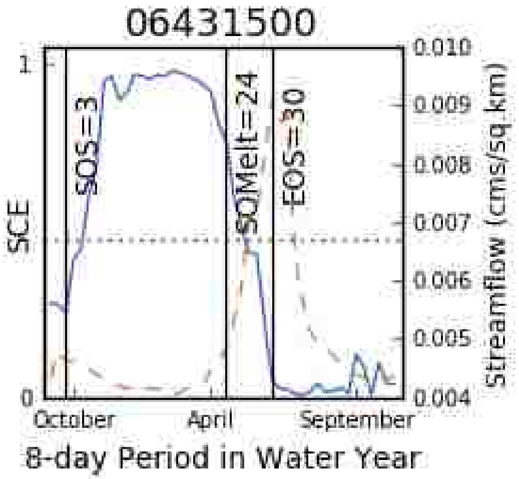
06431500
SCE
1
0
SOS=3
SOMelt=24
EOS=30
0.010
0.009
0.008
0.007
0.006
0.005
0.004
Streamflow (cms/sq.km)
October
April
September
8-day Period in Water Year

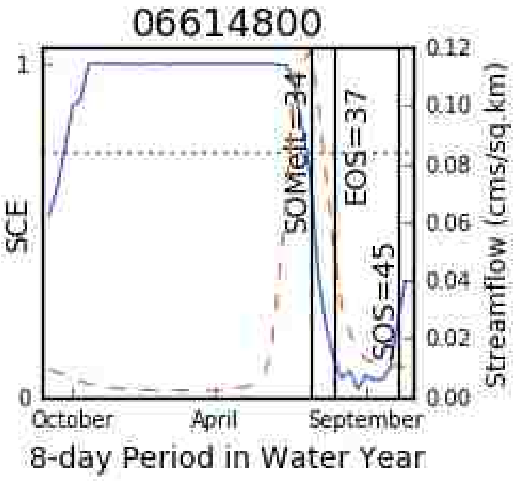
06614800
SCE
1
0
SOMelt=34
EOS=37
SOS=45
0.12
0.10
0.08
0.06
0.04
0.02
0.00
Streamflow (cms/sq.km)
October
April
September
8-day Period in Water Year

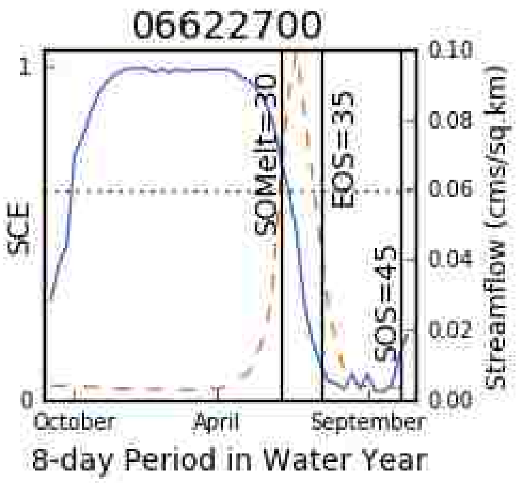
06622700
SCE
1
0
Streamflow (cms/sq.km)
0.10
0.08
0.06
0.04
0.02
0.00
SOMelt=30
EOS=35
SOS=45
October
April
September
8-day Period in Water Year

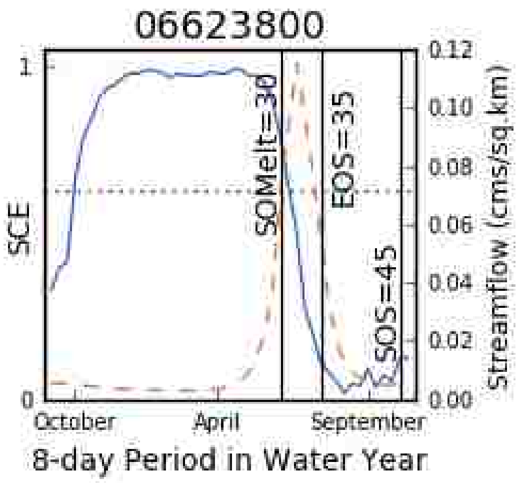
06623800
SCE
1
0
Streamflow (cms/sq.km)
0.12
0.10
0.08
0.06
0.04
0.02
0.00
SOMelt=30
EOS=35
SOS=45
October
April
September
8-day Period in Water Year

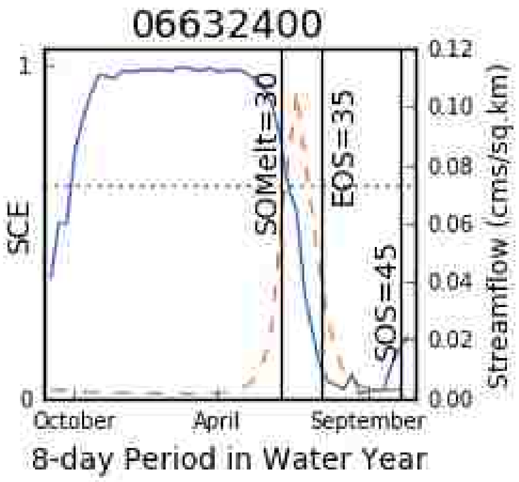
06632400
SCE
1
0
Streamflow (cms/sq.km)
0.12
0.10
0.08
0.06
0.04
0.02
0.00
SOMelt=30
EOS=35
SOS=45
October
April
September
8-day Period in Water Year

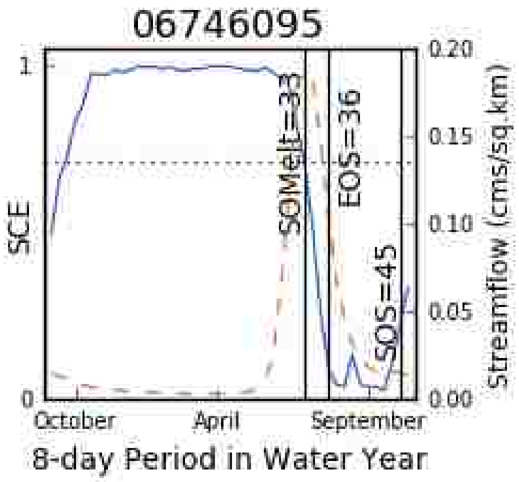
06746095
SCE
1
0
Streamflow (cms/sq.km)
0.20
0.15
0.10
0.05
0.00
SOMelt=33
EOS=36
SOS=45
October
April
September
8-day Period in Water Year

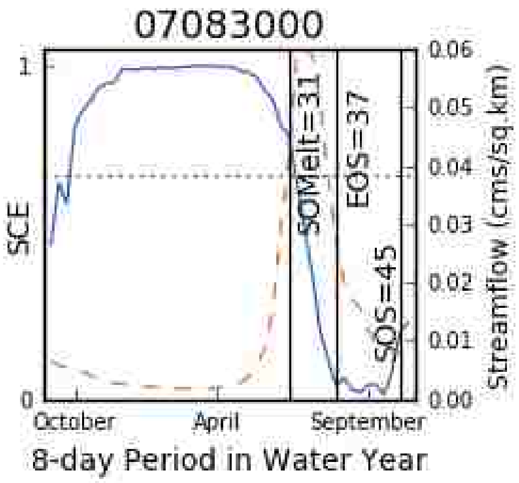
07083000
SCE
1
0
Streamflow (cms/sq.km)
0.06
0.05
0.04
0.03
0.02
0.01
0.00
SOMelt=31
EOS=37
SOS=45
October
April
September
8-day Period in Water Year

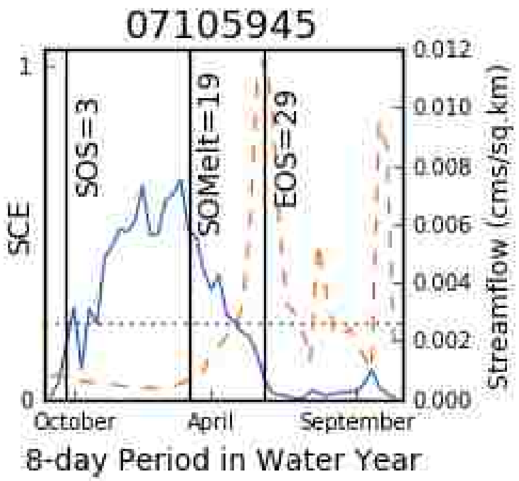
07105945
SCE
1
0
Streamflow (cms/sq.km)
0.012
0.010
0.008
0.006
0.004
0.002
0.000
SOS=3
SOMelt=19
EOS=29
October
April
September
8-day Period in Water Year

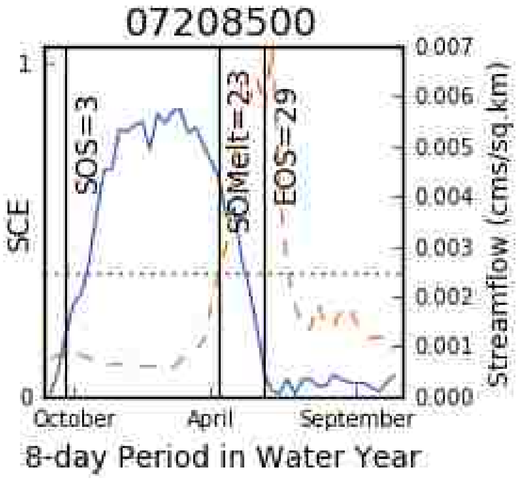
07208500

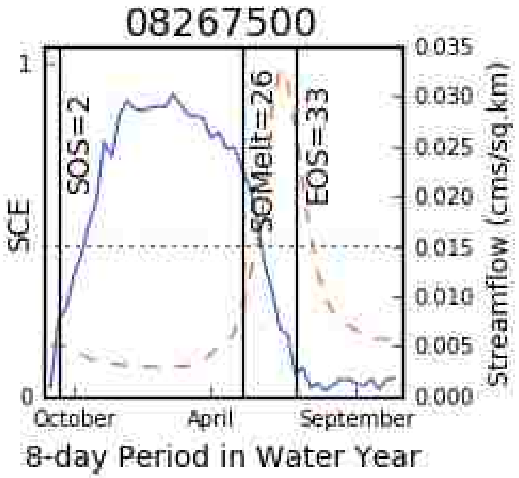
08267500

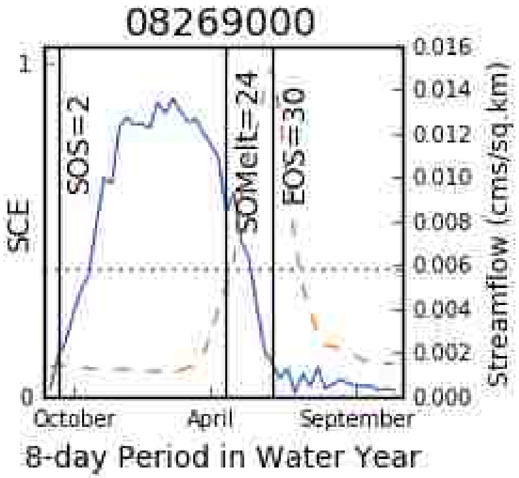
08269000

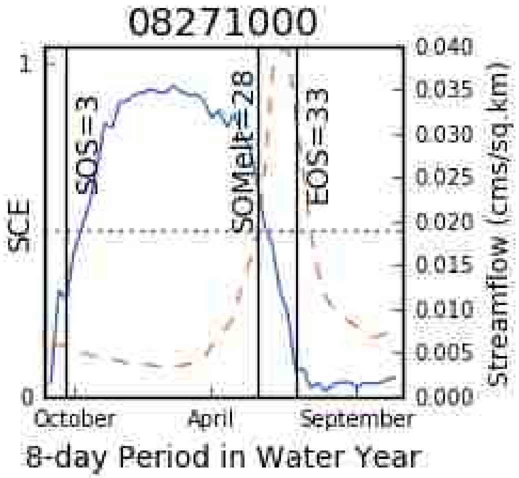
08271000

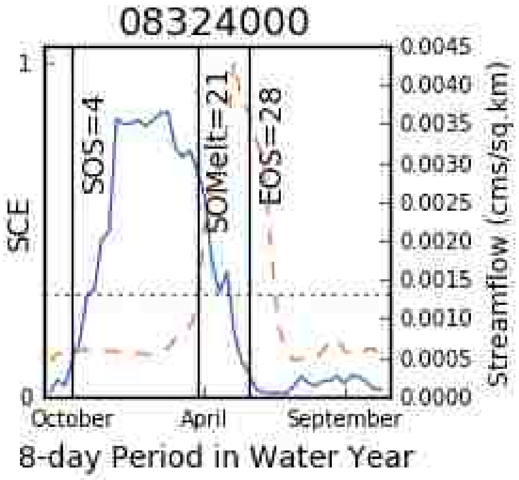
08324000

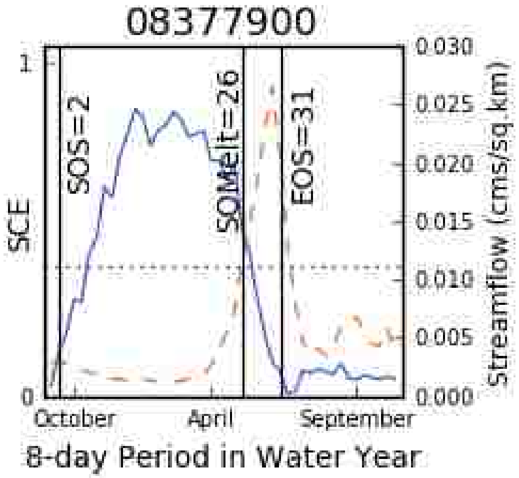
08377900

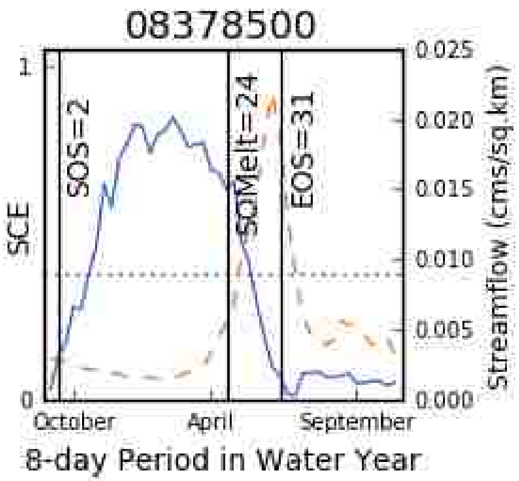
08378500
SCE
Streamflow (cms/sq.km)
SOS=2
SOMelt=24
EOS=31
1
0
0.025
0.020
0.015
0.010
0.005
0.000
October
April
September
8-day Period in Water Year

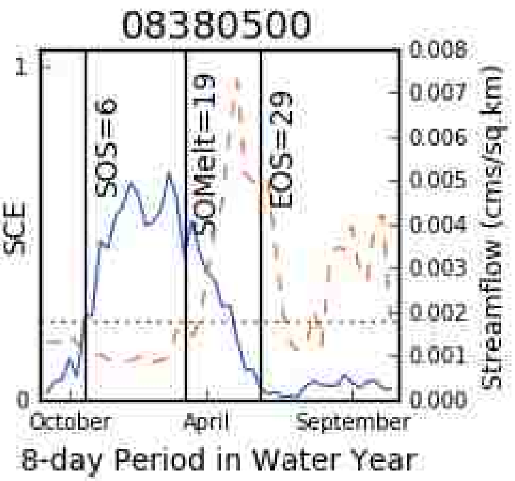
08380500
SCE
Streamflow (cms/sq.km)
SOS=6
SOMelt=19
EOS=29
1
0
0.008
0.007
0.006
0.005
0.004
0.003
0.002
0.001
0.000
October
April
September
8-day Period in Water Year

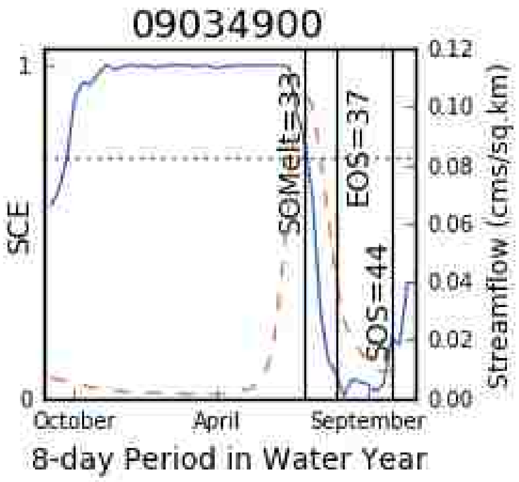
09034900
SCE
Streamflow (cms/sq.km)
SOMelt=33
EOS=37
SOS=44
1
0
0.12
0.10
0.08
0.06
0.04
0.02
0.00
October
April
September
8-day Period in Water Year

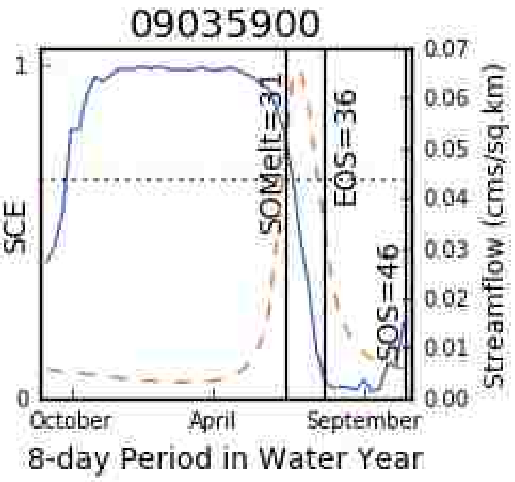
09035900
SCE
Streamflow (cms/sq.km)
SOMelt=31
EOS=36
SOS=46
1
0
0.07
0.06
0.05
0.04
0.03
0.02
0.01
0.00
October
April
September
8-day Period in Water Year

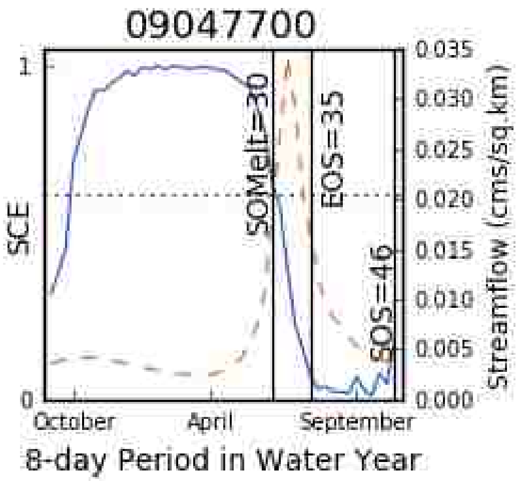
09047700
SCE
Streamflow (cms/sq.km)
SOMelt=30
EOS=35
SOS=46
1
0
0.035
0.030
0.025
0.020
0.015
0.010
0.005
0.000
October
April
September
8-day Period in Water Year

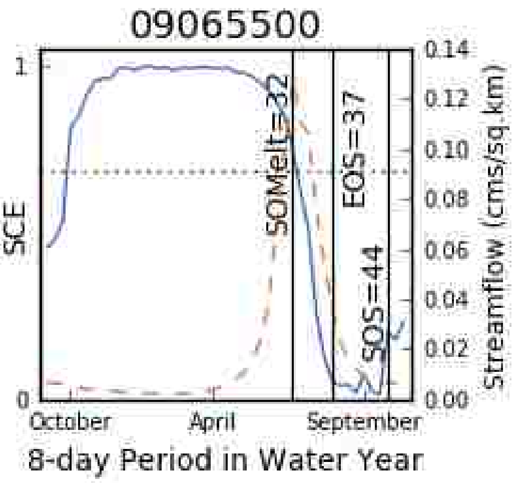
09065500
SCE
Streamflow (cms/sq.km)
SOMelt=32
EOS=37
SOS=44
1
0
0.14
0.12
0.10
0.08
0.06
0.04
0.02
0.00
October
April
September
8-day Period in Water Year

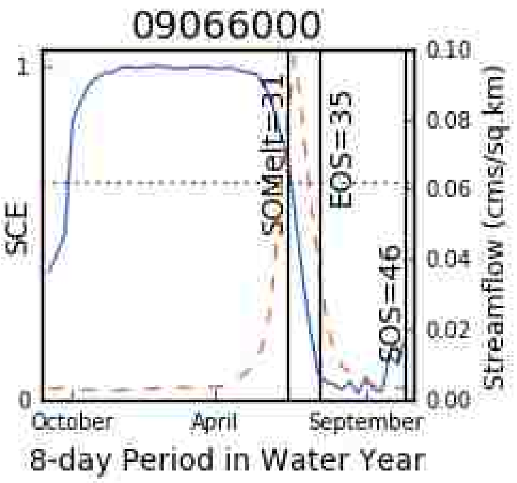
09066000
SCE
0
1
Streamflow (cms/sq.km)
0.00
0.02
0.04
0.06
0.08
0.10
SOMelt=31
EOS=35
SOS=46
October
April
September
8-day Period in Water Year

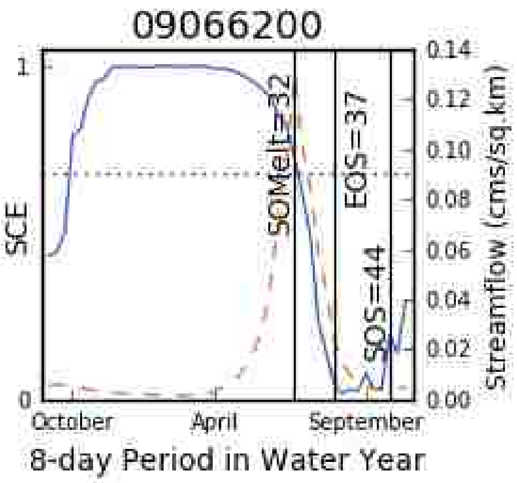
09066200
SCE
0
1
Streamflow (cms/sq.km)
0.00
0.02
0.04
0.06
0.08
0.10
0.12
0.14
SOMelt=32
EOS=37
SOS=44
October
April
September
8-day Period in Water Year

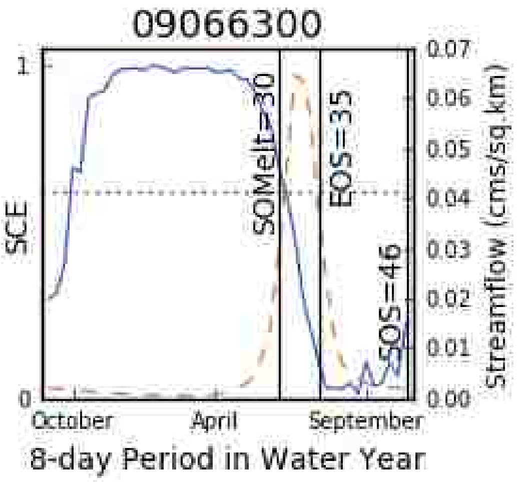
09066300
SCE
0
1
Streamflow (cms/sq.km)
0.00
0.01
0.02
0.03
0.04
0.05
0.06
0.07
SOMelt=30
EOS=35
SOS=46
October
April
September
8-day Period in Water Year

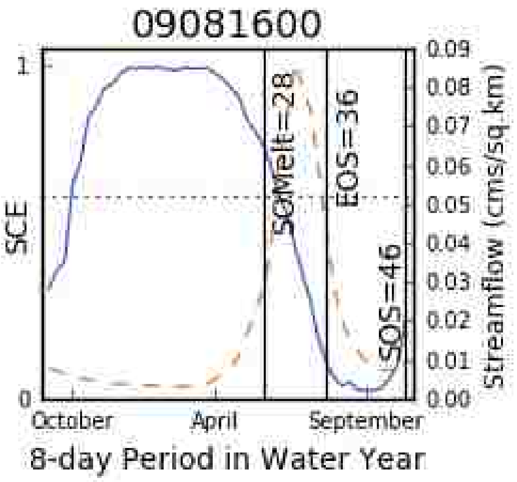
09081600
SCE
0
1
Streamflow (cms/sq.km)
0.00
0.01
0.02
0.03
0.04
0.05
0.06
0.07
0.08
0.09
SOMelt=28
EOS=36
SOS=46
October
April
September
8-day Period in Water Year

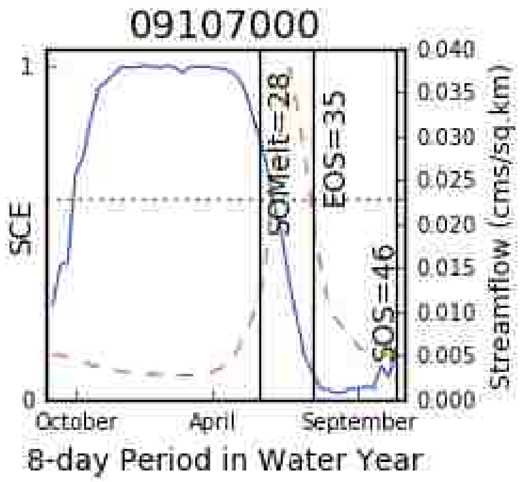
09107000
SCE
0
1
Streamflow (cms/sq.km)
0.000
0.005
0.010
0.015
0.020
0.025
0.030
0.035
0.040
SOMelt=28
EOS=35
SOS=46
October
April
September
8-day Period in Water Year

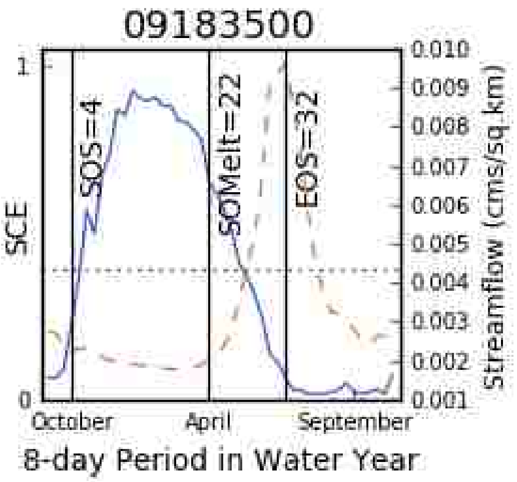
09183500
SCE
0
1
Streamflow (cms/sq.km)
0.001
0.002
0.003
0.004
0.005
0.006
0.007
0.008
0.009
0.010
SOS=4
SOMelt=22
EOS=32
October
April
September
8-day Period in Water Year

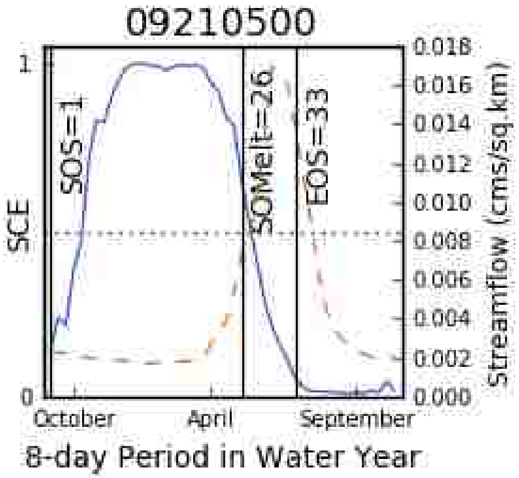
09210500
SOS=1
SOMelt=26
EOS=33
SCE
1
0
0.018
0.016
0.014
0.012
0.010
0.008
0.006
0.004
0.002
0.000
Streamflow (cms/sq.km)
October
April
September
8-day Period in Water Year

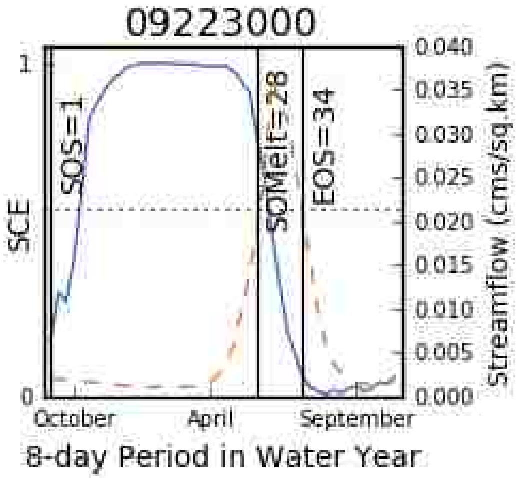
09223000
SOS=1
SOMelt=28
EOS=34
SCE
1
0
0.040
0.035
0.030
0.025
0.020
0.015
0.010
0.005
0.000
Streamflow (cms/sq.km)
October
April
September
8-day Period in Water Year

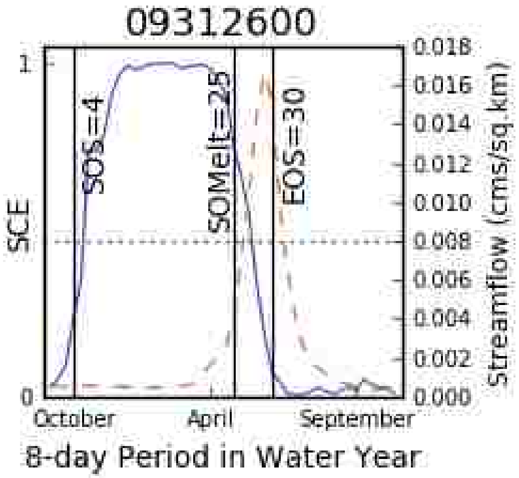
09312600
SOS=4
SOMelt=25
EOS=30
SCE
1
0
0.018
0.016
0.014
0.012
0.010
0.008
0.006
0.004
0.002
0.000
Streamflow (cms/sq.km)
October
April
September
8-day Period in Water Year

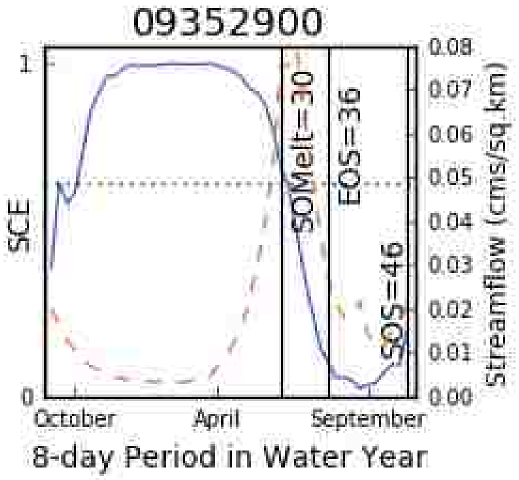
09352900
SOMelt=30
EOS=36
SOS=46
SCE
1
0
0.08
0.07
0.06
0.05
0.04
0.03
0.02
0.01
0.00
Streamflow (cms/sq.km)
October
April
September
8-day Period in Water Year

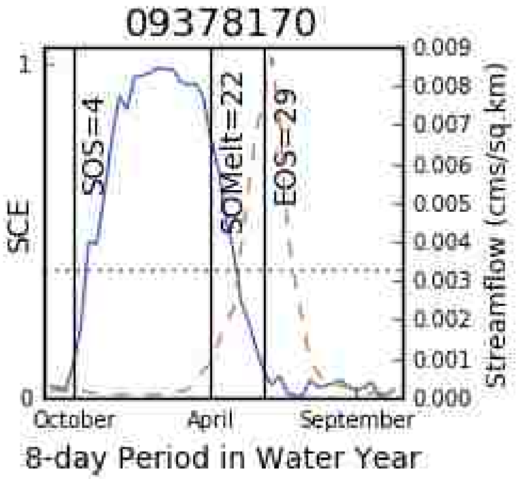
09378170
SOS=4
SOMelt=22
EOS=29
SCE
1
0
0.009
0.008
0.007
0.006
0.005
0.004
0.003
0.002
0.001
0.000
Streamflow (cms/sq.km)
October
April
September
8-day Period in Water Year

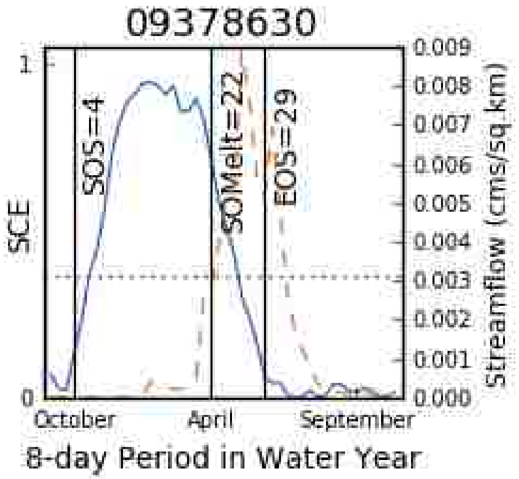
09378630
SOS=4
SOMelt=22
EOS=29
SCE
1
0
0.009
0.008
0.007
0.006
0.005
0.004
0.003
0.002
0.001
0.000
Streamflow (cms/sq.km)
October
April
September
8-day Period in Water Year

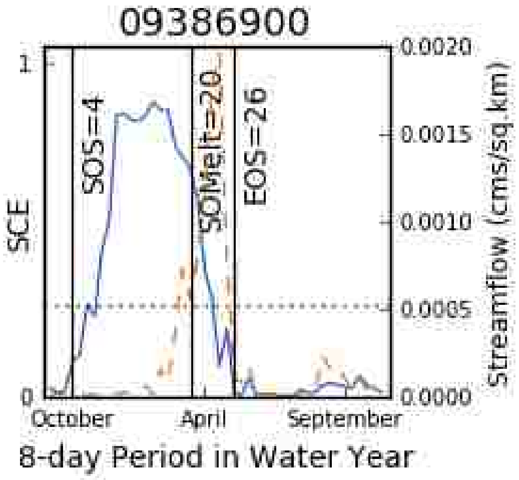
09386900
SCE
1
0
0.0020
0.0015
0.0010
0.0005
0.0000
Streamflow (cms/sq.km)
SOS=4
SOMelt=20
EOS=26
October
April
September
8-day Period in Water Year

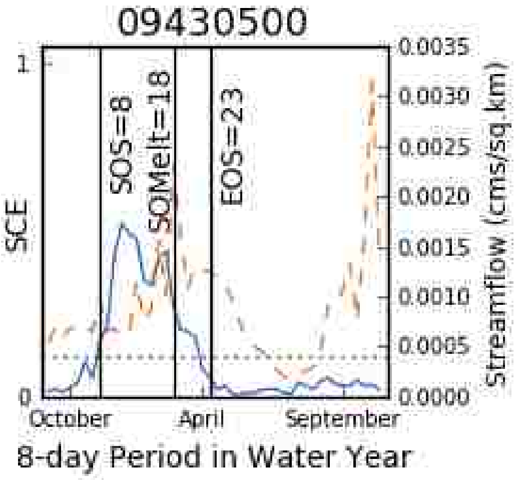
09430500
SCE
1
0
0.0035
0.0030
0.0025
0.0020
0.0015
0.0010
0.0005
0.0000
Streamflow (cms/sq.km)
SOS=8
SOMelt=18
EOS=23
October
April
September
8-day Period in Water Year

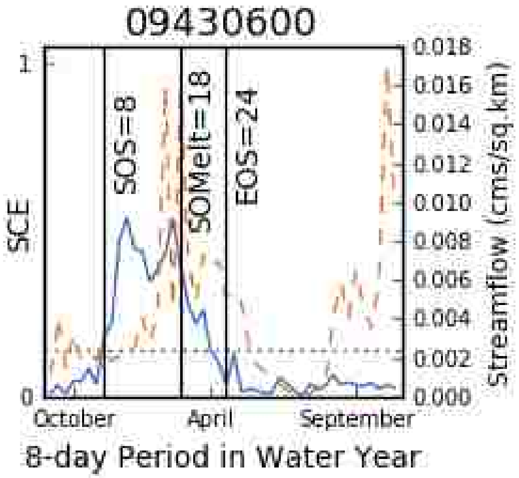
09430600
SCE
1
0
0.018
0.016
0.014
0.012
0.010
0.008
0.006
0.004
0.002
0.000
Streamflow (cms/sq.km)
SOS=8
SOMelt=18
EOS=24
October
April
September
8-day Period in Water Year

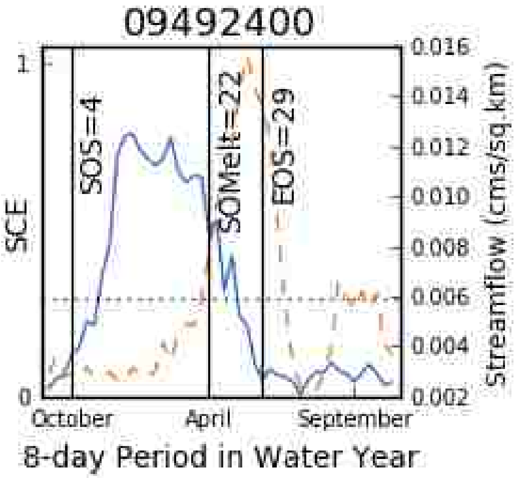
09492400
SCE
1
0
0.016
0.014
0.012
0.010
0.008
0.006
0.004
0.002
Streamflow (cms/sq.km)
SOS=4
SOMelt=22
EOS=29
October
April
September
8-day Period in Water Year

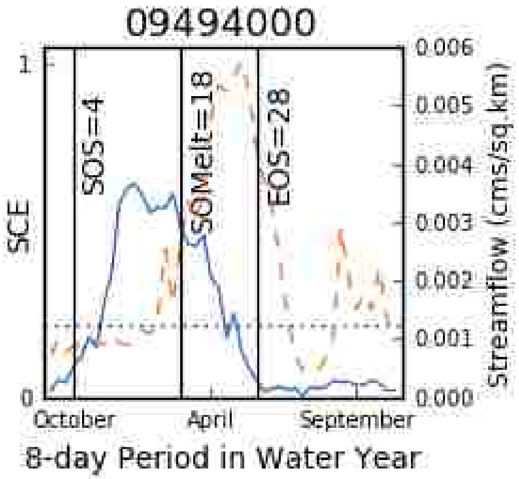
09494000
SCE
1
0
0.006
0.005
0.004
0.003
0.002
0.001
0.000
Streamflow (cms/sq.km)
SOS=4
SOMelt=18
EOS=28
October
April
September
8-day Period in Water Year

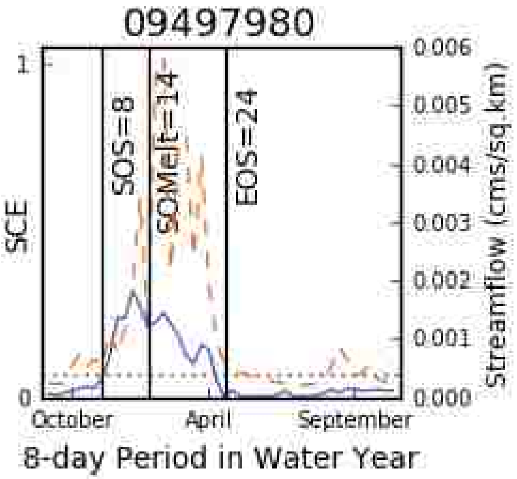
09497980
SCE
1
0
0.006
0.005
0.004
0.003
0.002
0.001
0.000
Streamflow (cms/sq.km)
SOS=8
SOMelt=14
EOS=24
October
April
September
8-day Period in Water Year

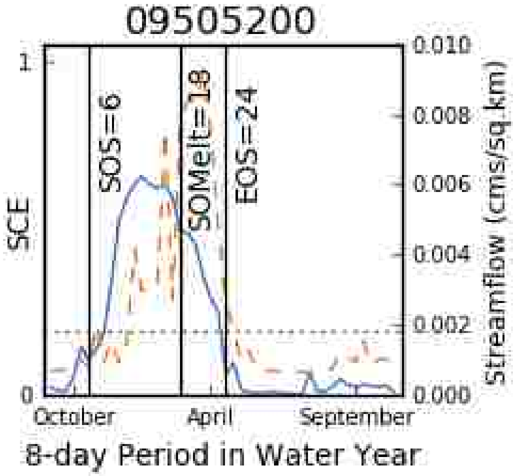
09505200
SCE
Streamflow (cms/sq.km)
SOS=6
SOMelt=18
EOS=24
0
1
0.000
0.002
0.004
0.006
0.008
0.010
October
April
September
8-day Period in Water Year

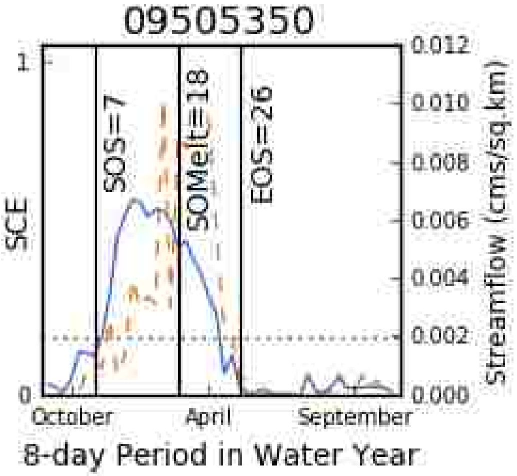
09505350
SCE
Streamflow (cms/sq.km)
SOS=7
SOMelt=18
EOS=26
0
1
0.000
0.002
0.004
0.006
0.008
0.010
0.012
October
April
September
8-day Period in Water Year

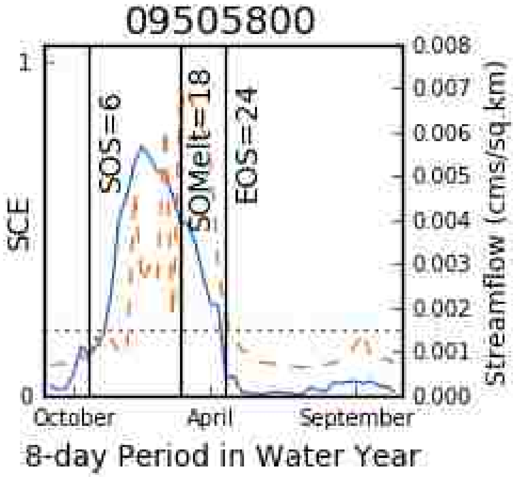
09505800
SCE
Streamflow (cms/sq.km)
SOS=6
SOMelt=18
EOS=24
0
1
0.000
0.001
0.002
0.003
0.004
0.005
0.006
0.007
0.008
October
April
September
8-day Period in Water Year

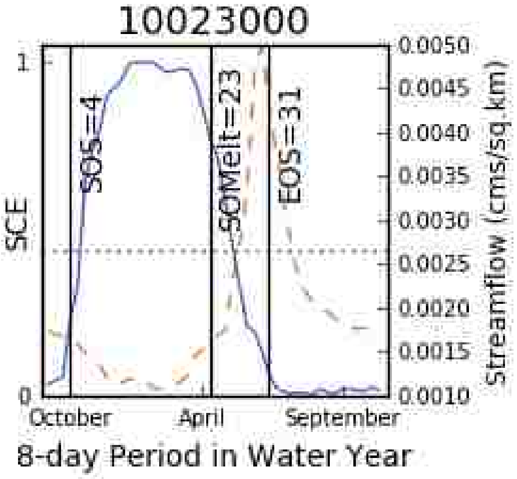
10023000
SCE
Streamflow (cms/sq.km)
SOS=4
SOMelt=23
EOS=31
0
1
0.0010
0.0015
0.0020
0.0025
0.0030
0.0035
0.0040
0.0045
0.0050
October
April
September
8-day Period in Water Year

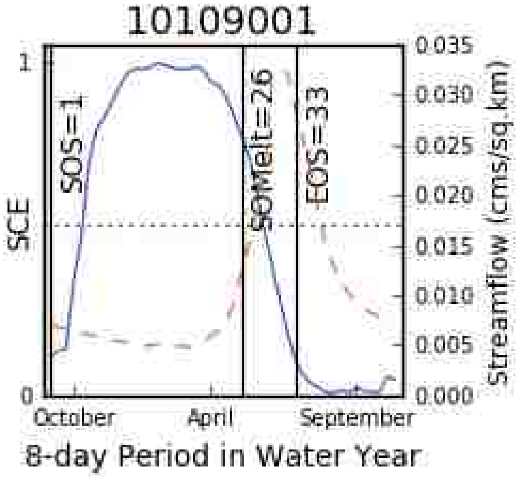
10109001
SCE
Streamflow (cms/sq.km)
SOS=1
SOMelt=26
EOS=33
0
1
0.000
0.005
0.010
0.015
0.020
0.025
0.030
0.035
October
April
September
8-day Period in Water Year

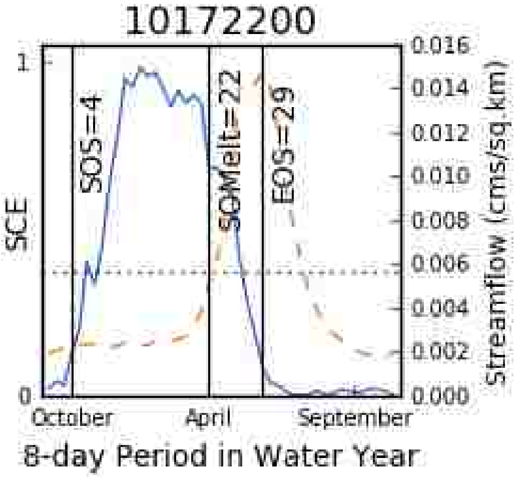
10172200
SCE
Streamflow (cms/sq.km)
SOS=4
SOMelt=22
EOS=29
0
1
0.000
0.002
0.004
0.006
0.008
0.010
0.012
0.014
0.016
October
April
September
8-day Period in Water Year

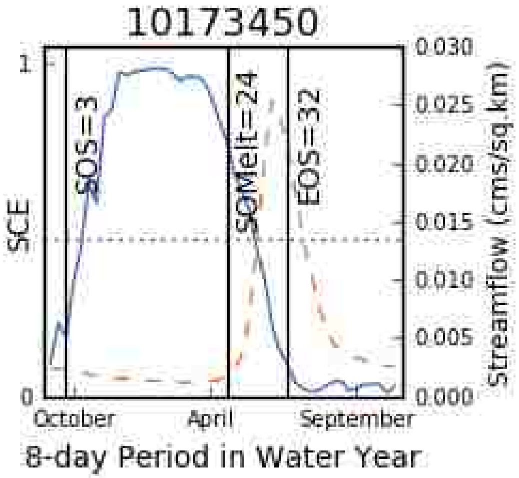
10173450
SCE
1
0
SOS=3
SOMelt=24
EOS=32
0.030
0.025
0.020
0.015
0.010
0.005
0.000
Streamflow (cms/sq.km)
October
April
September
8-day Period in Water Year

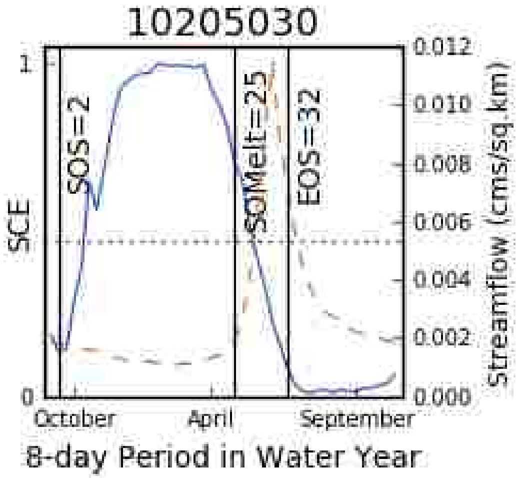
10205030
SCE
1
0
SOS=2
SOMelt=25
EOS=32
0.012
0.010
0.008
0.006
0.004
0.002
0.000
Streamflow (cms/sq.km)
October
April
September
8-day Period in Water Year

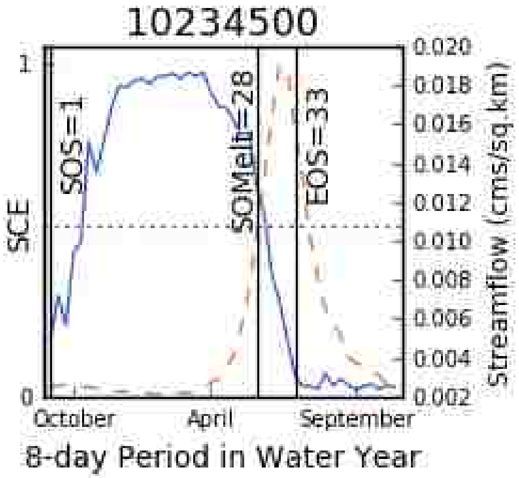
10234500
SCE
1
0
SOS=1
SOMelt=28
EOS=33
0.020
0.018
0.016
0.014
0.012
0.010
0.008
0.006
0.004
0.002
Streamflow (cms/sq.km)
October
April
September
8-day Period in Water Year

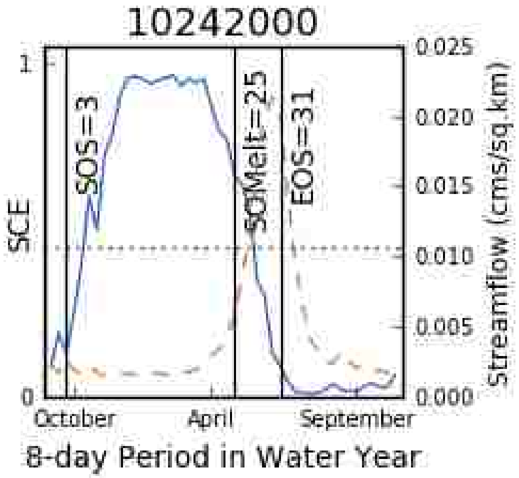
10242000
SCE
1
0
SOS=3
SOMelt=25
EOS=31
0.025
0.020
0.015
0.010
0.005
0.000
Streamflow (cms/sq.km)
October
April
September
8-day Period in Water Year

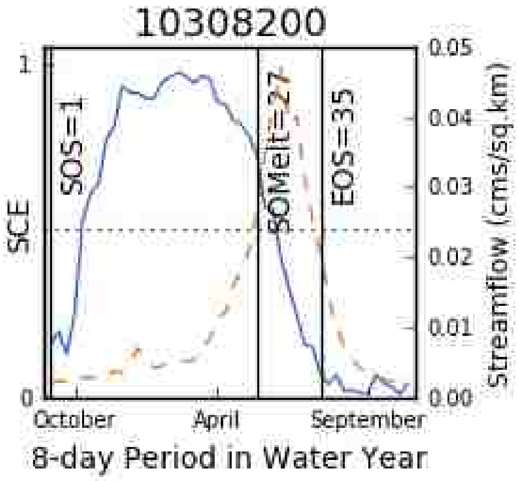
10308200
SCE
1
0
SOS=1
SOMelt=27
EOS=35
0.05
0.04
0.03
0.02
0.01
0.00
Streamflow (cms/sq.km)
October
April
September
8-day Period in Water Year

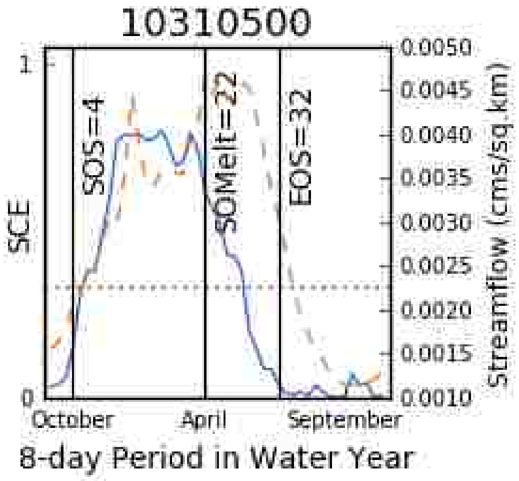
10310500
SCE
1
0
SOS=4
SOMelt=22
EOS=32
0.0050
0.0045
0.0040
0.0035
0.0030
0.0025
0.0020
0.0015
0.0010
Streamflow (cms/sq.km)
October
April
September
8-day Period in Water Year

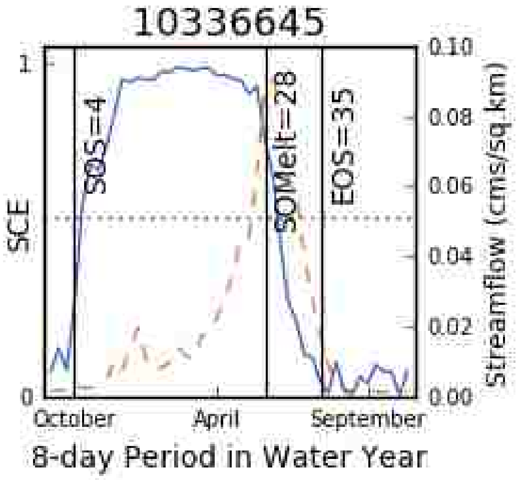
10336645
SCE
1
0
Streamflow (cms/sq.km)
0.10
0.08
0.06
0.04
0.02
0.00
SOS=4
SOMelt=28
EOS=35
October
April
September
8-day Period in Water Year

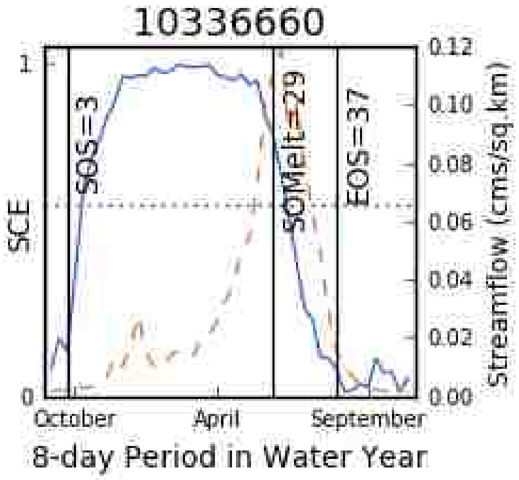
10336660
SCE
1
0
Streamflow (cms/sq.km)
0.12
0.10
0.08
0.06
0.04
0.02
0.00
SOS=3
SOMelt=29
EOS=37
October
April
September
8-day Period in Water Year

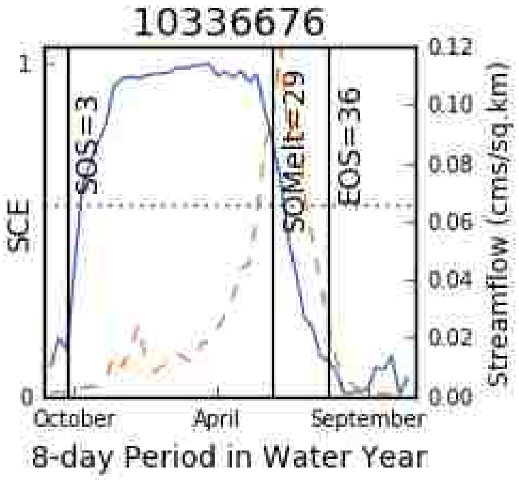
10336676
SCE
1
0
Streamflow (cms/sq.km)
0.12
0.10
0.08
0.06
0.04
0.02
0.00
SOS=3
SOMelt=29
EOS=36
October
April
September
8-day Period in Water Year

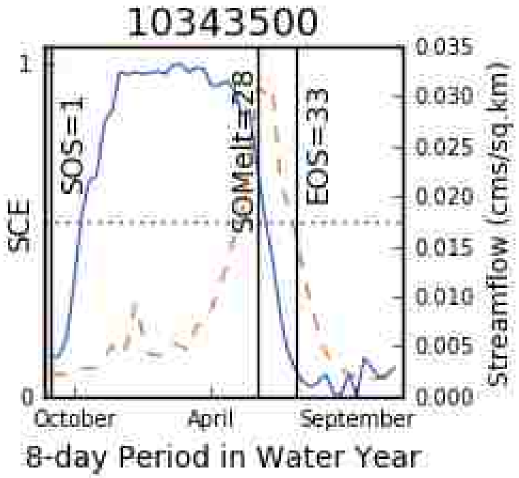
10343500
SCE
1
0
Streamflow (cms/sq.km)
0.035
0.030
0.025
0.020
0.015
0.010
0.005
0.000
SOS=1
SOMelt=28
EOS=33
October
April
September
8-day Period in Water Year

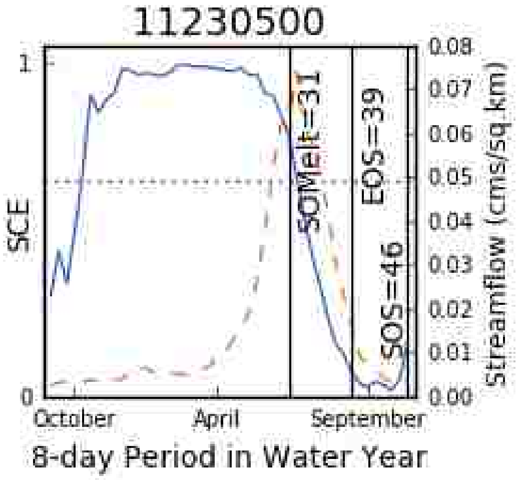
11230500
SCE
1
0
Streamflow (cms/sq.km)
0.08
0.07
0.06
0.05
0.04
0.03
0.02
0.01
0.00
SOMelt=31
EOS=39
SOS=46
October
April
September
8-day Period in Water Year

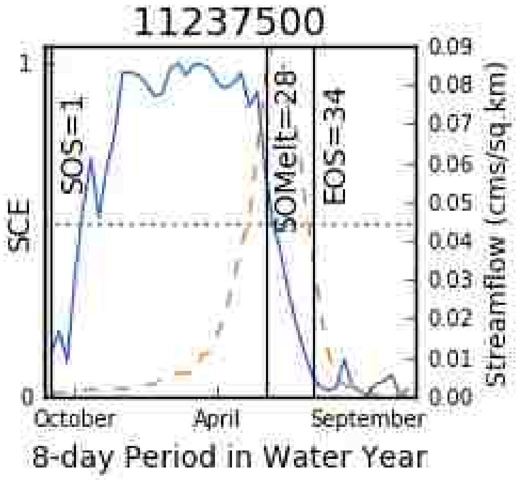
11237500
SCE
1
0
Streamflow (cms/sq.km)
0.09
0.08
0.07
0.06
0.05
0.04
0.03
0.02
0.01
0.00
SOS=1
SOMelt=28
EOS=34
October
April
September
8-day Period in Water Year

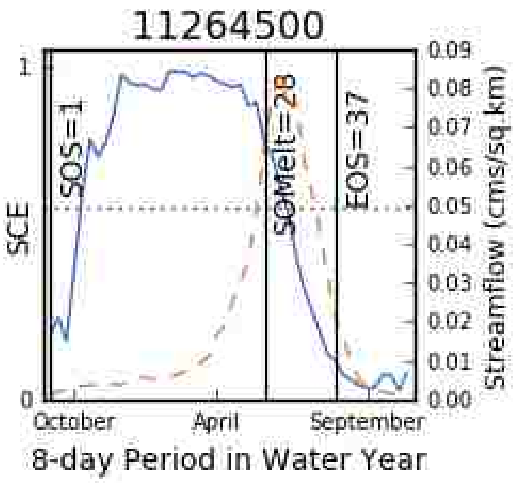
11264500
SOS=1
SOMelt=28
EOS=37
SCE
Streamflow (cms/sq.km)
0
1
0.00
0.01
0.02
0.03
0.04
0.05
0.06
0.07
0.08
0.09
October
April
September
8-day Period in Water Year

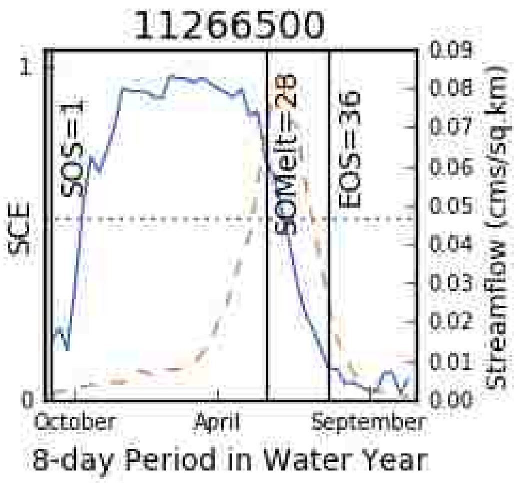
11266500
SOS=1
SOMelt=28
EOS=36
SCE
Streamflow (cms/sq.km)
0
1
0.00
0.01
0.02
0.03
0.04
0.05
0.06
0.07
0.08
0.09
October
April
September
8-day Period in Water Year

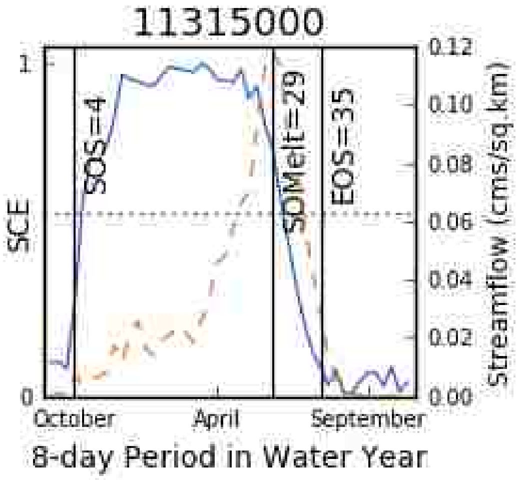
11315000
SOS=4
SOMelt=29
EOS=35
SCE
Streamflow (cms/sq.km)
0
1
0.00
0.02
0.04
0.06
0.08
0.10
0.12
October
April
September
8-day Period in Water Year

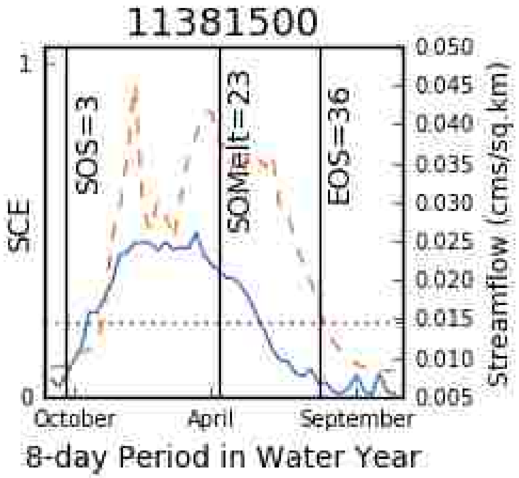
11381500
SOS=3
SOMelt=23
EOS=36
SCE
Streamflow (cms/sq.km)
0
1
0.005
0.010
0.015
0.020
0.025
0.030
0.035
0.040
0.045
0.050
October
April
September
8-day Period in Water Year

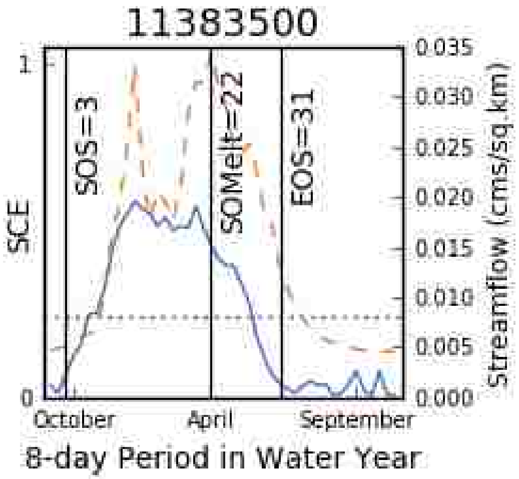
11383500
SOS=3
SOMelt=22
EOS=31
SCE
Streamflow (cms/sq.km)
0
1
0.000
0.005
0.010
0.015
0.020
0.025
0.030
0.035
October
April
September
8-day Period in Water Year

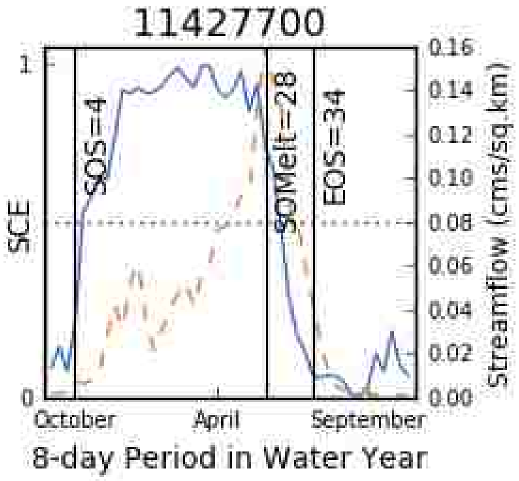
11427700
SOS=4
SOMelt=28
EOS=34
SCE
Streamflow (cms/sq.km)
0
1
0.00
0.02
0.04
0.06
0.08
0.10
0.12
0.14
0.16
October
April
September
8-day Period in Water Year

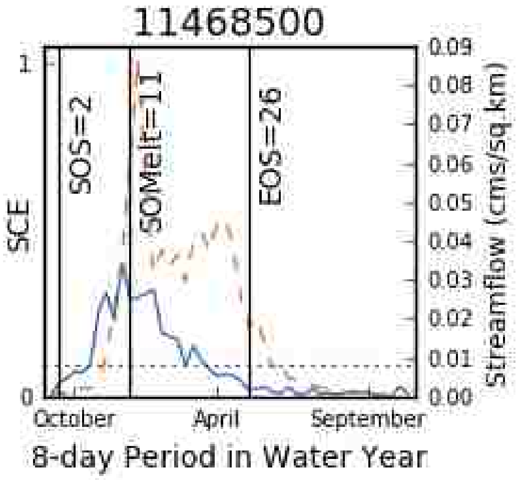
11468500
SCE
1
0
SOS=2
SOMelt=11
EOS=26
0.09
0.08
0.07
0.06
0.05
0.04
0.03
0.02
0.01
0.00
Streamflow (cms/sq.km)
October
April
September
8-day Period in Water Year

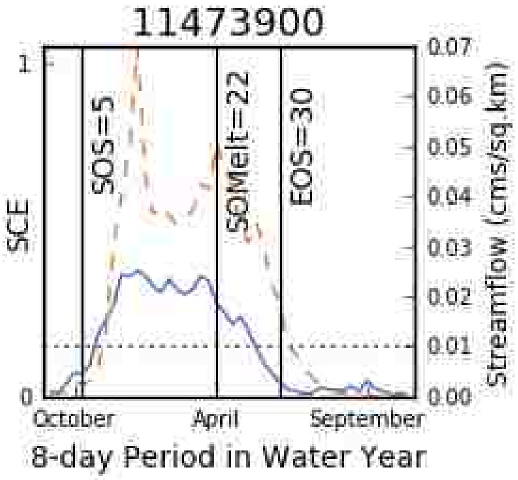
11473900
SCE
1
0
SOS=5
SOMelt=22
EOS=30
0.07
0.06
0.05
0.04
0.03
0.02
0.01
0.00
Streamflow (cms/sq.km)
October
April
September
8-day Period in Water Year

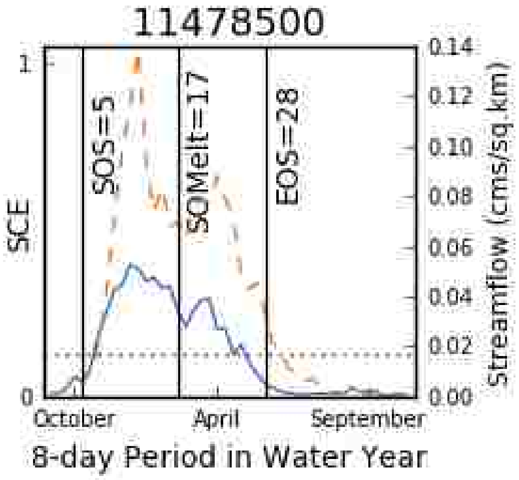
11478500
SCE
1
0
SOS=5
SOMelt=17
EOS=28
0.14
0.12
0.10
0.08
0.06
0.04
0.02
0.00
Streamflow (cms/sq.km)
October
April
September
8-day Period in Water Year

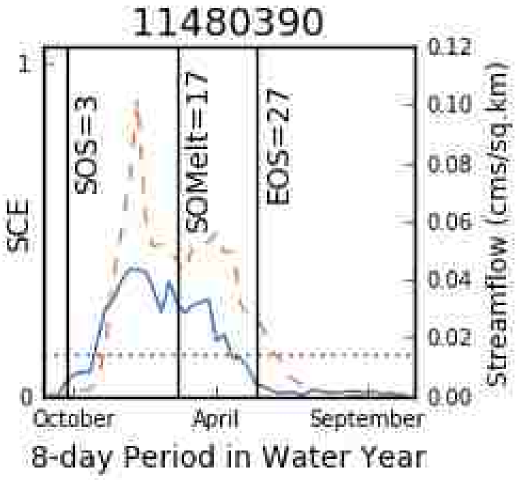
11480390
SCE
1
0
SOS=3
SOMelt=17
EOS=27
0.12
0.10
0.08
0.06
0.04
0.02
0.00
Streamflow (cms/sq.km)
October
April
September
8-day Period in Water Year

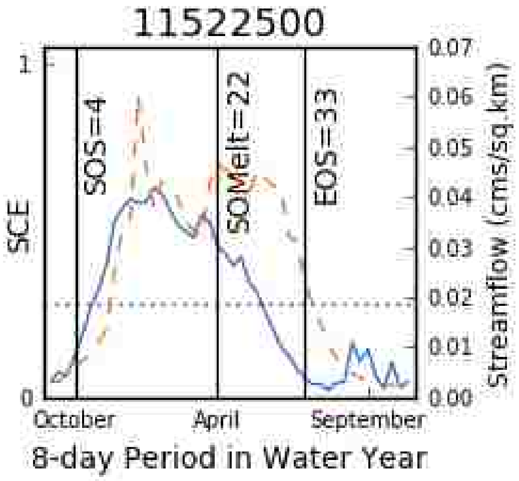
11522500
SCE
1
0
SOS=4
SOMelt=22
EOS=33
0.07
0.06
0.05
0.04
0.03
0.02
0.01
0.00
Streamflow (cms/sq.km)
October
April
September
8-day Period in Water Year

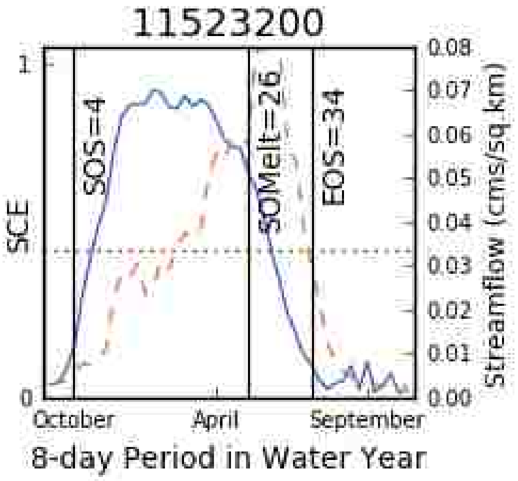
11523200
SCE
1
0
SOS=4
SOMelt=26
EOS=34
0.08
0.07
0.06
0.05
0.04
0.03
0.02
0.01
0.00
Streamflow (cms/sq.km)
October
April
September
8-day Period in Water Year

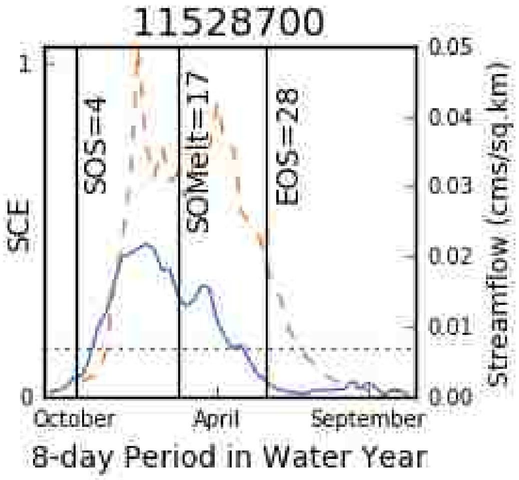
11528700
SCE
1
0
SOS=4
SOMelt=17
EOS=28
0.05
0.04
0.03
0.02
0.01
0.00
Streamflow (cms/sq.km)
October
April
September
8-day Period in Water Year

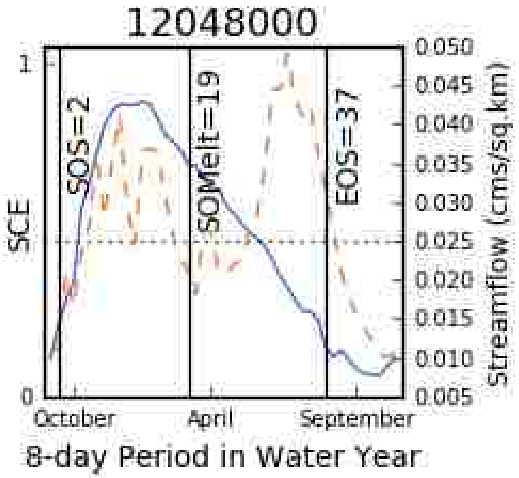
12048000
SCE
1
0
SOS=2
SOMelt=19
EOS=37
0.050
0.045
0.040
0.035
0.030
0.025
0.020
0.015
0.010
0.005
Streamflow (cms/sq.km)
October
April
September
8-day Period in Water Year

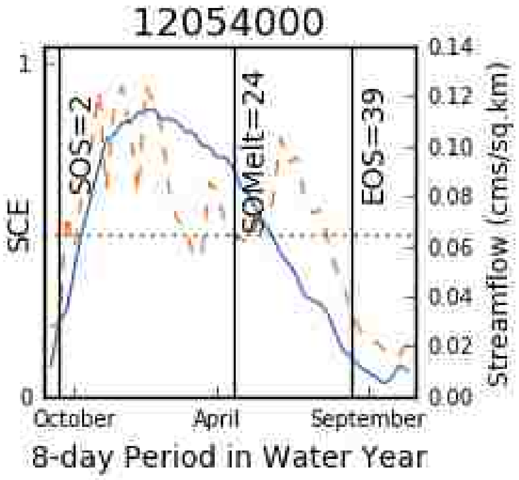
12054000
SCE
1
0
SOS=2
SOMelt=24
EOS=39
0.14
0.12
0.10
0.08
0.06
0.04
0.02
0.00
Streamflow (cms/sq.km)
October
April
September
8-day Period in Water Year

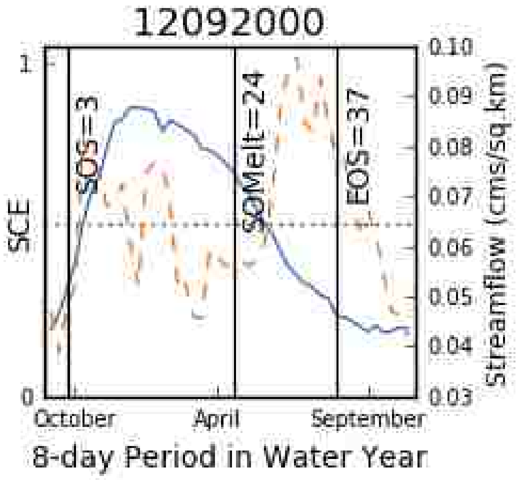
12092000
SCE
1
0
SOS=3
SOMelt=24
EOS=37
0.10
0.09
0.08
0.07
0.06
0.05
0.04
0.03
Streamflow (cms/sq.km)
October
April
September
8-day Period in Water Year

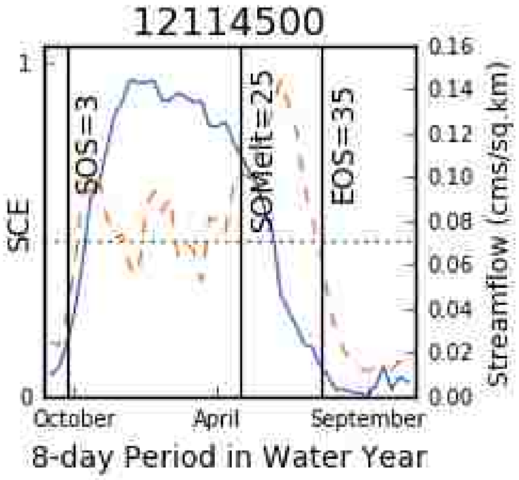
12114500
SCE
1
0
SOS=3
SOMelt=25
EOS=35
0.16
0.14
0.12
0.10
0.08
0.06
0.04
0.02
0.00
Streamflow (cms/sq.km)
October
April
September
8-day Period in Water Year

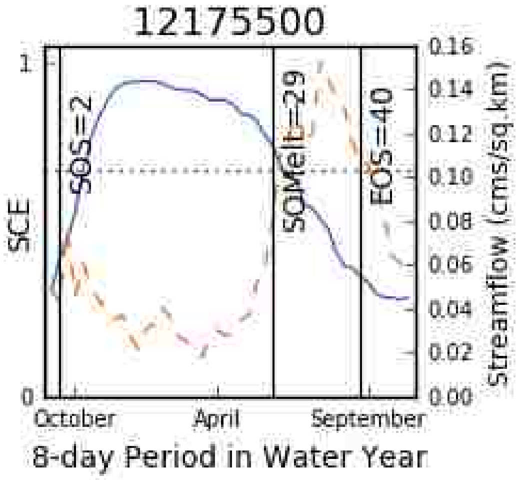
12175500
SCE
1
0
SOS=2
SOMelt=29
EOS=40
0.16
0.14
0.12
0.10
0.08
0.06
0.04
0.02
0.00
Streamflow (cms/sq.km)
October
April
September
8-day Period in Water Year

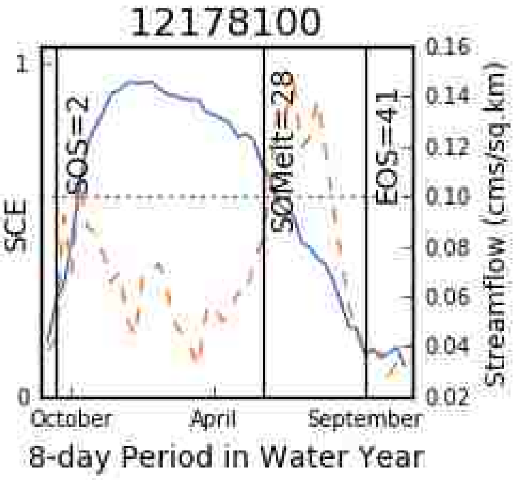
12178100
SCE
Streamflow (cms/sq.km)
SOS=2
SOMelt=28
EOS=41
October
April
September
8-day Period in Water Year

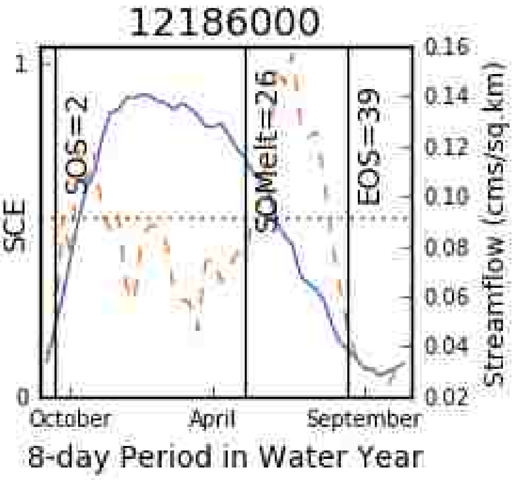
12186000
SCE
Streamflow (cms/sq.km)
SOS=2
SOMelt=26
EOS=39
October
April
September
8-day Period in Water Year

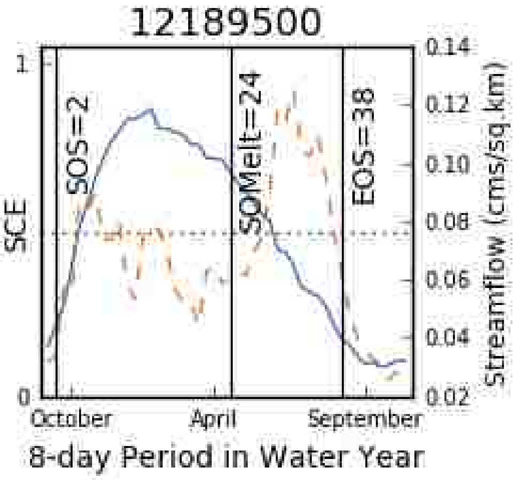
12189500
SCE
Streamflow (cms/sq.km)
SOS=2
SOMelt=24
EOS=38
October
April
September
8-day Period in Water Year

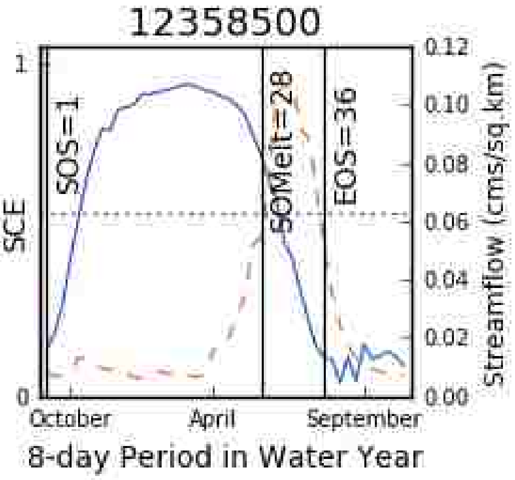
12358500
SCE
Streamflow (cms/sq.km)
SOS=1
SOMelt=28
EOS=36
October
April
September
8-day Period in Water Year

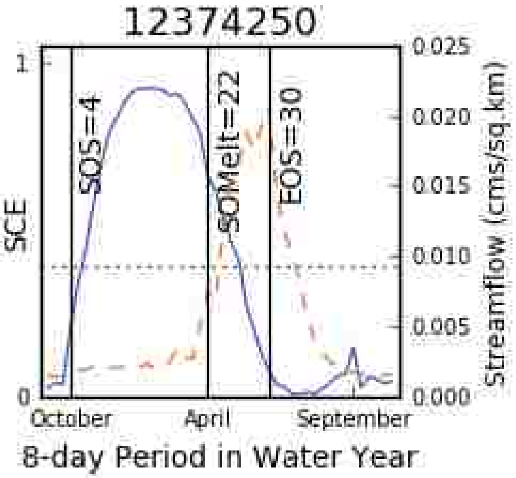
12374250
SCE
Streamflow (cms/sq.km)
SOS=4
SOMelt=22
EOS=30
October
April
September
8-day Period in Water Year

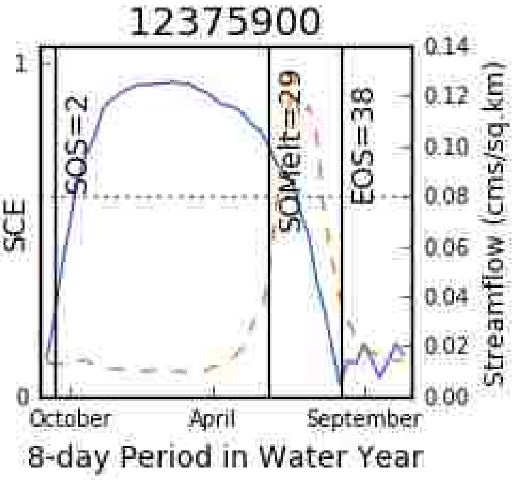
12375900
SCE
Streamflow (cms/sq.km)
SOS=2
SOMelt=29
EOS=38
October
April
September
8-day Period in Water Year

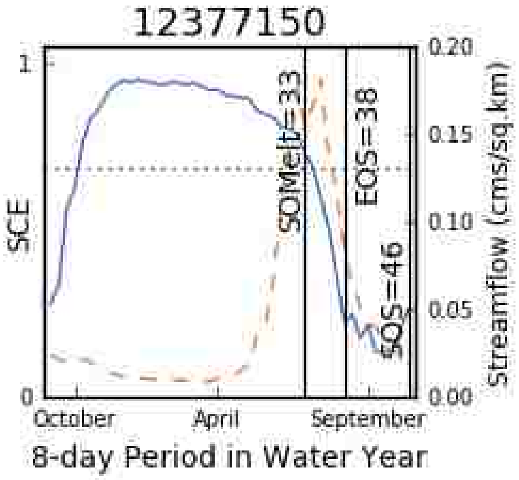
12377150
SCE
Streamflow (cms/sq.km)
SOMelt=33
EOS=38
SOS=46
0
1
0.00
0.05
0.10
0.15
0.20
October
April
September
8-day Period in Water Year

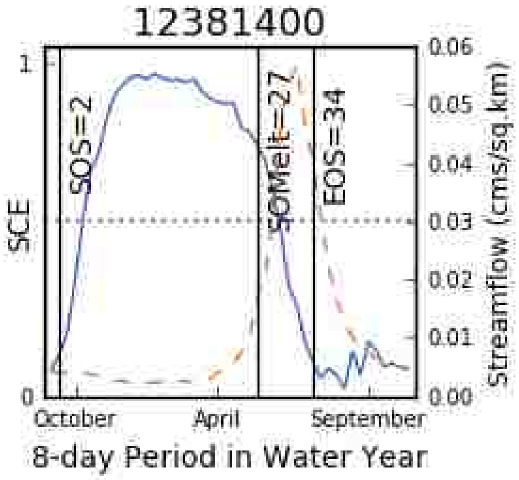
12381400
SCE
Streamflow (cms/sq.km)
SOS=2
SOMelt=27
EOS=34
0
1
0.00
0.01
0.02
0.03
0.04
0.05
0.06
October
April
September
8-day Period in Water Year

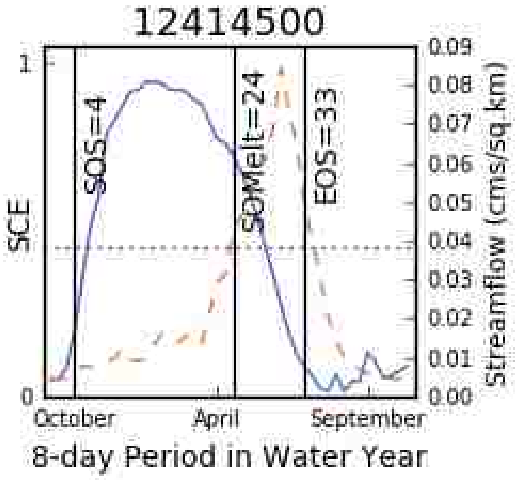
12414500
SCE
Streamflow (cms/sq.km)
SOS=4
SOMelt=24
EOS=33
0
1
0.00
0.01
0.02
0.03
0.04
0.05
0.06
0.07
0.08
0.09
October
April
September
8-day Period in Water Year

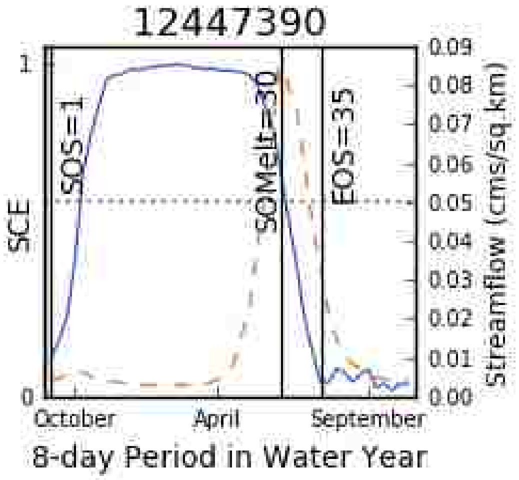
12447390
SCE
Streamflow (cms/sq.km)
SOS=1
SOMelt=30
EOS=35
0
1
0.00
0.01
0.02
0.03
0.04
0.05
0.06
0.07
0.08
0.09
October
April
September
8-day Period in Water Year

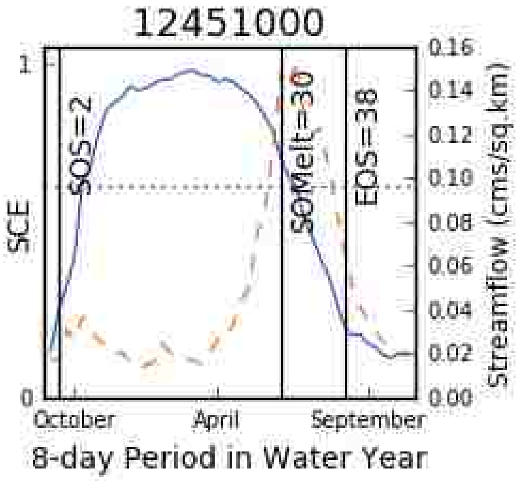
12451000
SCE
Streamflow (cms/sq.km)
SOS=2
SOMelt=30
EOS=38
0
1
0.00
0.02
0.04
0.06
0.08
0.10
0.12
0.14
0.16
October
April
September
8-day Period in Water Year

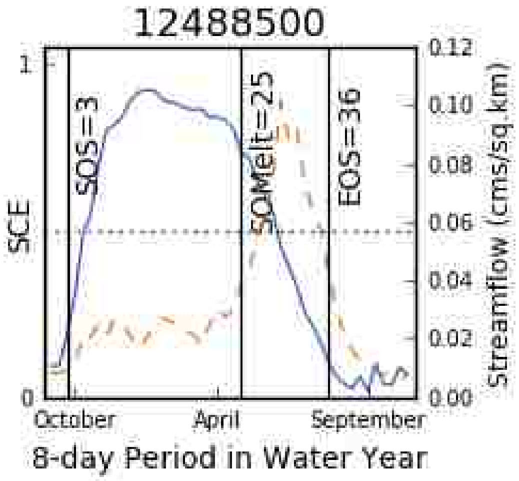
12488500
SCE
Streamflow (cms/sq.km)
SOS=3
SOMelt=25
EOS=36
0
1
0.00
0.02
0.04
0.06
0.08
0.10
0.12
October
April
September
8-day Period in Water Year

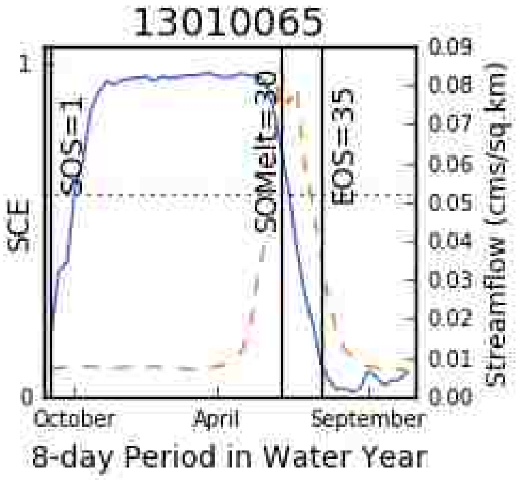
13010065
SCE
1
0
SOS=1
SOMelt=30
EOS=35
0.09
0.08
0.07
0.06
0.05
0.04
0.03
0.02
0.01
0.00
Streamflow (cms/sq.km)
October
April
September
8-day Period in Water Year

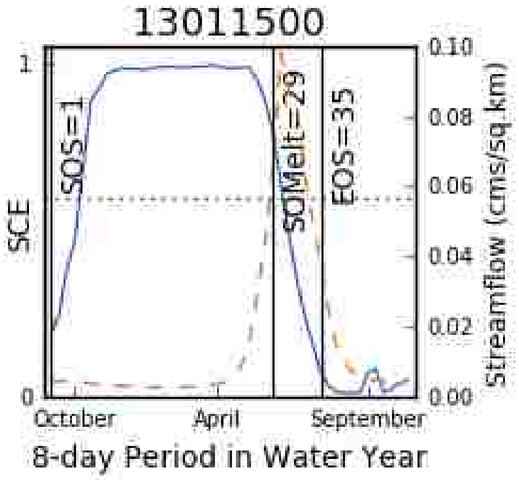
13011500
SCE
1
0
SOS=1
SOMelt=29
EOS=35
0.10
0.08
0.06
0.04
0.02
0.00
Streamflow (cms/sq.km)
October
April
September
8-day Period in Water Year

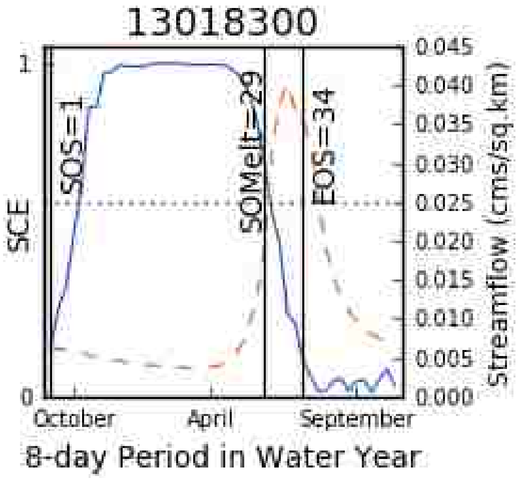
13018300
SCE
1
0
SOS=1
SOMelt=29
EOS=34
0.045
0.040
0.035
0.030
0.025
0.020
0.015
0.010
0.005
0.000
Streamflow (cms/sq.km)
October
April
September
8-day Period in Water Year

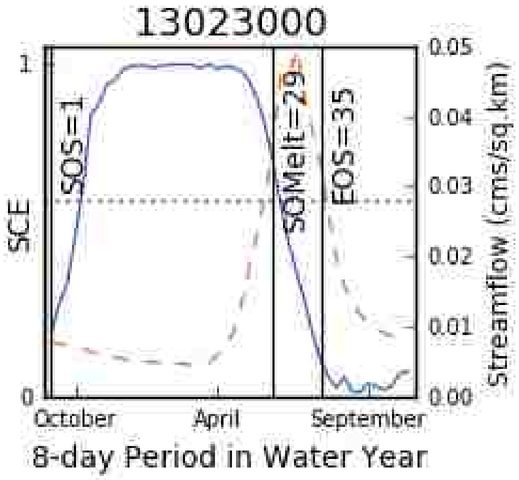
13023000
SCE
1
0
SOS=1
SOMelt=29
EOS=35
0.05
0.04
0.03
0.02
0.01
0.00
Streamflow (cms/sq.km)
October
April
September
8-day Period in Water Year

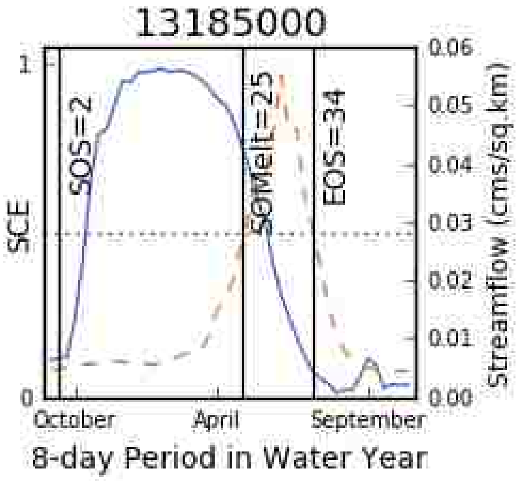
13185000
SCE
1
0
SOS=2
SOMelt=25
EOS=34
0.06
0.05
0.04
0.03
0.02
0.01
0.00
Streamflow (cms/sq.km)
October
April
September
8-day Period in Water Year

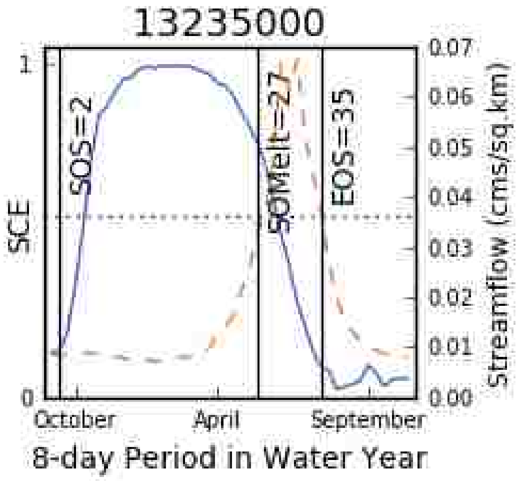
13235000
SCE
1
0
SOS=2
SOMelt=27
EOS=35
0.07
0.06
0.05
0.04
0.03
0.02
0.01
0.00
Streamflow (cms/sq.km)
October
April
September
8-day Period in Water Year

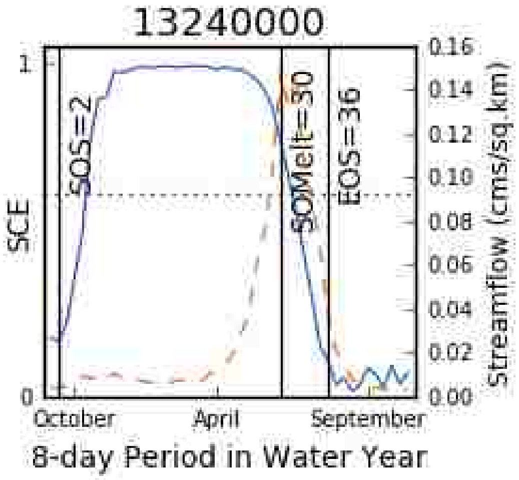
13240000
SCE
1
0
SOS=2
SOMelt=30
EOS=36
0.16
0.14
0.12
0.10
0.08
0.06
0.04
0.02
0.00
Streamflow (cms/sq.km)
October
April
September
8-day Period in Water Year

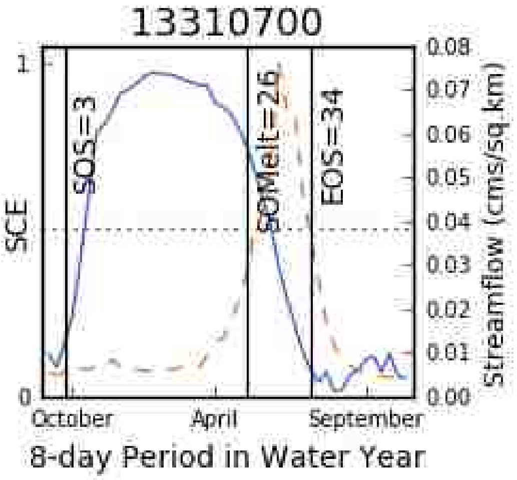
13310700
SCE
1
0
SOS=3
SOMelt=26
EOS=34
0.08
0.07
0.06
0.05
0.04
0.03
0.02
0.01
0.00
Streamflow (cms/sq.km)
October
April
September
8-day Period in Water Year

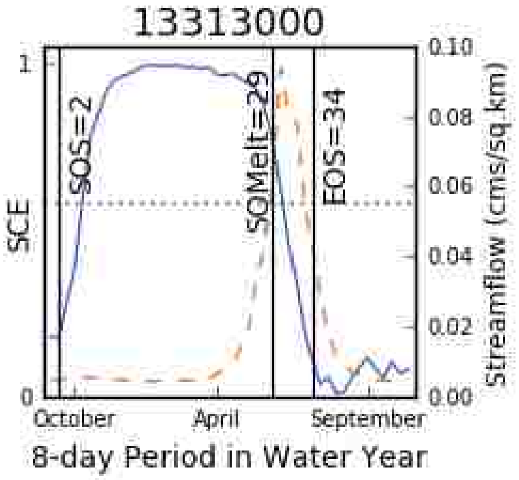
13313000
SCE
1
0
SOS=2
SOMelt=29
EOS=34
0.10
0.08
0.06
0.04
0.02
0.00
Streamflow (cms/sq.km)
October
April
September
8-day Period in Water Year

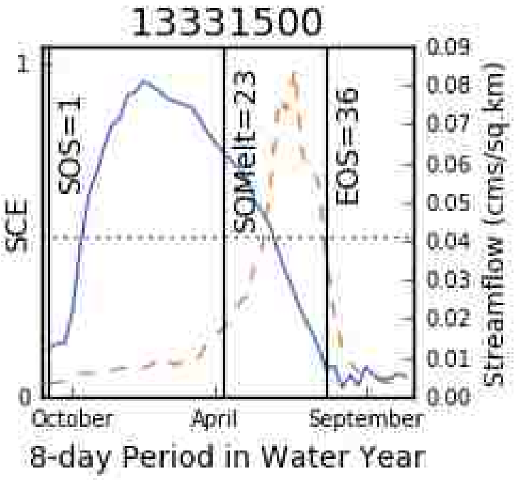
13331500
SCE
1
0
SOS=1
SOMelt=23
EOS=36
0.09
0.08
0.07
0.06
0.05
0.04
0.03
0.02
0.01
0.00
Streamflow (cms/sq.km)
October
April
September
8-day Period in Water Year

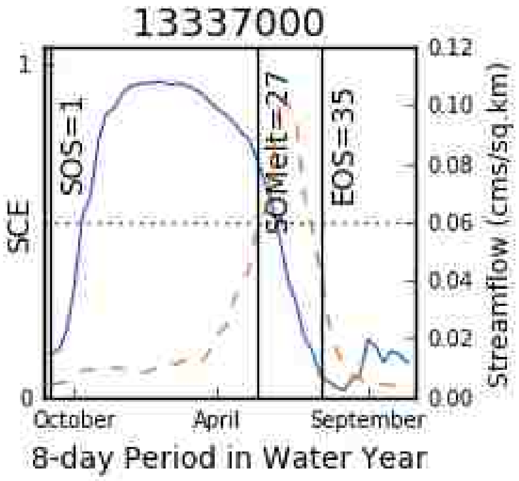
13337000
SCE
1
0
SOS=1
SOMelt=27
EOS=35
0.12
0.10
0.08
0.06
0.04
0.02
0.00
Streamflow (cms/sq.km)
October
April
September
8-day Period in Water Year

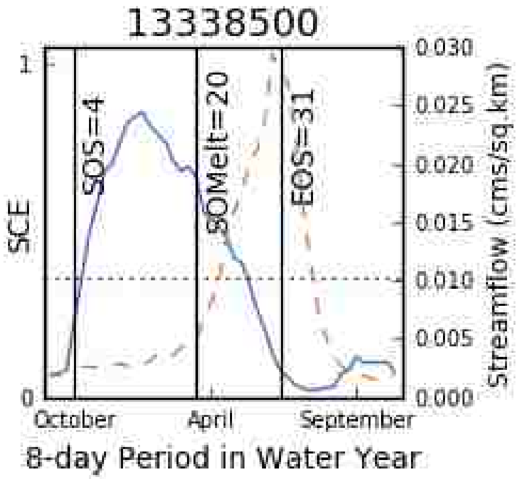
13338500
SCE
1
0
SOS=4
SOMelt=20
EOS=31
0.030
0.025
0.020
0.015
0.010
0.005
0.000
Streamflow (cms/sq.km)
October
April
September
8-day Period in Water Year

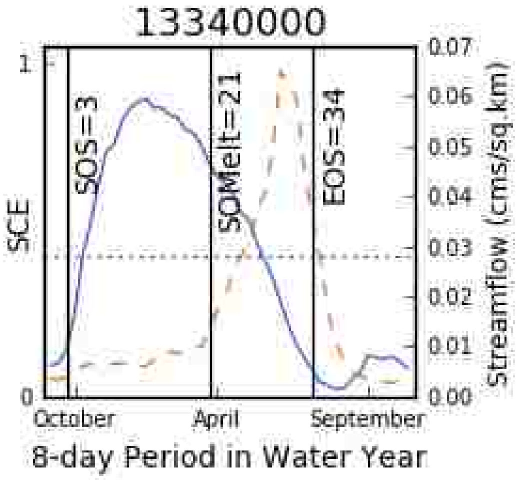
13340000
SCE
0
1
SOS=3
SOMelt=21
EOS=34
Streamflow (cms/sq.km)
0.00
0.01
0.02
0.03
0.04
0.05
0.06
0.07
October
April
September
8-day Period in Water Year

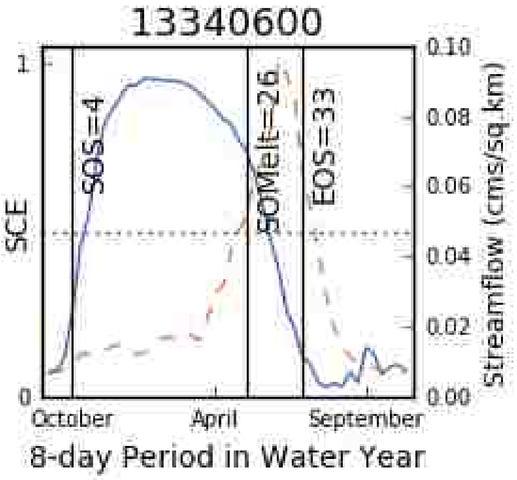
13340600
SCE
0
1
SOS=4
SOMelt=26
EOS=33
Streamflow (cms/sq.km)
0.00
0.02
0.04
0.06
0.08
0.10
October
April
September
8-day Period in Water Year

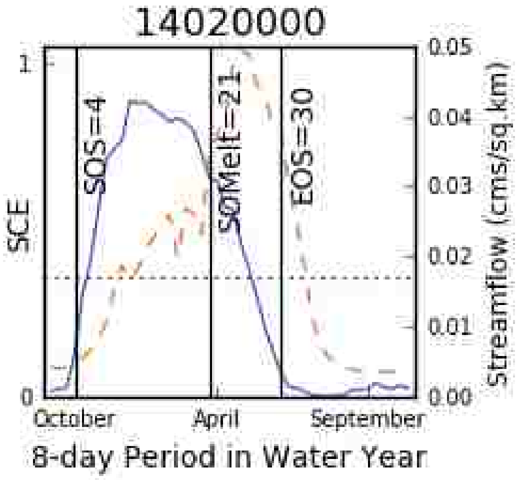
14020000
SCE
0
1
SOS=4
SOMelt=21
EOS=30
Streamflow (cms/sq.km)
0.00
0.01
0.02
0.03
0.04
0.05
October
April
September
8-day Period in Water Year

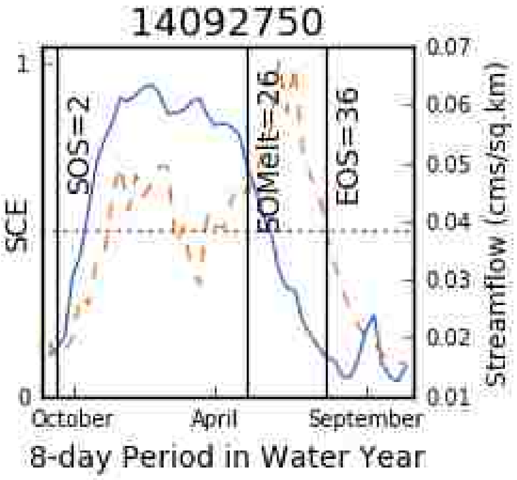
14092750
SCE
0
1
SOS=2
SOMelt=26
EOS=36
Streamflow (cms/sq.km)
0.01
0.02
0.03
0.04
0.05
0.06
0.07
October
April
September
8-day Period in Water Year

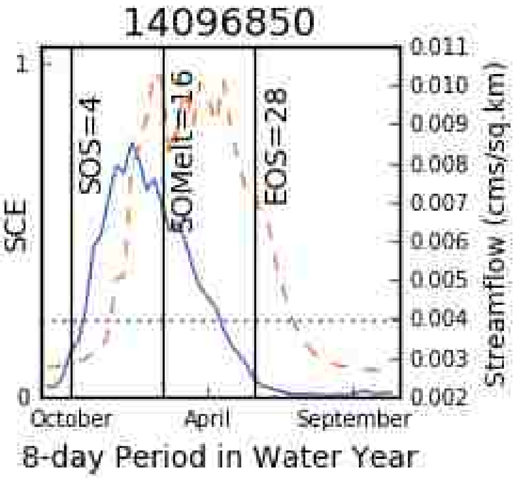

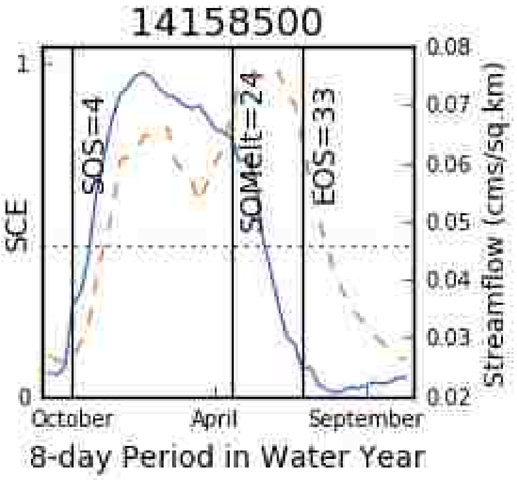

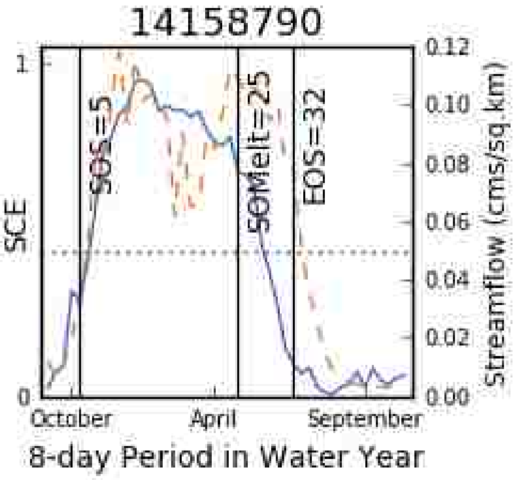

The script below takes the snow cover extent for the average water year for each watershed and calculates the appropriate SCE metrics as detailed in Section 2.6.

```
import re
import csv
import os
import sys


#############################################
### Input: text file with gage ID's for each basin. These gage IDs are used to get the appropriate
### CSV from "../Results_SCE/" that contains 8-day SCE data for an "average" water year.
###
### Output: CSV file with each line as the SCE metrics for a given gage.
###########################################

### Define the workspace (but NOT the arcpy.env.workspace)
workspace = "D:/Thesis/"

### Get the text file of gage ID's from the command line.
if len(sys.argv) != 2:
    print "Need this form: python modis-sce-metrics.py <gage_IDs.txt>"
    print sys.argv
    sys.exit()

gageFilename = sys.argv[1]
inputFolder = os.path.join(workspace, "Results_SCE/")

### Open the gage ID file and create a list of the gage IDs.
gageFile = open(gageFilename, 'r+')
reader = csv.reader(gageFile, delimiter=',')

gages = []
for row in reader:
    # QC for row format
    if len(row) != 1:
        print "Improper text file format. One gageID per row: %s" % row
        sys.exit()

    # Get the gage ID and add it to the "gages" list.
    gages.append(row[0])

### Open the output file and write the header.
outfileName = os.path.join(workspace, "Results_Metrics/sce-metrics.csv")
outfile = open(outfileName, 'wb')
writer = csv.writer(outfile, delimiter=',')
writer.writerow(['Gage ID', 'SOS', 'EOS', 'LOS', 'Min SCE', 'POWY Min SCE', 'Peak SCE', 'POWY Peak SCE', 'Avg Peak SCE', 'Avg SCE', 'SOMain', 'SOMelt', 'Persistence', 'LOMelt'])

############
### Main ###
############
for gageID in gages:

    print "Processing gage %s" % gageID

    ### Locate the sce file labeled "sce-averages-<gageID>.csv".
    sceFilename = os.path.join(inputFolder, "sce-averages-%s.csv" % gageID)
    if not os.path.exists(sceFilename):
        print "The snow directory does not exist: %s" % sceFilename
        sys.exit()


    ##############################
    ### Read in the SCE values ###
    ##############################
    sceFile = open(sceFilename, 'r+')
    sceReader = csv.reader(sceFile, delimiter=',')

    # Skip the header.
    sceReader.next()

    # Read the rows into a buffer so the algorithm can skip around.
    rows = []
    for row in sceReader:
        rows.append(row)

    # Set record length, N, and make sure there are 46 of them to match
    # the number of 8-day periods in a water year.
    N = len(rows)
    if N != 46:
        print "There are not enough SCE records for gage %s " % gageID
        sys.exit()


    ##########################################################################
    ### Iterate through the rows and pick out the first set of SCE metrics ###
    ##########################################################################

    peakSCE = None
    datePeakSCE = None
    minSCE = rows[0][1] # set minSCE as first values in water year
    dateMinSCE = rows[0][0] # set date of minSCE as first period of water year (powy)
    sumSCE = 0.0

    i = 0
    while i < N:

        data = rows[i]
        powy = int(data[0]) # period of water year
        sce = float(data[1]) # snow cover extent as proportion of watershed

        # Check to see if this value exceeds the current peakSCE.
            if sce >= peakSCE:
                peakSCE = sce
                datePeakSCE = powy

            # Check to see if this value is below the current minSCE.
            if sce <= minSCE:
                minSCE = sce
                dateMinSCE = powy

            # Add to sumSCE to average later into AvgSCE.
            sumSCE = sumSCE + sce

            # Increment the index.
            i = i + 1

        # Calculate average SCE.
        avgSCE = sumSCE / N


        #################################################################
        ### Iterate through rows and pick out secondary set of metrics. ###
        #################################################################

        # The main snow season is defined as the periods which are
     all consecutive and within - 20% of the peakSCE.
        mainThreshold = peakSCE - (0.2*peakSCE)

    # The snow season is defined as the periods which are
all consecutive and are above the minimum SCE by 10% of the maximum SCE.
    # This definition helps account for permanent snowpacks at high
elevations and watersheds with low maximum SCEs.
    allThreshold = minSCE + (0.1*peakSCE)

    SOS = None
    EOS = None
    SOMain = None
    SOMelt = None
    sosFound = False
    origSOS = None
    i = 0
    while i < N:

        data = rows[i]
        powy = int(data[0])
        sce = float(data[1])

        # If the start of the snow season has not been found and
this SCE is over the allThreshold,
        # Then check to see if the next period is increasing.
        # If yes, then mark the original POWY as the SOS.
        if not SOS and sce >= allThreshold:

            isGood = True
            prevSCE = sce
            for m in [1]:
                j = i + m
                currSCE = float(rows[j][1])

                if currSCE < prevSCE:
                    isGood = False
                    break

                prevSCE = currSCE

            if isGood:
                SOS = powy

        # Restart the season for early, temporary snow.
        elif SOS and not SOMain and sce < allThreshold:
            SOS = None

        # If the snow season has started but not yet ended and this sce

        # is less than allThreshold, set EOS to current period.
        elif SOS and not EOS and sce < allThreshold:
            EOS = powy

        # If the snow season has started and the sce is above the
        # mainThreshold, SOMain (start of main season) is set to
current period.
        if SOS and not SOMain and sce >= mainThreshold:
            SOMain = powy

        # If the main snow season has started but not yet melted and
        # this sce is less than the mainThreshold, set SOMelt to current
period.
        elif SOMain and not SOMelt and sce < mainThreshold:
            SOMelt = powy

            # If the SCE goes back above the mainThreshold, reopen the main
    season.
            elif SOMelt and sce >= mainThreshold:
                SOMelt = None

            # If SCE goes back above the allThreshold and the main season
            # hasn't started (i.e. SOMain = None), reopen the snow season.
            elif EOS and not SOMain and sce >= allThreshold:
                EOS = None

            # Catch SOS's that fall before the start of the water year.
            # Make sure false spikes at end of season don't trigger it by
            # checking if it's greater than 2 periods away from EOS.
            elif SOS and EOS and not sosFound and sce >= allThreshold:

                if (powy - EOS) > 2:

                    origSOS = SOS
                    SOS = (powy - 46) - 1
                    sosFound = True

            # Catch false SOS's that are temporary early snow that triggered
     the case above.
            elif SOS and EOS and sosFound and sce < allThreshold:

                SOS = origSOS
                sosFound = False

            # Increment the index.
            i = i + 1


        # Calculate the duration of the snow season from SOS and EOS.
        LOS = EOS - SOS

        # Calculate the persistence of the snow season from SOMain and SOMelt.
        persistence = SOMelt - SOMain + 1

        # Calculate the length of the snow melt from EOS and SOMelt.
        LOMelt = EOS - SOMelt + 1


        ##############################################################
        ### Iterate through the rows and calculate the AvgPeakSCE. ###
        ##############################################################
        i = 0
        sumPeakSCE = 0.0
        while i < N:

            data = rows[i]
            powy = int(data[0])
            sce = float(data[1])

            if powy >= SOMain and powy < SOMelt:
                sumPeakSCE = sumPeakSCE + sce

            # Increment the index.
            i = i + 1

        # Calculate average peak SCE.
        avgPeakSCE = sumPeakSCE / (SOMelt - SOMain)


        ##################################
        ### Write out the SCE metrics ###
        ##################################

        outRow = [gageID, SOS, EOS, LOS, minSCE, dateMinSCE, peakSCE,
    datePeakSCE, avgPeakSCE, avgSCE, SOMain, SOMelt, persistence, LOMelt]
        writer.writerow(outRow)


    ### Close the output file.
    outfile.close()


    print "Done!"
```

Appendix D: Selecting metrics for analysis

Dozens of metrics were originally gathered from SWE, SCE, streamflow, and PRISM datasets for each watershed. A correlational analysis was done to generate the R and p values for each possible linear regression pairing. The R values for the analysis are shown in the images below. This data was used to determine which values were redundant or irrelevant to pinpoint the most important set of variables. The final metrics are SOS, SOMelt, EOS, AvgSCE, AvgAnnualTemp, AvgAnnualPPT, PeakSWE, and PeakQ. See Appendix A for the definition of each metric.

	SOS	EOS	LOS	MinSCE	POWYMinSCE	PeakSCE
SOS	1	-0.7961	-0.91901	-0.40621	-0.434605295	-0.671641256
EOS	-0.79612	1	0.97021	0.601408	0.559156232	0.734134173
LOS	-0.91901	0.97021	1	0.554432	0.538273812	0.747167837
MinSCE	-0.40621	0.60141	0.55443	1	0.339961932	0.155715709
POWYMinSCE	-0.43461	0.55916	0.53827	0.339962	1	0.274847725
PeakSCE	-0.67164	0.73413	0.74717	0.155716	0.274847725	1
POWYPeakSCE	-0.41591	0.36313	0.40308	-0.10439	0.158010889	0.445641351
AvgPeakSCE	-0.68656	0.73421	0.75319	0.142433	0.288650523	0.995632562
AvgSCE	-0.86642	0.89804	0.93193	0.349821	0.453709932	0.865625251
SOMain	0.783044	-0.6007	-0.70481	-0.25986	-0.341003943	-0.392523354
SOMelt	-0.74674	0.77782	0.8057	0.271947	0.46650833	0.581036572
Persistence	-0.80682	0.76725	0.82286	0.285215	0.453623085	0.554033889
LOMelt	-0.32985	0.61522	0.53286	0.615657	0.3043879	0.439099508
VarianceAvgSCE	0.293284	-0.1287	-0.20124	-0.08385	0.028757346	-0.03928979
VariancePeakSCE	0.509622	-0.6341	-0.61715	-0.13377	-0.172438678	-0.8421214
VariancePeakQcms	0.095278	-0.0305	-0.05803	0.007472	-0.000500106	-0.140795104
VariancePeakQnormcmssqkm	0.055105	0.0587	0.01618	0.064839	0.311797286	-0.185247644
Q20	-0.48985	0.37326	0.43929	-0.03353	0.057541253	0.497080307
Q50	-0.66821	0.63814	0.68326	0.204673	0.114617339	0.724880441
Q80	-0.53115	0.51403	0.54753	0.319676	0.010828972	0.499030934
PeakPOWY	-0.50534	0.49678	0.52596	0.258423	0.002943115	0.601418627
PeakQcms	0.017572	0.09868	0.05725	0.098144	0.016760136	-0.009002602
PeakQnormbyDrainageAreacmssqkm	-0.42848	0.60989	0.56887	0.425918	0.536858477	0.231715536
PeakQnormbyMeanAnnualPeak	0.048168	0.08179	0.034	0.117572	0.0557362	-0.083948425
PeakQnormbyMeanAnnualMean	-0.1834	0.00393	0.07599	-0.22875	-0.091783675	0.165129485
SCEatPeakQ	-0.3913	0.50801	0.48762	0.161326	0.53133416	0.246753006
DRAIN_SQKM	0.108059	-0.0503	-0.07606	0.014349	-0.125706901	-0.101571587
LAT_GAGE	-0.3905	0.532	0.50292	0.435553	0.283160998	0.31813897
LNG_GAGE	-0.22951	-0.0772	0.04157	-0.21929	-0.492758058	0.213985409
Meanm	-0.47911	0.28848	0.37976	-0.10806	-0.038842241	0.487531496
Minm	-0.42673	0.17279	0.28342	-0.24942	-0.088498754	0.474847446
Maxm	-0.4642	0.36399	0.42298	0.121505	0.045317526	0.368885967
Rangem	0.016863	0.20338	0.12574	0.47895	0.172572497	-0.195079553
MeanAnnualpptmm	-0.11845	0.40322	0.31011	0.473461	0.445125697	-0.014980719
MeanAnnualtmeanC	0.835218	-0.729	-0.80929	-0.2333	-0.20369349	-0.791966739
MeanAnnualtminC	0.742355	-0.5637	-0.66443	-0.09289	-0.079178559	-0.711805481
MeanAnnualtmaxC	0.860589	-0.8248	-0.88187	-0.3405	-0.298971952	-0.809121787
MeanDecMarpptmm	0.018309	0.28412	0.17776	0.359056	0.508379903	-0.11749991
MeanAprJulpptmm	-0.43719	0.53729	0.52506	0.423123	0.164225705	0.260309117
MeanAugNovpptmm	-0.18586	0.42957	0.35427	0.564894	0.302293535	0.053998054
MeanDecMartmeanC	0.756764	-0.6073	-0.69863	-0.12792	-0.056196828	-0.747290516
MeanAprJultmeanC	0.869929	-0.8271	-0.88709	-0.32463	-0.389776591	-0.791732056
MeanAugNovtmeanC	0.831453	-0.7274	-0.80677	-0.25765	-0.194226214	-0.783091483
MeanDecMartminC	0.6385	-0.4331	-0.5378	0.003028	0.067955936	-0.648312949
MeanAprJultminC	0.816018	-0.7035	-0.78502	-0.20902	-0.291977901	-0.74189386
MeanAugNovtminC	0.75317	-0.5686	-0.67196	-0.11369	-0.085871061	-0.708371514
MeanDecMartmaxC	0.816276	-0.7377	-0.8074	-0.25362	-0.18086159	-0.787500053
MeanAprJultmaxC	0.862781	-0.876	-0.91612	-0.3956	-0.443366567	-0.785822304
MeanAugNovtmaxC	0.842912	-0.8098	-0.86501	-0.35705	-0.269022107	-0.794677037

	POWYPeakSCE	AvgPeakSCE	AvgSCE	SOMain	SOMelt	Persistence
SOS	-0.415906088	-0.68655754	-0.86642	0.7830439	-0.746742	-0.8068151
EOS	0.363127669	0.73420833	0.898041	-0.600651	0.777821	0.76725363
LOS	0.403081241	0.75318816	0.931932	-0.70481	0.805696	0.82286344
MinSCE	-0.104388474	0.14243349	0.349821	-0.259863	0.271947	0.28521536
POWYMinSCE	0.158010889	0.28865052	0.45371	-0.341004	0.466508	0.45362309
PeakSCE	0.445641351	0.99563256	0.865625	-0.392523	0.581037	0.55403389
POWYPeakSCE	1	0.47703212	0.529246	-0.400729	0.572417	0.55058768
AvgPeakSCE	0.477032125	1	0.88329	-0.429168	0.616704	0.59231273
AvgSCE	0.529246373	0.88328953	1	-0.722053	0.867701	0.87360138
SOMain	-0.400728934	-0.42916762	-0.72205	1	-0.732142	-0.8700614
SOMelt	0.572417025	0.61670352	0.867701	-0.732142	1	0.97277788
Persistence	0.550587681	0.59231273	0.873601	-0.870061	0.972778	1
LOMelt	-0.140321856	0.39447805	0.340277	-0.0372	-0.016933	0.00040192
VarianceAvgSCE	-0.166266042	-0.08492793	-0.28528	0.5984894	-0.342733	-0.4516493
VariancePeakSCE	-0.332597875	-0.83127104	-0.66355	0.2505248	-0.399327	-0.3742223
VariancePeakQcms	-0.116273395	-0.1449487	-0.11416	0.0408066	-0.106313	-0.0908208
VariancePeakQnormcmssqkm	0.020977544	-0.1789333	-0.02672	0.0284054	0.134011	0.08731872
Q20	0.468850859	0.52304106	0.593911	-0.51713	0.585998	0.60001793
Q50	0.46267272	0.7354707	0.78107	-0.586068	0.650672	0.67027537
Q80	0.26628696	0.48934476	0.528192	-0.385748	0.34324	0.37963792
PeakPOWY	0.250170792	0.60150822	0.587241	-0.346095	0.37576	0.38968141
PeakQcms	-0.071019994	-0.01876912	0.012842	-0.032432	-0.038726	-0.0169917
PeakQnormbyDrainageAreacmssqkm	0.175790224	0.23734878	0.51284	-0.437383	0.586558	0.5732921
PeakQnormbyMeanAnnualPeak	-0.111757561	-0.09401704	-0.03918	-0.009268	-0.062255	-0.0419005
PeakQnormbyMeanAnnualMean	0.2830682	0.20248842	0.253716	-0.350514	0.326748	0.35571494
SCEatPeakQ	0.351275469	0.27056962	0.498558	-0.4306	0.607458	0.5861096
DRAIN_SQKM	-0.111259133	-0.1092654	-0.10453	0.0371874	-0.154682	-0.1245937
LAT_GAGE	-0.030154738	0.30620182	0.397778	-0.393046	0.231025	0.30091179
LNG_GAGE	0.268842335	0.23433736	0.174511	-0.285364	0.123108	0.18617757
Meanm	0.502546874	0.51570703	0.52903	-0.397053	0.529968	0.51861731
Minm	0.526600364	0.50572946	0.472915	-0.379846	0.471807	0.47067224
Maxm	0.377791855	0.3859811	0.459287	-0.330605	0.468361	0.451426
Rangem	-0.253716221	-0.21600112	-0.08454	0.113633	-0.072221	-0.0909253
MeanAnnualpptmm	-0.163911827	-0.04288189	0.124264	-0.021898	0.14507	0.11243596
MeanAnnualtmeanC	-0.504115043	-0.81088598	-0.89128	0.7520772	-0.734168	-0.7871803
MeanAnnualtminC	-0.520924733	-0.73799136	-0.78884	0.7047803	-0.662536	-0.7192491
MeanAnnualtmaxC	-0.455705594	-0.82042092	-0.92129	0.7431568	-0.747729	-0.7939588
MeanDecMarpptmm	-0.184008843	-0.13958283	0.013398	0.0855608	0.089403	0.03559086
MeanAprJulpptmm	0.038439065	0.23769963	0.401832	-0.357078	0.341793	0.36883598
MeanAugNovpptmm	-0.172069633	0.02136519	0.157987	-0.054817	0.100109	0.09109756
MeanDecMartmeanC	-0.499594489	-0.77196966	-0.81068	0.7132377	-0.666276	-0.7248335
MeanAprJultmeanC	-0.490270089	-0.80517877	-0.93194	0.750816	-0.785083	-0.8235979
MeanAugNovtmeanC	-0.482324662	-0.79861515	-0.88022	0.7403005	-0.710925	-0.7663529
MeanDecMartminC	-0.504111386	-0.67800409	-0.6847	0.625649	-0.570892	-0.6260059
MeanAprJultminC	-0.519091807	-0.76332047	-0.87204	0.7419212	-0.754648	-0.7985457
MeanAugNovtminC	-0.498624232	-0.73157571	-0.78731	0.7173535	-0.647199	-0.7124281
MeanDecMartmaxC	-0.452796676	-0.80487675	-0.87369	0.7444446	-0.709563	-0.7667767
MeanAprJultmaxC	-0.440583775	-0.79236194	-0.92594	0.7156237	-0.764584	-0.7967896
MeanAugNovtmaxC	-0.439558165	-0.80309442	-0.90039	0.7130667	-0.718153	-0.7623184

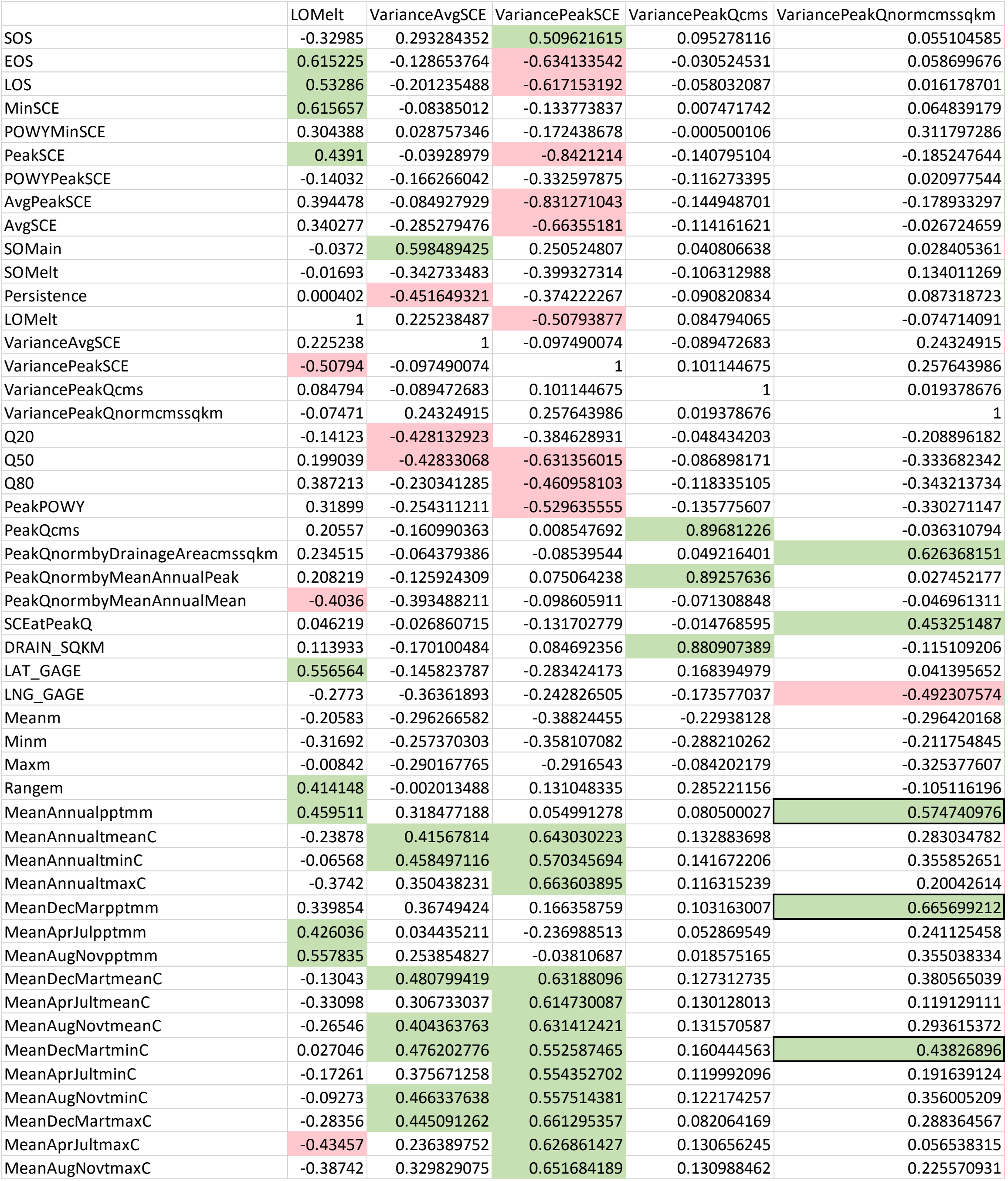

	LOMelt	VarianceAvgSCE	VariancePeakSCE	VariancePeakQcms	VariancePeakQnormcmssqkm
SOS	-0.32985	0.293284352	0.509621615	0.095278116	0.055104585
EOS	0.615225	-0.128653764	-0.634133542	-0.030524531	0.058699676
LOS	0.53286	-0.201235488	-0.617153192	-0.058032087	0.016178701
MinSCE	0.615657	-0.08385012	-0.133773837	0.007471742	0.064839179
POWYMinSCE	0.304388	0.028757346	-0.172438678	-0.000500106	0.311797286
PeakSCE	0.4391	-0.03928979	-0.8421214	-0.140795104	-0.185247644
POWYPeakSCE	-0.14032	-0.166266042	-0.332597875	-0.116273395	0.020977544
AvgPeakSCE	0.394478	-0.084927929	-0.831271043	-0.144948701	-0.178933297
AvgSCE	0.340277	-0.285279476	-0.66355181	-0.114161621	-0.026724659
SOMain	-0.0372	0.598489425	0.250524807	0.040806638	0.028405361
SOMelt	-0.01693	-0.342733483	-0.399327314	-0.106312988	0.134011269
Persistence	0.000402	-0.451649321	-0.374222267	-0.090820834	0.087318723
LOMelt	1	0.225238487	-0.50793877	0.084794065	-0.074714091
VarianceAvgSCE	0.225238	1	-0.097490074	-0.089472683	0.24324915
VariancePeakSCE	-0.50794	-0.097490074	1	0.101144675	0.257643986
VariancePeakQcms	0.084794	-0.089472683	0.101144675	1	0.019378676
VariancePeakQnormcmssqkm	-0.07471	0.24324915	0.257643986	0.019378676	1
Q20	-0.14123	-0.428132923	-0.384628931	-0.048434203	-0.208896182
Q50	0.199039	-0.42833068	-0.631356015	-0.086898171	-0.333682342
Q80	0.387213	-0.230341285	-0.460958103	-0.118335105	-0.343213734
PeakPOWY	0.31899	-0.254311211	-0.529635555	-0.135775607	-0.330271147
PeakQcms	0.20557	-0.160990363	0.008547692	0.89681226	-0.036310794
PeakQnormbyDrainageAreacmssqkm	0.234515	-0.064379386	-0.08539544	0.049216401	0.626368151
PeakQnormbyMeanAnnualPeak	0.208219	-0.125924309	0.075064238	0.89257636	0.027452177
PeakQnormbyMeanAnnualMean	-0.4036	-0.393488211	-0.098605911	-0.071308848	-0.046961311
SCEatPeakQ	0.046219	-0.026860715	-0.131702779	-0.014768595	0.453251487
DRAIN_SQKM	0.113933	-0.170100484	0.084692356	0.880907389	-0.115109206
LAT_GAGE	0.556564	-0.145823787	-0.283424173	0.168394979	0.041395652
LNG_GAGE	-0.2773	-0.36361893	-0.242826505	-0.173577037	-0.492307574
Meanm	-0.20583	-0.296266582	-0.38824455	-0.22938128	-0.296420168
Minm	-0.31692	-0.257370303	-0.358107082	-0.288210262	-0.211754845
Maxm	-0.00842	-0.290167765	-0.2916543	-0.084202179	-0.325377607
Rangem	0.414148	-0.002013488	0.131048335	0.285221156	-0.105116196
MeanAnnualpptmm	0.459511	0.318477188	0.054991278	0.080500027	0.574740976
MeanAnnualtmeanC	-0.23878	0.41567814	0.643030223	0.132883698	0.283034782
MeanAnnualtminC	-0.06568	0.458497116	0.570345694	0.141672206	0.355852651
MeanAnnualtmaxC	-0.3742	0.350438231	0.663603895	0.116315239	0.20042614
MeanDecMarpptmm	0.339854	0.36749424	0.166358759	0.103163007	0.665699212
MeanAprJulpptmm	0.426036	0.034435211	-0.236988513	0.052869549	0.241125458
MeanAugNovpptmm	0.557835	0.253854827	-0.03810687	0.018575165	0.355038334
MeanDecMartmeanC	-0.13043	0.480799419	0.63188096	0.127312735	0.380565039
MeanAprJultmeanC	-0.33098	0.306733037	0.614730087	0.130128013	0.119129111
MeanAugNovtmeanC	-0.26546	0.404363763	0.631412421	0.131570587	0.293615372
MeanDecMartminC	0.027046	0.476202776	0.552587465	0.160444563	0.43826896
MeanAprJultminC	-0.17261	0.375671258	0.554352702	0.119992096	0.191639124
MeanAugNovtminC	-0.09273	0.466337638	0.557514381	0.122174257	0.356005209
MeanDecMartmaxC	-0.28356	0.445091262	0.661295357	0.082064169	0.288364567
MeanAprJultmaxC	-0.43457	0.236389752	0.626861427	0.130656245	0.056538315
MeanAugNovtmaxC	-0.38742	0.329829075	0.651684189	0.130988462	0.225570931

	Q20	Q50	Q80	PeakPOWY	PeakQcms	PeakQnormbyDrainageAreacmssqkm
SOS	-0.48985	-0.66821	-0.5312	-0.5053388	0.0175724	-0.428480296
EOS	0.37326	0.638143	0.51403	0.49678295	0.09868213	0.609891002
LOS	0.43929	0.683259	0.54753	0.52595921	0.05725263	0.568873544
MinSCE	-0.03353	0.204673	0.31968	0.25842288	0.09814369	0.425917672
POWYMinSCE	0.05754	0.114617	0.01083	0.00294311	0.01676014	0.536858477
PeakSCE	0.49708	0.72488	0.49903	0.60141863	-0.0090026	0.231715536
POWYPeakSCE	0.46885	0.462673	0.26629	0.25017079	-0.07102	0.175790224
AvgPeakSCE	0.52304	0.735471	0.48934	0.60150822	-0.0187691	0.237348778
AvgSCE	0.59391	0.78107	0.52819	0.58724119	0.01284168	0.512839966
SOMain	-0.51713	-0.58607	-0.3857	-0.3460949	-0.032432	-0.43738329
SOMelt	0.586	0.650672	0.34324	0.37576004	-0.0387259	0.586558402
Persistence	0.60002	0.670275	0.37964	0.38968141	-0.0169917	0.5732921
LOMelt	-0.14123	0.199039	0.38721	0.31899002	0.2055697	0.234514919
VarianceAvgSCE	-0.42813	-0.42833	-0.2303	-0.2543112	-0.1609904	-0.064379386
VariancePeakSCE	-0.38463	-0.63136	-0.461	-0.5296356	0.00854769	-0.08539544
VariancePeakQcms	-0.04843	-0.0869	-0.1183	-0.1357756	0.89681226	0.049216401
VariancePeakQnormcmssqkm	-0.2089	-0.33368	-0.3432	-0.3302711	-0.0363108	0.626368151
Q20	1	0.79786	0.35992	0.4654409	0.01971759	0.165421048
Q50	0.79786	1	0.70918	0.73019744	0.02194753	0.136959773
Q80	0.35992	0.709181	1	0.81380684	-0.0301614	-0.009383835
PeakPOWY	0.46544	0.730197	0.81381	1	0.00056662	0.053322823
PeakQcms	0.01972	0.021948	-0.0302	0.00056662	1	0.15136944
PeakQnormbyDrainageAreacmssqkm	0.16542	0.13696	-0.0094	0.05332282	0.15136944	1
PeakQnormbyMeanAnnualPeak	-0.06079	-0.06257	-0.0851	-0.0717491	0.98173355	0.18489737
PeakQnormbyMeanAnnualMean	0.76091	0.439375	-0.049	0.19553381	-0.0769055	0.094640044
SCEatPeakQ	0.21843	0.069294	-0.1567	-0.1633441	0.00955887	0.722269613
DRAIN_SQKM	-0.01715	-0.02699	0.01007	0.03658194	0.92012354	-0.027854987
LAT_GAGE	-0.08931	0.182601	0.19495	0.1277511	0.3322667	0.442354727
LNG_GAGE	0.49288	0.528121	0.46219	0.4588333	-0.1836412	-0.415544525
Meanm	0.73414	0.686892	0.47475	0.51969481	-0.2518534	-0.123772541
Minm	0.67706	0.605401	0.38025	0.44337602	-0.3438911	-0.131864643
Maxm	0.62368	0.627553	0.51173	0.49947967	-0.0688489	-0.097731232
Rangem	-0.16147	-0.06094	0.10212	0.0029945	0.37808464	0.0597955
MeanAnnualpptmm	-0.41312	-0.29348	-0.1338	-0.1924807	0.1420453	0.710134274
MeanAnnualtmeanC	-0.6935	-0.86045	-0.6498	-0.6490373	0.0186821	-0.236477127
MeanAnnualtminC	-0.73813	-0.83845	-0.5992	-0.6124879	0.05562853	-0.0764919
MeanAnnualtmaxC	-0.6081	-0.82217	-0.6506	-0.637606	-0.0148734	-0.360582668
MeanDecMarpptmm	-0.45444	-0.41883	-0.3179	-0.3541135	0.13219228	0.680762135
MeanAprJulpptmm	-0.0561	0.179353	0.30134	0.21553786	0.16491021	0.594047125
MeanAugNovpptmm	-0.36952	-0.182	0.0618	-0.0071399	0.09764382	0.572627945
MeanDecMartmeanC	-0.71143	-0.87655	-0.6445	-0.6532013	0.02661915	-0.088223784
MeanAprJultmeanC	-0.62237	-0.78028	-0.5866	-0.5768185	0.01543914	-0.406084606
MeanAugNovtmeanC	-0.6822	-0.84641	-0.6625	-0.6587425	0.0106582	-0.240385394
MeanDecMartminC	-0.72864	-0.83391	-0.6001	-0.6192957	0.0932406	0.080627826
MeanAprJultminC	-0.69193	-0.77657	-0.5385	-0.5491082	0.02449273	-0.288461045
MeanAugNovtminC	-0.7256	-0.82395	-0.5979	-0.6041049	0.02627242	-0.098002716
MeanDecMartmaxC	-0.63356	-0.84715	-0.6365	-0.6335135	-0.0450421	-0.256771866
MeanAprJultmaxC	-0.53387	-0.73944	-0.5909	-0.5658811	0.00759261	-0.474049564
MeanAugNovtmaxC	-0.60542	-0.81225	-0.6733	-0.6619081	-0.0025014	-0.339583469

	PeakQnormbyMeanAnnualPeak	PeakQnormbyMeanAnnualMean	SCEatPeakQ	DRAIN_SQKM
SOS	0.048168404	-0.183400896	-0.391302215	0.108058542
EOS	0.081794989	0.003933877	0.508011876	-0.050345835
LOS	0.034001549	0.075990784	0.487617788	-0.076061881
MinSCE	0.117571919	-0.228745174	0.161326236	0.014348816
POWYMinSCE	0.0557362	-0.091783675	0.53133416	-0.125706901
PeakSCE	-0.083948425	0.165129485	0.246753006	-0.101571587
POWYPeakSCE	-0.111757561	0.2830682	0.351275469	-0.111259133
AvgPeakSCE	-0.094017037	0.202488423	0.270569623	-0.109265397
AvgSCE	-0.039181471	0.253715723	0.498557694	-0.104533558
SOMain	-0.0092683	-0.350513866	-0.430600368	0.037187374
SOMelt	-0.06225545	0.326747538	0.607458439	-0.154681991
Persistence	-0.041900457	0.355714937	0.586109597	-0.124593696
LOMelt	0.208218635	-0.403602847	0.046219328	0.113932864
VarianceAvgSCE	-0.125924309	-0.393488211	-0.026860715	-0.170100484
VariancePeakSCE	0.075064238	-0.098605911	-0.131702779	0.084692356
VariancePeakQcms	0.89257636	-0.071308848	-0.014768595	0.880907389
VariancePeakQnormcmssqkm	0.027452177	-0.046961311	0.453251487	-0.115109206
Q20	-0.060794516	0.760912181	0.218434498	-0.017145172
Q50	-0.062569424	0.439375079	0.069293726	-0.026992111
Q80	-0.085074138	-0.049028445	-0.156706041	0.010069024
PeakPOWY	-0.071749147	0.195533811	-0.163344051	0.036581939
PeakQcms	0.98173355	-0.076905472	0.009558865	0.920123542
PeakQnormbyDrainageAreacmssqkm	0.18489737	0.094640044	0.722269613	-0.027854987
PeakQnormbyMeanAnnualPeak	1	-0.125769696	0.020897532	0.887121715
PeakQnormbyMeanAnnualMean	-0.125769696	1	0.164938363	-0.091136945
SCEatPeakQ	0.020897532	0.164938363	1	-0.103922922
DRAIN_SQKM	0.887121715	-0.091136945	-0.103922922	1
LAT_GAGE	0.343170538	-0.266740682	0.212962649	0.188485847
LNG_GAGE	-0.255609683	0.460133995	-0.378263958	-0.095616676
Meanm	-0.322315356	0.547311309	0.064687416	-0.202083818
Minm	-0.414158457	0.593718425	0.067157931	-0.297279868
Maxm	-0.10663066	0.365055117	0.01783755	-0.026274108
Rangem	0.427020701	-0.358763936	-0.068590599	0.366536069
MeanAnnualpptmm	0.228449462	-0.426892061	0.391692804	-0.007909793
MeanAnnualtmeanC	0.086295557	-0.367998366	-0.25331925	0.07946686
MeanAnnualtminC	0.132245127	-0.463304432	-0.159093675	0.064415199
MeanAnnualtmaxC	0.040345121	-0.260042349	-0.318789179	0.087320605
MeanDecMarpptmm	0.224329549	-0.422390374	0.448375604	-0.009865998
MeanAprJulpptmm	0.192842229	-0.22098921	0.20531108	0.033316725
MeanAugNovpptmm	0.172141104	-0.391202176	0.230629796	-0.02344764
MeanDecMartmeanC	0.103551178	-0.427847015	-0.129870016	0.0590107
MeanAprJultmeanC	0.065930875	-0.273479331	-0.405921527	0.107782075
MeanAugNovtmeanC	0.077410206	-0.353585044	-0.241717738	0.071811513
MeanDecMartminC	0.176932	-0.501070826	-0.022680048	0.072713191
MeanAprJultminC	0.083642015	-0.378289154	-0.351597068	0.071338842
MeanAugNovtminC	0.101734407	-0.444871375	-0.1618064	0.040898
MeanDecMartmaxC	0.018363471	-0.315491728	-0.2306485	0.039767723
MeanAprJultmaxC	0.0485798	-0.177334796	-0.425081074	0.129849741
MeanAugNovtmaxC	0.053164049	-0.258707356	-0.290812267	0.092140055

	LAT_GAGE	LNG_GAGE	Mean Elev (m)	Min Elev (m)	Max Elev (m)	Range Elev (m)
SOS	-0.390497935	-0.229508018	-0.479108943	-0.42673442	-0.464197136	0.016863448
EOS	0.531997934	-0.077235491	0.288481876	0.172791837	0.363992155	0.203380301
LOS	0.502921886	0.041571534	0.379756477	0.283419196	0.422978653	0.125743804
MinSCE	0.435553309	-0.219291137	-0.108064702	-0.249422453	0.121505204	0.478950145
POWYMinSCE	0.283160998	-0.492758058	-0.038842241	-0.088498754	0.045317526	0.172572497
PeakSCE	0.31813897	0.213985409	0.487531496	0.474847446	0.368885967	-0.195079553
POWYPeakSCE	-0.030154738	0.268842335	0.502546874	0.526600364	0.377791855	-0.253716221
AvgPeakSCE	0.30620182	0.234337358	0.515707033	0.505729463	0.385981099	-0.216001118
AvgSCE	0.397777699	0.174511289	0.529029821	0.472914623	0.459286871	-0.08453964
SOMain	-0.393046335	-0.285364179	-0.397053264	-0.379846391	-0.330605289	0.113633002
SOMelt	0.231025137	0.12310759	0.529968162	0.471806573	0.468360936	-0.072220654
Persistence	0.300911794	0.186177567	0.518617309	0.470672236	0.451426	-0.090925297
LOMelt	0.556564106	-0.277295839	-0.205829245	-0.316924314	-0.008422051	0.414148464
VarianceAvgSCE	-0.145823787	-0.36361893	-0.296266582	-0.257370303	-0.290167765	-0.002013488
VariancePeakSCE	-0.283424173	-0.242826505	-0.38824455	-0.358107082	-0.2916543	0.131048335
VariancePeakQcms	0.168394979	-0.173577037	-0.22938128	-0.288210262	-0.084202179	0.285221156
VariancePeakQnormcmssqkm	0.041395652	-0.492307574	-0.296420168	-0.211754845	-0.325377607	-0.105116196
Q20	-0.089311142	0.492875543	0.734140397	0.677055584	0.623679911	-0.161472943
Q50	0.182600975	0.528120918	0.686891686	0.60540117	0.627553348	-0.060937452
Q80	0.194948986	0.462194346	0.474753965	0.380249931	0.51172771	0.102115347
PeakPOWY	0.127751104	0.4588333	0.519694809	0.443376017	0.499479668	0.002994502
PeakQcms	0.332266697	-0.18364125	-0.251853427	-0.343891104	-0.068848885	0.378084639
PeakQnormbyDrainageAreacmssqkm	0.442354727	-0.415544525	-0.123772541	-0.131864643	-0.097731232	0.0597955
PeakQnormbyMeanAnnualPeak	0.343170538	-0.255609683	-0.322315356	-0.414158457	-0.10663066	0.427020701
PeakQnormbyMeanAnnualMean	-0.266740682	0.460133995	0.547311309	0.593718425	0.365055117	-0.358763936
SCEatPeakQ	0.212962649	-0.378263958	0.064687416	0.067157931	0.01783755	-0.068590599
DRAIN_SQKM	0.188485847	-0.095616676	-0.202083818	-0.297279868	-0.026274108	0.366536069
LAT_GAGE	1	-0.326137763	-0.463345306	-0.4547139	-0.401581684	0.129086844
LNG_GAGE	-0.326137763	1	0.711808447	0.719502588	0.537104997	-0.321672578
Meanm	-0.463345306	0.711808447	1	0.931178782	0.871500213	-0.205682672
Minm	-0.4547139	0.719502588	0.931178782	1	0.693703042	-0.510118041
Maxm	-0.401581684	0.537104997	0.871500213	0.693703042	1	0.26562933
Rangem	0.129086844	-0.321672578	-0.205682672	-0.510118041	0.26562933	1
MeanAnnualpptmm	0.511102064	-0.680561842	-0.544905688	-0.545542718	-0.390011217	0.264478885
MeanAnnualtmeanC	-0.302466053	-0.485362461	-0.687521746	-0.640654448	-0.590495504	0.152377103
MeanAnnualtminC	-0.110140924	-0.614940134	-0.786204203	-0.749967688	-0.660136659	0.215531315
MeanAnnualtmaxC	-0.450441516	-0.339585778	-0.555250187	-0.502218933	-0.490108846	0.086957434
MeanDecMarpptmm	0.397884612	-0.838333177	-0.608471582	-0.602296577	-0.453616388	0.264489855
MeanAprJulpptmm	0.667421066	-0.09694067	-0.221698156	-0.20925576	-0.169461538	0.077726923
MeanAugNovpptmm	0.473155038	-0.419027179	-0.387702955	-0.40947396	-0.233804025	0.268885583
MeanDecMartmeanC	-0.229003642	-0.635104661	-0.729588071	-0.695724088	-0.604504567	0.209359243
MeanAprJultmeanC	-0.37135941	-0.249913779	-0.58159809	-0.52855204	-0.518451402	0.088359063
MeanAugNovtmeanC	-0.303600559	-0.482778101	-0.679576008	-0.626480997	-0.592872857	0.130566897
MeanDecMartminC	-0.000416794	-0.759304845	-0.826044144	-0.796615607	-0.677218315	0.257571758
MeanAprJultminC	-0.219232352	-0.358759809	-0.684695481	-0.639012548	-0.598852399	0.140199968
MeanAugNovtminC	-0.154779517	-0.587878993	-0.750346438	-0.716396509	-0.6313293	0.204996518
MeanDecMartmaxC	-0.447946347	-0.452159102	-0.567604158	-0.531969774	-0.477799313	0.141478678
MeanAprJultmaxC	-0.467876951	-0.151976171	-0.469517399	-0.4137639	-0.427410726	0.043431029
MeanAugNovtmaxC	-0.404060243	-0.368879673	-0.581042267	-0.51588831	-0.525555079	0.06292566

	MeanAnnualpptmm	MeanAnnualtmeanC	MeanAnnualtminC	MeanAnnualtmaxC
SOS	-0.118453386	0.835217885	0.74235491	0.86058941
EOS	0.403220191	-0.728957753	-0.563670044	-0.824773633
LOS	0.310109385	-0.809286552	-0.664427752	-0.881865332
MinSCE	0.473461208	-0.23330235	-0.092891118	-0.340501774
POWYMinSCE	0.445125697	-0.20369349	-0.079178559	-0.298971952
PeakSCE	-0.014980719	-0.791966739	-0.711805481	-0.809121787
POWYPeakSCE	-0.163911827	-0.504115043	-0.520924733	-0.455705594
AvgPeakSCE	-0.042881891	-0.810885976	-0.737991363	-0.820420925
AvgSCE	0.124263685	-0.891282772	-0.788837703	-0.921285655
SOMain	-0.021897712	0.75207725	0.704780329	0.743156766
SOMelt	0.145070238	-0.73416837	-0.662535633	-0.747728516
Persistence	0.112435957	-0.787180301	-0.719249137	-0.793958752
LOMelt	0.459510841	-0.238780919	-0.065678787	-0.374204799
VarianceAvgSCE	0.318477188	0.41567814	0.458497116	0.350438231
VariancePeakSCE	0.054991278	0.643030223	0.570345694	0.663603895
VariancePeakQcms	0.080500027	0.132883698	0.141672206	0.116315239
VariancePeakQnormcmssqkm	0.574740976	0.283034782	0.355852651	0.20042614
Q20	-0.413124018	-0.693501202	-0.738132468	-0.608098921
Q50	-0.293480156	-0.860452684	-0.838445821	-0.822167669
Q80	-0.133819404	-0.649792017	-0.599233512	-0.650562342
PeakPOWY	-0.192480707	-0.649037279	-0.612487948	-0.637605994
PeakQcms	0.142045302	0.018682101	0.05562853	-0.014873357
PeakQnormbyDrainageAreacmssqkm	0.710134274	-0.236477127	-0.0764919	-0.360582668
PeakQnormbyMeanAnnualPeak	0.228449462	0.086295557	0.132245127	0.040345121
PeakQnormbyMeanAnnualMean	-0.426892061	-0.367998366	-0.463304432	-0.260042349
SCEatPeakQ	0.391692804	-0.25331925	-0.159093675	-0.318789179
DRAIN_SQKM	-0.007909793	0.07946686	0.064415199	0.087320605
LAT_GAGE	0.511102064	-0.302466053	-0.110140924	-0.450441516
LNG_GAGE	-0.680561842	-0.485362461	-0.614940134	-0.339585778
Meanm	-0.544905688	-0.687521746	-0.786204203	-0.555250187
Minm	-0.545542718	-0.640654448	-0.749967688	-0.502218933
Maxm	-0.390011217	-0.590495504	-0.660136659	-0.490108846
Rangem	0.264478885	0.152377103	0.215531315	0.086957434
MeanAnnualpptmm	1	0.147107743	0.348706117	-0.039038951
MeanAnnualtmeanC	0.147107743	1	0.959121801	0.968889064
MeanAnnualtminC	0.348706117	0.959121801	1	0.859243009
MeanAnnualtmaxC	-0.039038951	0.968889064	0.859243009	1
MeanDecMarpptmm	0.949422273	0.308427734	0.482876796	0.135238142
MeanAprJulpptmm	0.695557527	-0.308774601	-0.12461306	-0.449188311
MeanAugNovpptmm	0.902682245	0.005349356	0.198686666	-0.164094291
MeanDecMartmeanC	0.315006982	0.970277246	0.970258087	0.90541961
MeanAprJultmeanC	-0.059755147	0.956460071	0.872426513	0.966002819
MeanAugNovtmeanC	0.123381787	0.996342636	0.949185253	0.970967604
MeanDecMartminC	0.500056246	0.896547728	0.971084744	0.7714158
MeanAprJultminC	0.116118144	0.955155938	0.947960393	0.897586287
MeanAugNovtminC	0.315044372	0.962393062	0.995850153	0.868785599
MeanDecMartmaxC	0.095608657	0.965386168	0.887665412	0.968810397
MeanAprJultmaxC	-0.192038499	0.903895867	0.765312876	0.964659956
MeanAugNovtmaxC	-0.037686147	0.962144939	0.853343484	0.992967985

	MeanDecMarpptmm	MeanAprJulpptmm	MeanAugNovpptmm
SOS	0.018309262	-0.437194685	-0.185860686
EOS	0.284115174	0.537287132	0.42957408
LOS	0.177760989	0.525063543	0.354265834
MinSCE	0.359055777	0.423123112	0.564893629
POWYMinSCE	0.508379903	0.164225705	0.302293535
PeakSCE	-0.11749991	0.260309117	0.053998054
POWYPeakSCE	-0.184008843	0.038439065	-0.172069633
AvgPeakSCE	-0.139582831	0.237699626	0.021365186
AvgSCE	0.013397987	0.401832443	0.15798734
SOMain	0.085560752	-0.357077736	-0.054817307
SOMelt	0.089402947	0.341792504	0.10010876
Persistence	0.035590859	0.368835978	0.09109756
LOMelt	0.339854128	0.426035781	0.55783537
VarianceAvgSCE	0.36749424	0.034435211	0.253854827
VariancePeakSCE	0.166358759	-0.236988513	-0.03810687
VariancePeakQcms	0.103163007	0.052869549	0.018575165
VariancePeakQnormcmssqkm	0.665699212	0.241125458	0.355038334
Q20	-0.454443437	-0.056099448	-0.369516213
Q50	-0.418832895	0.179353398	-0.181996796
Q80	-0.317867333	0.301344778	0.061795561
PeakPOWY	-0.354113479	0.215537862	-0.007139902
PeakQcms	0.132192277	0.164910215	0.097643821
PeakQnormbyDrainageAreacmssqkm	0.680762135	0.594047125	0.572627945
PeakQnormbyMeanAnnualPeak	0.224329549	0.192842229	0.172141104
PeakQnormbyMeanAnnualMean	-0.422390374	-0.22098921	-0.391202176
SCEatPeakQ	0.448375604	0.20531108	0.230629796
DRAIN_SQKM	-0.009865998	0.033316725	-0.02344764
LAT_GAGE	0.397884612	0.667421066	0.473155038
LNG_GAGE	-0.838333177	-0.09694067	-0.419027179
Meanm	-0.608471582	-0.221698156	-0.387702955
Minm	-0.602296577	-0.20925576	-0.40947396
Maxm	-0.453616388	-0.169461538	-0.233804025
Rangem	0.264489855	0.077726923	0.268885583
MeanAnnualpptmm	0.949422273	0.695557527	0.902682245
MeanAnnualtmeanC	0.308427734	-0.308774601	0.005349356
MeanAnnualtminC	0.482876796	-0.12461306	0.198686666
MeanAnnualtmaxC	0.135238142	-0.449188311	-0.164094291
MeanDecMarpptmm	1	0.48570999	0.746747449
MeanAprJulpptmm	0.48570999	1	0.710170109
MeanAugNovpptmm	0.746747449	0.710170109	1
MeanDecMartmeanC	0.477645049	-0.213203842	0.14803311
MeanAprJultmeanC	0.071974133	-0.386979601	-0.133698597
MeanAugNovtmeanC	0.297416024	-0.327390899	-0.038943692
MeanDecMartminC	0.637947577	-0.029719835	0.317240784
MeanAprJultminC	0.22383152	-0.224889515	0.034877486
MeanAugNovtminC	0.455514631	-0.155261985	0.162662322
MeanDecMartmaxC	0.2703364	-0.386469342	-0.040789035
MeanAprJultmaxC	-0.049166768	-0.490305756	-0.256212874
MeanAugNovtmaxC	0.152501468	-0.445047155	-0.197973082

	MeanDecMartmeanC	MeanAprJultmeanC	MeanAugNovtmeanC
SOS	0.756763732	0.869929169	0.831453354
EOS	-0.607318493	-0.827053484	-0.727402564
LOS	-0.698632086	-0.887089925	-0.806766199
MinSCE	-0.127920363	-0.32462974	-0.257647904
POWYMinSCE	-0.056196828	-0.389776591	-0.194226214
PeakSCE	-0.747290516	-0.791732056	-0.783091483
POWYPeakSCE	-0.499594489	-0.490270089	-0.482324662
AvgPeakSCE	-0.771969661	-0.805178765	-0.798615146
AvgSCE	-0.81067847	-0.931940985	-0.880224978
SOMain	0.713237733	0.750815996	0.740300522
SOMelt	-0.666276147	-0.785083341	-0.710925302
Persistence	-0.724833466	-0.823597892	-0.766352866
LOMelt	-0.130427033	-0.330975159	-0.265462104
VarianceAvgSCE	0.480799419	0.306733037	0.404363763
VariancePeakSCE	0.63188096	0.614730087	0.631412421
VariancePeakQcms	0.127312735	0.130128013	0.131570587
VariancePeakQnormcmssqkm	0.380565039	0.119129111	0.293615372
Q20	-0.711431167	-0.622370686	-0.682199524
Q50	-0.876553026	-0.780280159	-0.846407249
Q80	-0.644534347	-0.586602233	-0.662473933
PeakPOWY	-0.65320133	-0.576818476	-0.658742522
PeakQcms	0.026619155	0.015439138	0.010658198
PeakQnormbyDrainageAreacmssqkm	-0.088223784	-0.406084606	-0.240385394
PeakQnormbyMeanAnnualPeak	0.103551178	0.065930875	0.077410206
PeakQnormbyMeanAnnualMean	-0.427847015	-0.273479331	-0.353585044
SCEatPeakQ	-0.129870016	-0.405921527	-0.241717738
DRAIN_SQKM	0.0590107	0.107782075	0.071811513
LAT_GAGE	-0.229003642	-0.37135941	-0.303600559
LNG_GAGE	-0.635104661	-0.249913779	-0.482778101
Meanm	-0.729588071	-0.58159809	-0.679576008
Minm	-0.695724088	-0.52855204	-0.626480997
Maxm	-0.604504567	-0.518451402	-0.592872857
Rangem	0.209359243	0.088359063	0.130566897
MeanAnnualpptmm	0.315006982	-0.059755147	0.123381787
MeanAnnualtmeanC	0.970277246	0.956460071	0.996342636
MeanAnnualtminC	0.970258087	0.872426513	0.949185253
MeanAnnualtmaxC	0.90541961	0.966002819	0.970967604
MeanDecMarpptmm	0.477645049	0.071974133	0.297416024
MeanAprJulpptmm	-0.213203842	-0.386979601	-0.327390899
MeanAugNovpptmm	0.14803311	-0.133698597	-0.038943692
MeanDecMartmeanC	1	0.860489018	0.958296453
MeanAprJultmeanC	0.860489018	1	0.956028241
MeanAugNovtmeanC	0.958296453	0.956028241	1
MeanDecMartminC	0.960458435	0.752219773	0.881003639
MeanAprJultminC	0.89386228	0.958842092	0.949704976
MeanAugNovtminC	0.964065153	0.882717615	0.957121778
MeanDecMartmaxC	0.956973204	0.900845512	0.958127836
MeanAprJultmaxC	0.786557339	0.97573182	0.907358885
MeanAugNovtmaxC	0.894639808	0.95583098	0.972726272

	MeanDecMartminC	MeanAprJultminC	MeanAugNovtminC
SOS	0.638499567	0.81601797	0.753170146
EOS	-0.433127665	-0.703510709	-0.568580371
LOS	-0.537803359	-0.785021615	-0.671956747
MinSCE	0.003028188	-0.209020159	-0.1136858
POWYMinSCE	0.067955936	-0.291977901	-0.085871061
PeakSCE	-0.648312949	-0.74189386	-0.708371514
POWYPeakSCE	-0.504111386	-0.519091807	-0.498624232
AvgPeakSCE	-0.67800409	-0.763320474	-0.731575707
AvgSCE	-0.68470281	-0.872035869	-0.787313673
SOMain	0.625648994	0.741921218	0.71735349
SOMelt	-0.570892302	-0.754647662	-0.647199448
Persistence	-0.626005884	-0.798545719	-0.712428086
LOMelt	0.027046453	-0.172608731	-0.092727816
VarianceAvgSCE	0.476202776	0.375671258	0.466337638
VariancePeakSCE	0.552587465	0.554352702	0.557514381
VariancePeakQcms	0.160444563	0.119992096	0.122174257
VariancePeakQnormcmssqkm	0.43826896	0.191639124	0.356005209
Q20	-0.728644216	-0.691929746	-0.725600098
Q50	-0.833912243	-0.776570689	-0.823945254
Q80	-0.600107684	-0.538460843	-0.597945219
PeakPOWY	-0.619295681	-0.549108186	-0.604104939
PeakQcms	0.093240597	0.024492734	0.026272418
PeakQnormbyDrainageAreacmssqkm	0.080627826	-0.288461045	-0.098002716
PeakQnormbyMeanAnnualPeak	0.176932	0.083642015	0.101734407
PeakQnormbyMeanAnnualMean	-0.501070826	-0.378289154	-0.444871375
SCEatPeakQ	-0.022680048	-0.351597068	-0.1618064
DRAIN_SQKM	0.072713191	0.071338842	0.040898
LAT_GAGE	-0.000416794	-0.219232352	-0.154779517
LNG_GAGE	-0.759304845	-0.358759809	-0.587878993
Meanm	-0.826044144	-0.684695481	-0.750346438
Minm	-0.796615607	-0.639012548	-0.716396509
Maxm	-0.677218315	-0.598852399	-0.6313293
Rangem	0.257571758	0.140199968	0.204996518
MeanAnnualpptmm	0.500056246	0.116118144	0.315044372
MeanAnnualtmeanC	0.896547728	0.955155938	0.962393062
MeanAnnualtminC	0.971084744	0.947960393	0.995850153
MeanAnnualtmaxC	0.7714158	0.897586287	0.868785599
MeanDecMarpptmm	0.637947577	0.22383152	0.455514631
MeanAprJulpptmm	-0.029719835	-0.224889515	-0.155261985
MeanAugNovpptmm	0.317240784	0.034877486	0.162662322
MeanDecMartmeanC	0.960458435	0.89386228	0.964065153
MeanAprJultmeanC	0.752219773	0.958842092	0.882717615
MeanAugNovtmeanC	0.881003639	0.949704976	0.957121778
MeanDecMartminC	1	0.847013174	0.953741991
MeanAprJultminC	0.847013174	1	0.955408931
MeanAugNovtminC	0.953741991	0.955408931	1
MeanDecMartmaxC	0.838341113	0.867395025	0.893614348
MeanAprJultmaxC	0.636986078	0.873398716	0.777219685
MeanAugNovtmaxC	0.76848501	0.886629102	0.863823117

	MeanDecMartmaxC	MeanAprJultmaxC	MeanAugNovtmaxC
SOS	0.816275757	0.862781265	0.842912403
EOS	-0.737705995	-0.876005387	-0.809760665
LOS	-0.8074019	-0.916118641	-0.865007567
MinSCE	-0.253621502	-0.395603577	-0.357047267
POWYMinSCE	-0.18086159	-0.443366567	-0.269022107
PeakSCE	-0.787500053	-0.785822304	-0.794677037
POWYPeakSCE	-0.452796676	-0.440583775	-0.439558165
AvgPeakSCE	-0.804876754	-0.79236194	-0.80309442
AvgSCE	-0.87368539	-0.925942134	-0.900392317
SOMain	0.744444585	0.715623717	0.713066686
SOMelt	-0.709562819	-0.764583816	-0.718153437
Persistence	-0.76677673	-0.796789564	-0.762318385
LOMelt	-0.283562863	-0.434566557	-0.387418696
VarianceAvgSCE	0.445091262	0.236389752	0.329829075
VariancePeakSCE	0.661295357	0.626861427	0.651684189
VariancePeakQcms	0.082064169	0.130656245	0.130988462
VariancePeakQnormcmssqkm	0.288364567	0.056538315	0.225570931
Q20	-0.633560131	-0.533870086	-0.605419832
Q50	-0.847154773	-0.739438449	-0.81224827
Q80	-0.636542018	-0.59087295	-0.673329786
PeakPOWY	-0.633513524	-0.565881105	-0.6619081
PeakQcms	-0.045042062	0.007592606	-0.002501412
PeakQnormbyDrainageAreacmssqkm	-0.256771866	-0.474049564	-0.339583469
PeakQnormbyMeanAnnualPeak	0.018363471	0.0485798	0.053164049
PeakQnormbyMeanAnnualMean	-0.315491728	-0.177334796	-0.258707356
SCEatPeakQ	-0.2306485	-0.425081074	-0.290812267
DRAIN_SQKM	0.039767723	0.129849741	0.092140055
LAT_GAGE	-0.447946347	-0.467876951	-0.404060243
LNG_GAGE	-0.452159102	-0.151976171	-0.368879673
Meanm	-0.567604158	-0.469517399	-0.581042267
Minm	-0.531969774	-0.4137639	-0.51588831
Maxm	-0.477799313	-0.427410726	-0.525555079
Rangem	0.141478678	0.043431029	0.06292566
MeanAnnualpptmm	0.095608657	-0.192038499	-0.037686147
MeanAnnualtmeanC	0.965386168	0.903895867	0.962144939
MeanAnnualtminC	0.887665412	0.765312876	0.853343484
MeanAnnualtmaxC	0.968810397	0.964659956	0.992967985
MeanDecMarpptmm	0.2703364	-0.049166768	0.152501468
MeanAprJulpptmm	-0.386469342	-0.490305756	-0.445047155
MeanAugNovpptmm	-0.040789035	-0.256212874	-0.197973082
MeanDecMartmeanC	0.956973204	0.786557339	0.894639808
MeanAprJultmeanC	0.900845512	0.97573182	0.95583098
MeanAugNovtmeanC	0.958127836	0.907358885	0.972726272
MeanDecMartminC	0.838341113	0.636986078	0.76848501
MeanAprJultminC	0.867395025	0.873398716	0.886629102
MeanAugNovtminC	0.893614348	0.777219685	0.863823117
MeanDecMartmaxC	1	0.876186713	0.950757727
MeanAprJultmaxC	0.876186713	1	0.955663507
MeanAugNovtmaxC	0.950757727	0.955663507	1

References

Clow, D. W. (2009). Changes in the Timing of Snowmelt and Streamflow in Colorado: A Response to Recent Warming. *Journal of Climate*, *23*(9), 2293–2306. https://doi.org/10.1175/2009JCLI2951.1

Daly, C., Gibson, W. P., Taylor, G. H., Johnson, G. L., & Pasteris, P. (2002). A knowledge-based approach to the statistical mapping of climate. *Climate Research*, *22*(2), 99–113. https://doi.org/10.3354/cr022099

Dudley, R. W., Hodgkins, G. A., McHale, M. R., Kolian, M. J., & Renard, B. (2017). Trends in snowmelt-related streamflow timing in the conterminous United States. *Journal of Hydrology*, *547*(Supplement C), 208–221. https://doi.org/10.1016/j.jhydrol.2017.01.051

Eckhardt, K., & Ulbrich, U. (2003). Potential impacts of climate change on groundwater recharge and streamflow in a central European low mountain range. *Journal of Hydrology*, *284*(1), 244–252. https://doi.org/10.1016/j.jhydrol.2003.08.005

Falcone, J. A. (2011). *GAGES-II: Geospatial Attributes of Gages for Evaluating Streamflow* (USGS Unnumbered Series). Reston, VA: U.S. Geological Survey. Retrieved from http://pubs.er.usgs.gov/publication/70046617

Feng, S., & Hu, Q. (2007). Changes in winter snowfall/precipitation ratio in the contiguous United States. *Journal of Geophysical Research: Atmospheres*, *112*(D15), D15109. https://doi.org/10.1029/2007JD008397

Fyfe, J. C., Derksen, C., Mudryk, L., Flato, G. M., Santer, B. D., Swart, N. C., … Jiao, Y. (2017). Large near-term projected snowpack loss over the western United States. *Nature Communications*, *8*, 14996. https://doi.org/10.1038/ncomms14996

Guan, B., Molotch, N. P., Waliser, D. E., Fetzer, E. J., & Neiman, P. J. (2010). Extreme snowfall events linked to atmospheric rivers and surface air temperature via satellite measurements. *Geophysical Research Letters*, *37*(20), L20401. https://doi.org/10.1029/2010GL044696

Hall, D. K., & Riggs, G. A. (2007). Accuracy assessment of the MODIS snow products. *Hydrological Processes*, *21*(12), 1534–1547. https://doi.org/10.1002/hyp.6715

Hall, D. K., Riggs, G. A., & Salomonson, V. V. (1995). Development of methods for mapping global snow cover using moderate resolution imaging spectroradiometer data. *Remote Sensing of Environment*, *54*(2), 127–140. https://doi.org/10.1016/0034-4257(95)00137-P

Hall, D. K., Riggs, G. A., Salomonson, V. V., DiGirolamo, N. E., & Bayr, K. J. (2002). MODIS snow-cover products. *Remote Sensing of Environment*, *83*(1), 181–194. https://doi.org/10.1016/S0034-4257(02)00095-0

Hay, L. E., Markstrom, S. L., & Ward-Garrison, C. (2010). Watershed-Scale Response to Climate Change through the Twenty-First Century for Selected Basins across the United States. *Earth Interactions*, *15*(17), 1–37. https://doi.org/10.1175/2010EI370.1

Hidalgo, H. G., Das, T., Dettinger, M. D., Cayan, D. R., Pierce, D. W., Barnett, T. P., … Nozawa, T. (2009). Detection and Attribution of Streamflow Timing Changes to Climate Change in the Western United States. *Journal of Climate*, *22*(13), 3838–3855. https://doi.org/10.1175/2009JCLI2470.1

Immerzeel, W. W., Droogers, P., de Jong, S. M., & Bierkens, M. F. P. (2009). Large-scale monitoring of snow cover and runoff simulation in Himalayan river basins using remote sensing. *Remote Sensing of Environment*, *113*(1), 40–49. https://doi.org/10.1016/j.rse.2008.08.010

Magand, C., Ducharne, A., Le Moine, N., & Gascoin, S. (2013). Introducing Hysteresis in Snow Depletion Curves to Improve the Water Budget of a Land Surface Model in an Alpine Catchment. *Journal of Hydrometeorology*, *15*(2), 631–649. https://doi.org/10.1175/JHM-D-13-091.1

Mankin, J. S., Viviroli, D., Singh, D., Hoekstra, A. Y., & Diffenbaugh, N. S. (2015). The potential for snow to supply human water demand in the present and future. *Environmental Research Letters*, *10*(11), 114016. https://doi.org/10.1088/1748-9326/10/11/114016

Martinec, J., & Rango, A. (1981). Areal distribution of snow water equivalent evaluated by snow cover monitoring. *Water Resources Research*, *17*(5), 1480–1488. https://doi.org/10.1029/WR017i005p01480

Miller, N. L., Bashford, K. E., & Strem, E. (2003). Potential Impacts of Climate Change on California Hydrology1. *JAWRA Journal of the American Water Resources Association*, *39*(4), 771–784. https://doi.org/10.1111/j.1752-1688.2003.tb04404.x

Milly, P. C. D., Dunne, K. A., & Vecchia, A. V. (2005). Global pattern of trends in streamflow and water availability in a changing climate. *Nature*, *438*(7066), 347. https://doi.org/10.1038/nature04312

Molotch, N. P., & Margulis, S. A. (2008). Estimating the distribution of snow water equivalent using remotely sensed snow cover data and a spatially distributed snowmelt model: A multi-resolution, multi-sensor comparison. *Advances in Water Resources*, *31*(11), 1503–1514. https://doi.org/10.1016/j.advwatres.2008.07.017

Morán-Tejeda, E., Lorenzo-Lacruz, J., López-Moreno, J. I., Rahman, K., & Beniston, M. (2014). Streamflow timing of mountain rivers in Spain: Recent changes and future projections. *Journal of Hydrology*, *517*(Supplement C), 1114–1127. https://doi.org/10.1016/j.jhydrol.2014.06.053

Nijssen, B., O’Donnell, G. M., Hamlet, A. F., & Lettenmaier, D. P. (2001). Hydrologic Sensitivity of Global Rivers to Climate Change. *Climatic Change*, *50*(1–2), 143–175. https://doi.org/10.1023/A:1010616428763

Rango, A. (1997). The response of areal snow cover to climate change in a snowmelt–runoff model. *Annals of Glaciology*, *25*, 232–236. https://doi.org/10.3189/S0260305500014099

Rahel, F. J., & Olden, J. D. (2008). Assessing the Effects of Climate Change on Aquatic Invasive Species. *Conservation Biology*, *22*(3), 521–533. https://doi.org/10.1111/j.1523-1739.2008.00950.x

Reed, B., Budde, M., Spencer, P., & Miller, A. E. (2009). Integration of MODIS-derived metrics to assess interannual variability in snowpack, lake ice, and NDVI in southwest Alaska. *Remote Sensing of Environment*, *113*(7), 1443–1452. https://doi.org/10.1016/j.rse.2008.07.020

Serreze, M. C., Clark, M. P., Armstrong, R. L., McGinnis, D. A., & Pulwarty, R. S. (1999). Characteristics of the western United States snowpack from snowpack telemetry (SNOTEL) data. *Water Resources Research*, *35*(7), 2145–2160. https://doi.org/10.1029/1999WR900090

Sławiński, C. (2011). Hysteresis in Soil. In *Encyclopedia of Agrophysics* (pp. 385–385). Springer, Dordrecht. https://doi.org/10.1007/978-90-481-3585-1_72

Stewart, I. T. (2009). Changes in snowpack and snowmelt runoff for key mountain regions. *Hydrological Processes*, *23*(1), 78–94. https://doi.org/10.1002/hyp.7128

Stewart, I. T., Cayan, D. R., & Dettinger, M. D. (2005). Changes toward Earlier Streamflow Timing across Western North America. *Journal of Climate*, *18*(8), 1136–1155. https://doi.org/10.1175/JCLI3321.1

Tahir, A. A., Chevallier, P., Arnaud, Y., & Ahmad, B. (2011). Snow cover dynamics and hydrological regime of the Hunza River basin, Karakoram Range, Northern Pakistan. *Hydrol. Earth Syst. Sci.*, *15*(7), 2275–2290. https://doi.org/10.5194/hess-15-2275-2011

Tekeli, A. E., Akyürek, Z., Arda Şorman, A., Şensoy, A., & Ünal Şorman, A. (2005). Using MODIS snow cover maps in modeling snowmelt runoff process in the eastern part of Turkey. *Remote Sensing of Environment*, *97*(2), 216–230. https://doi.org/10.1016/j.rse.2005.03.013

Trujillo, E., & Molotch, N. P. (2014). Snowpack regimes of the Western United States. *Water Resources Research*, *50*(7), 5611–5623. https://doi.org/10.1002/2013WR014753

Udall, B., & Overpeck, J. (2017). The twenty-first century Colorado River hot drought and implications for the future. *Water Resources Research*, *53*(3), 2404–2418. https://doi.org/10.1002/2016WR019638

U.S. Geological Survey. (2016). National Water Information System data available on the World Wide Web (USGS Water Data for the Nation), accessed January 28, 2017, at URL https://waterdata.usgs.gov/nwis/sw.

Verdin, K. L. (2011). ISLSCP II HYDRO1k Elevation-derived Products. ORNL Distributed Active Archive Center. https://doi.org/10.3334/ornldaac/1007

Vicuna, S., Leonardson, R., Hanemann, M. W., Dale, L. L., & Dracup, J. A. (2008). Climate change impacts on high elevation hydropower generation in California's Sierra Nevada: a case study in the Upper American River. *Climatic Change*, *87*(1), 123–137. https://doi.org/10.1007/s10584-007-9365-x

Westerling, A. L., Hidalgo, H. G., Cayan, D. R., & Swetnam, T. W. (2006). Warming and Earlier Spring Increase Western U.S. Forest Wildfire Activity. *Science*, *313*(5789), 940–943. https://doi.org/10.1126/science.1128834

Whitehead, P. G., Wilby, R. L., Battarbee, R. W., Kernan, M., & Wade, A. J. (2009). A review of the potential impacts of climate change on surface water quality. *Hydrological Sciences Journal*, *54*(1), 101–123. https://doi.org/10.1623/hysj.54.1.101

Yang, D., Robinson, D., Zhao, Y., Estilow, T., & Ye, B. (2003). Streamflow response to seasonal snow cover extent changes in large Siberian watersheds. *Journal of Geophysical Research: Atmospheres*, *108*(D18), 4578. https://doi.org/10.1029/2002JD003149

Yang, D., Zhao, Y., Armstrong, R., Robinson, D., & Brodzik, M.-J. (2007). Streamflow response to seasonal snow cover mass changes over large Siberian watersheds. *Journal of Geophysical Research: Earth Surface*, *112*(F2), F02S22. https://doi.org/10.1029/2006JF000518

Zhou, X., Xie, H., & Hendrickx, J. M. H. (2005). Statistical evaluation of remotely sensed snow-cover products with constraints from streamflow and SNOTEL measurements. *Remote Sensing of Environment*, *94*(2), 214–231. https://doi.org/10.1016/j.rse.2004.10.007